



**NTNU – Trondheim**  
Norwegian University of  
Science and Technology

# NON-LINEAR SOIL MODELS FOR PIPELINE AND RISER ANALYSIS

**Arifian Agusta Irman**

Marine Technology

Submission date: May 2015

Supervisor: Svein Sævik, IMT

Norwegian University of Science and Technology  
Department of Marine Technology





**NTNU – Trondheim**  
Norwegian University of  
Science and Technology

# NON-LINEAR SOIL MODELS FOR PIPELINE AND RISER ANALYSIS

Arifian Augusta Irman

Marine Structure

Submission date : May 2015

Supervisor : Svein Sævik, IMT

Norwegian University of Science and Technology

Department of Marine Technology





## MASTER THESIS SPRING 2015

for

**Stud. tech. Arifian Agusta**

### **Soil Interaction Model for Steel Catenary Risers at TDP**

*Jordinteraksjonsmodell for Fritthengende Stigerør*

The choice of soil model is an important issue when dealing with dynamic analysis of Steel Catenary Risers. The cyclic motions of the floater in a 3D sea environment induces stochastic vertical and lateral motions of the riser at the touch down point. The resulting stress histories and associated fatigue life of the riser depend on the state of the surrounding soil in terms of e.g. non-linear time dependent effects like suction and riser self-burial. Significant research efforts have been made into this in terms of model testing and formulation of models that can be implemented into a time-domain finite element framework to obtain reliable response predictions. The basic challenge with respect to the latter is the computing time which is governed by the following challenges:

1. The number of memory parameters needed to be able to predict the pipe/soil interaction force accurately as a function of time
2. The FE discretization method applied in terms of riser element length

With respect to item 1 above, the challenge is to minimize the number of memory parameters, still obtaining sufficient accuracy. When it comes to item 2, the standard implementation procedure in non-linear analysis is based on the concept of nodal springs which significantly limits the length of the riser beam elements that can be allowed, still maintaining the correct bending moment distribution. The master thesis will look into both aspects and is to be carried out as follows:

1. Literature study with focus on recent research efforts done to establish relevant pipe/soil interaction soil models (Pipestab, Carisima, Safebuck, Texas, etc.) and also finite element technologies such as the concept of hybrid mixed formulations.
2. Formulate and validate a soil interaction model that can be applied in a dynamic analysis framework
3. Implement the model in a 12 dof finite element framework using the concept of a hybrid mixed formulation.
4. Validate the model in terms of numerical analysis.



## 5. Conclusions and recommendations for further work

The work scope may prove to be larger than initially anticipated. Subject to approval from the supervisors, topics may be deleted from the list above or reduced in extent.

In the thesis the candidate shall present his personal contribution to the resolution of problems within the scope of the thesis work

Theories and conclusions should be based on mathematical derivations and/or logic reasoning identifying the various steps in the deduction.

The candidate should utilise the existing possibilities for obtaining relevant literature.

### **Thesis format**

The thesis should be organised in a rational manner to give a clear exposition of results, assessments, and conclusions. The text should be brief and to the point, with a clear language. Telegraphic language should be avoided.

The thesis shall contain the following elements: A text defining the scope, preface, list of contents, summary, main body of thesis, conclusions with recommendations for further work, list of symbols and acronyms, references and (optional) appendices. All figures, tables and equations shall be numerated.

The supervisors may require that the candidate, in an early stage of the work, presents a written plan for the completion of the work.

The original contribution of the candidate and material taken from other sources shall be clearly defined. Work from other sources shall be properly referenced using an acknowledged referencing system.

The report shall be submitted in two copies:

- Signed by the candidate
- The text defining the scope included
- In bound volume(s)
- Drawings and/or computer prints which cannot be bound should be organised in a separate folder.

### **Ownership**

NTNU has according to the present rules the ownership of the thesis. Any use of the thesis has to be approved by NTNU (or external partner when this applies). The department has the right to use the thesis as if the work was carried out by a NTNU employee, if nothing else has been agreed in advance.

**Thesis supervisors:**

Prof. Svein Sævik, NTNU


**Deadline: Juni 10, 2015**

Trondheim, January 2015

Svein Sævik

Candidate – date and signature:

Trondheim, January 2015



Arifian Agusta Irman

## ABSTRACT

This thesis describes the development and application of non-linear soil models in pipeline and riser design. A non-linear soil model is typically employed when investigating a complex pipe-soil interaction problem. Two main pipe-soil interactions are frequently studied: the vertical pipe-soil interaction at the touchdown point of the steel catenary riser (SCR) during cyclic heave motion, and the lateral pipe-soil interaction during the pipeline's lateral buckling.

Mathematical models for non-linear pipe-soil interaction are presented. The interaction typically is represented using a force-displacement curve found by fitting a high number of test data points. In the lateral direction, the soil model developed by Verley and Sotberg is widely used in industry for assessing pipeline walking. In the vertical direction, Aubeny proposed a fairly good soil model which can capture important soil behaviour such as suction force and pipe-soil separation.

The formulation and implementation of these models are the primarily focus of this thesis. New FORTRAN subroutines are created based on presented models. In lateral pipe-soil interaction, the soil subroutine, which is known as DNVMODEL-Y, includes mathematical models from DNV, PONDUS, and SAFEBUCK JIP. In vertical pipe-soil interaction, the soil subroutine, AUBENY-Z, includes the non-degradation vertical soil model developed by Aubeny. The soil subroutines are implemented inside the SIMLA software package to allow complete pipe-soil interaction analysis.

Validation of the soil subroutines is conducted and presented in detail. Two validation methods are employed: comparing the results with related works/software and ascertaining the soil behaviour by various test cases using forced displacement load.

Some applications of the developed soil subroutines in practical pipeline and riser analysis are presented in this thesis. Pipeline walking analysis using a non-linear soil model and Coulomb model is presented and discussed in detail. In regard to vertical pipe-soil interaction, deepwater SCR's response under forced heave motion is discussed. Sensitivity analysis of key parameters for several types of soil are also presented in respect to lateral and vertical pipe-soil interaction.

**Keywords:** pipeline, SCR, soil, interaction



## PREFACE

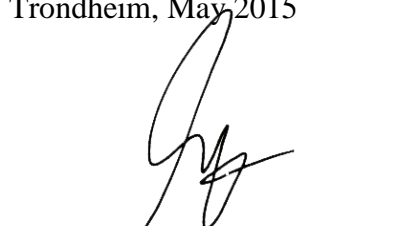
This thesis is submitted as part of the Spring 2015 curriculum at the Department of Marine Technology at Norwegian University of Science and Technology. Individuals wishing to read this thesis are assumed to have relevant backgrounds and knowledge of key terminology.

It should be noted that in the writing of this thesis, considerable expansion of scope of work have been agreed upon with the supervisor. Therefore, some major changes have been made in the list of contents and the title of the thesis from the agreed upon thesis contract.

In the completion of this thesis, I would like to thank Professor Svein Sævik for his guidance during development of the FORTRAN subroutine and writing of the thesis. I also would like to extend my appreciation to Guomin Ji for his extensive guidance during various stages of the development process. I want to thank all my friends in the Department of Marine Technology and in Trondheim for all the discussions and the emotional support during the writing process.

Last, I want to thank my parents for supporting me for the full two years during the process of attaining the Master's degree.

Trondheim, May 2015



---

Ariffan Agusta Irman

# Contents

LIST OF FIGURES .....	xi
LIST OF TABLES .....	xiii
LIST OF SYMBOLS AND ACRONYMS .....	xiv
CHAPTER 1 INTRODUCTION .....	1
CHAPTER 2 VERTICAL PIPE-SOIL INTERACTION .....	3
2.1 General Model.....	3
2.2 Backbone Curve.....	4
2.3 Bounding Loop.....	6
2.3.1 Elastic Rebound .....	6
2.3.2 Soil-Pipe Separation .....	6
2.3.3 Re-Contact .....	7
2.4 Arbitrary Loop .....	7
2.5 Memory Parameters .....	10
CHAPTER 3 LATERAL PIPE-SOIL INTERACTION .....	11
3.1 General Model.....	11
3.2 Passive Resistance Model.....	14
3.2.1 Elastic Regime.....	14
3.2.2 Plastic Regime.....	15
3.2.3 After Breakout .....	17
3.3 Berm Resistance .....	18
3.4 Soil Resistance Cycles .....	20
3.4.1 DNV Model .....	20
3.4.2 PONDUS Model .....	20
3.5 Memory Parameters .....	22
CHAPTER 4 FORMULATION AND IMPLEMENTATION.....	23
4.1 Lateral Soil Model (DNVMODEL-Y).....	23
4.1.1 General Process.....	23
4.1.2 IOP Case.....	25
4.1.3 Elastic Model .....	25
4.1.4 Plastic Regime.....	26
4.1.5 Residual Model.....	28
4.1.6 Berm Resistance Model.....	31
4.2 Vertical Soil Model (AUBENY-Z).....	32

4.2.1	General Process.....	32
4.2.2	Linear Model.....	34
4.2.3	Main Bounding Loop .....	34
4.2.4	Arbitrary Loop.....	36
4.3	SIMLA Implementation.....	38
CHAPTER 5 VALIDATION OF MODELS.....		39
5.1	Related Software .....	39
5.2	PONDUS Comparison .....	41
5.2.1	Case Description .....	41
5.2.2	Case 1 Results and Discussion .....	42
5.2.3	Case 2 Results and Discussion .....	44
5.2.4	Validation Conclusions .....	45
5.3	DNV-PONDUS Mode Comparison .....	46
5.3.1	Case Description .....	46
5.3.2	Case 1 Result and Discussion.....	46
5.3.3	Case 2 Results and Discussion .....	47
5.3.4	Validation Conclusion .....	49
5.4	Breakout Force Comparison .....	50
5.4.1	Case Description .....	50
5.4.2	Results and Discussion .....	50
5.5	DNV-BERM RESISTANCE MODEL .....	52
5.5.1	Case Description .....	52
5.5.2	Results .....	52
5.6	SIMLA Integration Validation .....	54
CHAPTER 6 APPLICATION OF PROGRAMS.....		56
6.1	Model Description .....	56
6.1.1	Lateral Pipe-Soil Model .....	56
6.1.2	Vertical Pipe-Soil Model .....	59
6.1.3	Constants.....	60
6.2	Elastic Soil Stiffness Sensitivity.....	62
6.2.1	Case Description .....	62
6.2.2	Results and Discussion .....	62
6.3	“Heavy” and “Light” Pipe .....	65
6.3.1	Case Description .....	65
6.3.2	Results and Discussion .....	65
6.4	Pipeline Walking.....	67

6.4.1	Introduction.....	67
6.4.2	Case Description.....	68
6.4.3	Results and Discussion .....	69
6.5	Coulomb Friction Model.....	73
6.5.1	Case Description.....	73
6.5.2	Results and Discussion .....	73
6.6	SCR Analysis.....	75
6.6.1	Introduction.....	75
6.6.2	Static Configuration.....	75
6.6.3	Dynamic Analysis.....	76
6.6.4	Soil Strength Sensitivity.....	79
6.6.5	Suction Force Sensitivity.....	82
6.6.6	Heave Amplitude Sensitivity.....	84
CHAPTER 7	CONCLUSION .....	86
CHAPTER 8	FURTHER WORKS.....	88
CHAPTER 9	REFERENCES .....	89
APPENDIX A	INPUT FILES.....	I
APPENDIX B	SOURCE CODES.....	V
APPENDIX C	Excerpt of SIMLA User Manual.....	XXI

## LIST OF FIGURES

Fig. 1-1.Touchdown region of SCR [1].	1
Fig. 1-2.Examples of pipeline walking in HP/HT pipeline [2].	2
Fig. 2-1.Typical load-displacement curve for vertically loaded pipeline [1].	4
Fig. 2-2.Seafloor and trench characteristics.	4
Fig. 2-3.Bounding loop description.	7
Fig. 2-4.Reversal paths from the main bounding loop.	8
Fig. 2-5.Arbitrary loop in P-y curve.	9
Fig. 3-1.Lateral pipe-soil model definition.	12
Fig. 3-2.Elastic and plastic displacement.	12
Fig. 3-3.Typical load-displacement curve for lateral soil resistance [12].	14
Fig. 3-4.Soil berm formation due to lateral movement [7].	18
Fig. 3-5.Cyclic lateral force–displacement curve for large displacement [7].	18
Fig. 3-6.Pipe buckle configuration: (a) without soil berm, and (b) with soil berm [13].	19
Fig. 3-7.Sketch of typical reversal scenario in DNV Model.	21
Fig. 3-8.Sketch of typical reversal scenario based on PONDUS mode for $v_{rev} < v_2$ .	21
Fig. 3-9.Sketch of typical reversal scenario based on PONDUS model for $y_{rev} > y_2$ .	22
Fig. 4-1.General process flowchart of DNVLATERAL-Y.	24
Fig. 4-2.Force-displacement movement after breakout in PONDUS model.	31
Fig. 4-3.Vertical soil model (AUBENY-Z) flowchart.	34
Fig. 4-4.PATHCARD sequence during main bounding loop in AUBENY-Z.	36
Fig. 4-5.Sequence of arbitrary loop in AUBENY-Z.	37
Fig. 4-6.Communication flowchart between soil subroutines and SIMLA.	38
Fig. 5-1.SIMLA program schematic [17].	40
Fig. 5-2.Forced displacement time history for PONDUS test case.	42
Fig. 5-3.Force-displacement curve for PONDUS Case 1.	42
Fig. 5-4.Soil force history (top) and penetration history (bottom) for Case 1.	43
Fig. 5-5.Force-displacement curve for PONDUS Case 2.	44
Fig. 5-6.Soil force history (top) and penetration history (bottom) for Case 2.	45
Fig. 5-7.Forced displacement time history for DNV test case.	46
Fig. 5-8.Result comparison of DNV and PONDUS analysis mode for small displacement, DNV Case 1.	47
Fig. 5-9 Force-displacement curve for DNV Case 1.	47
Fig. 5-10.Result comparison of DNV and PONDUS model for Case 2.	48
Fig. 5-11.Soil force vs. lateral displacement from DNV and PONDUS models for Case 2.	49
Fig. 5-12.Comparison of breakout penetration and initial penetration between models.	51
Fig. 5-13.Comparison of breakout resistance between different models.	51
Fig. 5-14.Lateral displacement history for berm resistance test case.	52
Fig. 5-15.Results of berm resistance model for large amplitude lateral displacement.	53
Fig. 5-16.SIMLA model used in the validation tests.	54
Fig. 5-17.Force-displacement curve of lateral motion from analytical solution and SIMLA.	55
Fig. 5-18.Force-displacement of vertical motion from analytical solution and SIMLA.	55
Fig. 6-1.Sketch of finite element model of the pipe and the seabed.	57
Fig. 6-2.Typical load factor history for lateral pipe-soil interaction.	58
Fig. 6-3.Typical EPCURVE model for axial pipe-soil interaction.	58
Fig. 6-4.SCR model for vertical pipe-soil interaction for 20 m water depth.	59
Fig. 6-5.Vertical soil stiffness calculation.	60

Fig. 6-6.The shape of pipeline after lateral buckling with high (top) and low (bottom) soil stiffness. .	63
Fig. 6-7.Force-displacement curve for Case 1A (top) and Case 1B (bottom). .....	64
Fig. 6-8.Bending moment history at the centre of pipeline for Case 1A and Case 1B. ....	64
Fig. 6-9.Non-dimensional soil force (top) and lateral displacement (bottom) vs. non-dimensional parameter S. ....	66
Fig. 6-10.A typical curve of lateral displacement development of pipeline under thermal cycling [2].	67
Fig. 6-11.Stress-strain curve for elastoplastic material model. ....	68
Fig. 6-12. Buckled form of pipeline for Case 2C with Coulomb Model (top) and Berm Model (bottom) .....	69
Fig. 6-13.Mid-node displacement, normalized against diameter, for various soil models from Case 2C. ....	70
Fig. 6-14.Walk/cycle, normalized against diameter, in the centre of pipeline vs. strain load amplitude. ....	71
Fig. 6-15.Bending moment range in the centre of the pipeline versus strain load amplitude .....	71
Fig. 6-16.Moment distribution along the pipeline for Case 2C with Coulomb model (top) and Berm model (bottom). ....	72
Fig. 6-17.Lifted pipeline segment with high friction coefficient ( $\mu > 0.9$ ). Displacement is scaled 3x. ....	73
Fig. 6-18.Lateral displacement in the centre of the pipeline for various friction coefficients. ....	74
Fig. 6-19.Moment distribution along the pipeline for various friction coefficients. ....	74
Fig. 6-20.Effective tension and bending moment along the riser length in the static configuration. ..	75
Fig. 6-21.Soil force and penetration along the riser length. ....	76
Fig. 6-22.Penetration development around the TDP region. ....	76
Fig. 6-23.Soil penetration and force at maximum penetration point (TDP Max) and TDP. ....	77
Fig. 6-24.Bending moment range (top) and history (bottom) for non-linear soil model analysis. ....	78
Fig. 6-25.Maximum and minimum bending moment at the tenth cycle. ....	79
Fig. 6-26.Soil penetration at the tenth cycle for various seabeds, verticals strength. ....	80
Fig. 6-27.Bending moment history for various seabeds, vertical strength at TDP. ....	81
Fig. 6-28.Effective tension history at TDP for various soil models. ....	81
Fig. 6-29.Soil penetration in TDP for various suction factors. ....	83
Fig. 6-30.Bending moment history at TDP for various suction factors. ....	83
Fig. 6-31.Effective tension history at TDP for various suction factors. ....	83
Fig. 6-32.Soil penetration (normalized) for various heave amplitudes. ....	84
Fig. 6-33.Bending moment history at TDP for various heave amplitudes. ....	85
Fig. 6-34.Effective tension history at TDP for various heave amplitudes. ....	85

**LIST OF TABLES**

Table 2-1 Power law coefficients [1] .....	5
Table 4-1 List of PATHCARD in Lateral Soil Model .....	23
Table 4-2 PATHCARD Description for Vertical Soil Model.....	33
Table 5-1 PONDUS Test Case Soil Parameters .....	41
Table 5-2 Soil Parameters for Analytical Test Cases .....	50
Table 5-3 Soil Parameters for SIMLA Integration Validation.....	54
Table 6-1 List of Constants .....	60
Table 6-2 List of Soil Parameters for Vertical Pipe-Soil Interaction .....	61
Table 6-3 Case Description for Elastic Soil Stiffness Sensitivity Analysis.....	62
Table 6-4 List of Cases for Pipeline Walking Analysis.....	68
Table 6-5 Bottom Point Locations and Penetration Depths .....	77
Table 6-6 Bending Moment Ranges at TDP.....	78
Table 6-7 Case List for Vertical Soil Strength Sensitivity Study .....	79
Table 6-8 Maximum Normalized Penetration ( $z/D$ ) for Various Soil Models.....	80
Table 6-9 Results Summary for Soil Strength Sensitivity Analysis.....	82
Table 6-10 Results Summary for Suction Factor Sensitivity Analysis.....	84
Table 6-11 Result Summary for Heave Amplitude Sensitivity Analysis.....	85

**LIST OF SYMBOLS AND ACRONYMS**

FEM	finite element method
HP/HT	high pressure/high temperature
JIP	Joint Industry Program
SCR	steel catenary riser
TDP	touchdown point
D	pipe outside diameter
$D_s$	remaining/passive soil resistance
$f_{suc}$	suction factor
E	accumulated energy (lateral soil model)
$F_{berm}$	berm resistance
$F_l$	lift force
$F_y$	lateral soil force
$F_z$	vertical soil force
$k_o$	unload slope during elastic rebound (vertical soil model)
$k_s$	soil elastic stiffness
Np	dimensionless bearing factor
$s_u$	soil undrained shear strength
$s_g$	soil strength gradient
$\mu$	Coulomb friction factor
v	lateral displacement
w	trench width
$w_s$	submerged weight
$\gamma_s$	soil submerged weight
$\omega$	asymptote of parabola during elastic rebound (vertical soil model)
z	soil penetration



## CHAPTER 1 INTRODUCTION

Offshore oil and gas exploration now continue to progress to deepwater areas, which present higher technical challenges compared to shallow water areas. One of the technical challenges is the effect of pipe-soil interaction in deepwater pipelines. In deepwater areas, soft clay soil is frequently encountered, and its interaction with risers and pipelines is the focus of many research projects. Two main types of pipe-soil interaction problem are typically studied: the first one is vertical riser/pipe-soil interaction, and the second one is lateral pipe-soil interaction. The vertical pipe-soil interaction problem is generally important in design of the steel catenary riser (SCR), especially in the touchdown point (TDP), as can be seen in Fig. 1-1. The interaction depends on various factors, such as soil properties and riser configuration. Typically, the contact between riser and soil at the TDP is often simplified by using a linear spring. This method, however, cannot simulate some important aspects of the vertical pipe-soil interaction, such as suction effect and deepening trench.

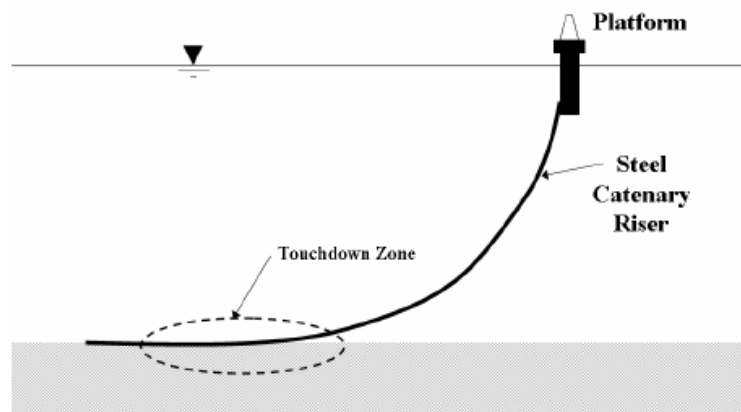


Fig. 1-1. Touchdown region of SCR [1].

The pipeline section that expands beyond the touchdown point is often observed to have high lateral displacement due to lateral buckle. The displacement could become very large, especially for pipelines operating with high pressure/high temperature (HP/HT). The cyclic thermal heating and cooling that pipelines experience during a lifetime lead to a phenomenon called 'pipeline walking'. The example of pipeline walking can be seen in Fig. 1-2. This phenomenon is very dependent on axial and lateral pipe-soil interaction. The interaction is often simplified by only considering the friction between the pipe and the soil (also known as the Coulomb model). As is the case with vertical pipe-soil interaction, this simplified model overlooks many important soil behaviours and can lead to poor design of the pipeline.

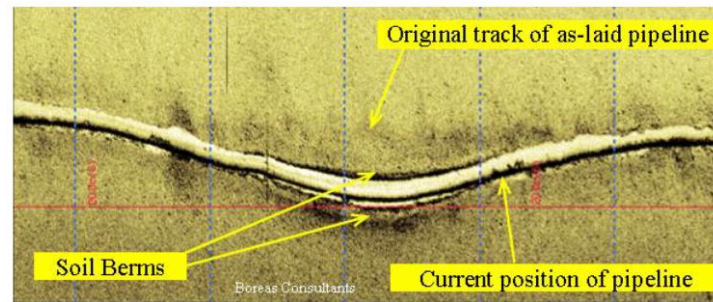


Fig. 1-2. Examples of pipeline walking in HP/HT pipeline [2].

It is therefore important to study the pipe-soil interaction by using a more realistic approach that considers non-linear soil behaviour. Some mathematical models that have been developed for non-linear vertical and lateral pipe-soil interaction are presented in this thesis. The pipe-soil interaction in those models is typically described in the form of soil resistance force and the soil displacement relationship. The relationship is derived from the process of fitting high number of test data from various research projects to correctly model soil behaviour. Chapter 2 and chapter 3 of this thesis describe some existing non-linear soil models for vertical and lateral pipe-soil interaction, respectively.

In this thesis, new FORTRAN 90 subroutines are developed based on the mathematical model presented. The subroutine for the vertical soil model is called AUBENY-Z, while that for the lateral soil model is called DNVMODEL-Y. The subroutines are integrated inside SIMLA software as custom material models for solving pipe-soil interaction problems. The formulation of the subroutines is discussed further in chapter 4.

Various validation tests have been performed for this thesis to confirm the results from the subroutines. The tests consist of comparing the results from other existing works or similar software, and confirmation of soil behaviours. The test cases also serve as a way to demonstrate the typical soil behaviour from the non-linear soil model implemented in the subroutines. The results and discussion of the validation cases are described in detail in chapter 5 of this thesis.

The last chapter of this thesis is focused on various applications of the subroutines in practical risers and pipeline design. Several design cases are presented to demonstrate the correct pipe-soil interaction. Sensitivity analysis also is conducted, generally in regard to soil characteristics, to study the changes in soil behaviour. This chapter also details the effect of a non-linear soil model in moment distribution along the riser/pipeline, and its comparison with a simplified model. Some discussions regarding the fatigue design in the form of moment variation is also presented in this thesis.

## CHAPTER 2 VERTICAL PIPE-SOIL INTERACTION

### 2.1 General Model

The soil resistance due to vertical motion of the SCR is a time-dependent process, and typically is characterized by a specific force-displacement curve. The force-displacement relationship for a vertically loaded pipeline has been investigated in the past ([3], [4]), and the typical curve is shown in Fig. 2-1. In general, the load-displacement relationship of a vertically loaded pipe is a path-dependent process. Path 0-1 is called the backbone curve; it is defined as the initial penetration of the pipe into the soil. The reversal/unloading path is defined by Path 1-2. Laboratory tests [3] show that suction force will develop during the unloading process, which in the curve is defined as a negative resistance. If the unloading continues, the suction force will not immediately disappear after reaching the maximum value, but will slowly lower, as shown in Path 2-3. Path 3-0 shows full separation between the pipe and soil. If the reloading occurs after full separation, the resistance of the soil will slowly increase to the maximum resistance value, as shown in Path 3-1. If the motion increases further, the P-y curve will continue the path along Path 0-1, or it can follow Path 1-2 again if the reversal occurs at the same point (Point 1).

Fig. 2-1 shows the complete cycles of pipe-soil interaction (initial penetration, unloading until full separation, and reloading to known maximum penetration). If the maximum motion of the pipe does not exceed maximum deflection in Point 1 and have cyclic properties, the load-deflection curve will follow Path 1-2, Path 2-3, Path 3-0, and Path 3-1, sequentially. This path combination is called the *bounding loop* [1] because exact repetition of the motion will generate the same soil resistance. It should be noted that, in reality, the repetition of the motion will degrade the soil, therefore changing the soil behaviour [1]. That effect is not included in this model.

The complete cycle of motion, as shown in Fig. 2-1, does not occur all the time. In reality, the reversal of the motion can occur within the bounding loop before the cycle can be completed. This arbitrary reversal is shown as a dashed lined in Fig. 2-1. Further reversals also can occur while following the dashed line.

A brief description of the mathematical model developed by Aubeny et al. [1] is presented in this thesis. For a more detailed analysis, further explanation of the model and experimental results can be found in Dunlap et al. [3], and Aubeny et al. [5].

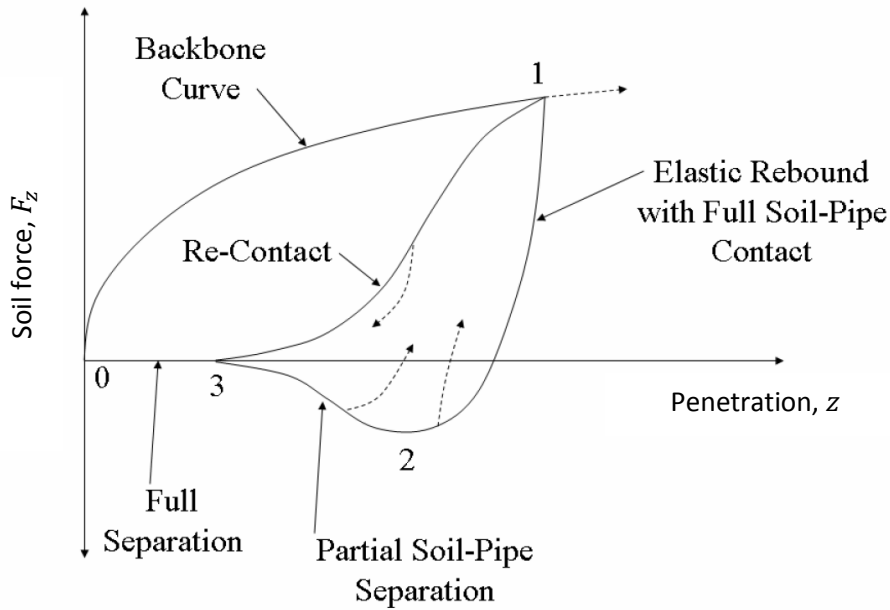


Fig. 2-1. Typical load-displacement curve for vertically loaded pipeline [1].

### 2.2 Backbone Curve

The backbone curve shows the load-displacement relationship during initial penetration of the pipe into the soil. The relationship is derived from the collapse load for a horizontal cylinder of diameter  $D$  embedded in a trench of depth  $D$  [1] with specified trench width,  $w$  (see Fig. 2-2).

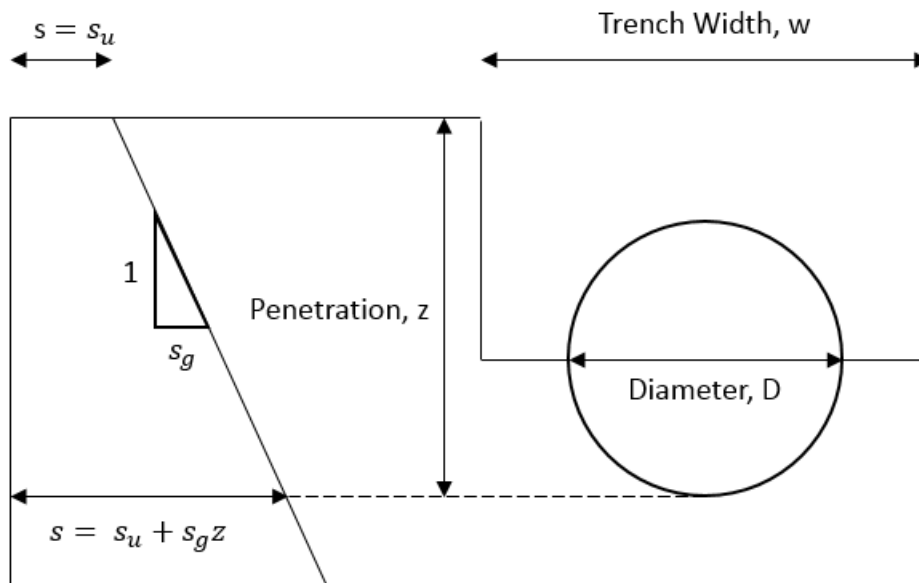


Fig. 2-2. Seafloor and trench characteristics.

The soil resistance per unit length is defined as follows [1]:

$$F_z = N_p s D \tag{2-1}$$

where  $N_p$  is the dimensionless bearing factor;  $s$  is soil strength; and  $D$  is pipe diameter. The soil strength is assumed to be linearly varying along the penetration depth,  $z$ , as follows [5]:

$$s = s_u + s_g z \quad [2-2]$$

where  $s_u$  is surface shear strength, and  $s_g$  is the gradient of shear strength. The dimensionless bearing factor,  $N_p$ , then can be found using the empirical power law function in relation to penetration depth,  $z$ , as follows [1]:

$$N_p = a(z/D)^b \quad [2-3]$$

where  $a$  and  $b$  are fitting coefficients and can be selected from Table 2-1. The soil resistance per unit length therefore has the following form:

$$F_z = a \left( \frac{z}{D} \right)^b (s_u + s_g z) D \quad [2-4]$$

It should be noted that Eq. [2-4] and Table 2-1 are valid if  $w/D=1$ . Along the riser length, the trench width can vary greatly, from very high in the touchdown region to narrow in other segments.

Table 2-1 Power law coefficients [1]

Surface roughness	$y/D < 0.5$	$y/D > 0.5$
Smooth	$a=4.97, b=0.23$	$a=4.88, b=0.21$
Rough	$a=6.73, b=0.29$	$a=6.15, b=0.15$

For other ratios of trench width and pipe diameter, the maximum value of  $N_p$  from Eq. [2-3] is limited by following these equations [1]:

$$\text{Rough Pipes} \quad N_{pmax} = 7.74 - 1.22 \left( \frac{w}{D} - 1 \right) \quad w/D < 2.75 \quad [2-5]$$

$$N_{pmax} = 5.60 \quad w/D > 2.75 \quad [2-6]$$

$$\text{Smooth Pipes} \quad N_{pmax} = 6.73 - 2.33 \left( \frac{w}{D} - 1 \right) \quad w/D < 2 \quad [2-7]$$

$$N_{pmax} = 4.40 \quad w/D < 2 \quad [2-8]$$

## 2.3 Bounding Loop

As stated before, the bounding loop will develop if sufficiently large motion cycles occur after the initial penetration. The bounding loop is defined as Path 1-2-3-1 in Fig. 2-1. The main paths in the loop are as described in following sections.

### 2.3.1 Elastic Rebound

This path connects Point 1 and Point 2 in Fig. 2-1, which defined the resistance of soil during the unloading process. Point 1 is the maximum initial penetration based on the backbone curve, while Point 2 is the point where the soil develops maximum suction force. The maximum suction force,  $F_{z2}$ , is defined as the ratio of maximum soil resistance,  $F_{z1}$ , as follows:

$$F_{z2} = -f_{suc}F_{z1} \quad [2-9]$$

The hyperbolic relationship is used to define the force-displacement curve in this path [1]:

$$F_z = F_{z1} + \frac{z - z_1}{\frac{1}{k_o} - \frac{z - z_1}{(1 + \omega)F_{z1}}} \quad [2-10]$$

where  $F_{z1}$  and  $z_1$  are soil resistance and penetration depth, respectively, at Point 1. The parameter  $k_o$  is the initial slope of the hyperbola and can be defined from surface soil strength  $s_u$  and assumed as  $k_o=660s_u$  [1]. The parameter  $\omega$  defined the asymptote of the parabola and location of  $z_2$  as follows:

$$z_2 = z_1 - \frac{(1 + \omega)F_{z1}}{k_o} \frac{1 + f_{suc}}{\omega - f_{suc}} \quad [2-11]$$

### 2.3.2 Soil-Pipe Separation

After maximum suction force is reached (Point 2), the suction force decreases slowly until the pipe is fully separated from the soil (Point 3). The penetration depth and soil resistance force at Point 3 is given by the following equations:

$$(z_2 - z_3) = \psi(z_1 - z_2) \quad [2-12]$$

$$F_{z3} = 0 \quad [2-13]$$

The parameter  $\psi$  is defined as the riser-soil separation parameter and needs to be acquired from the model test. If the motion continues to decrease below  $z_3$ , the soil resistance will be zero, as shown in Eq. [2-13].

The soil resistance between Point 2 and Point 3 is given by a cubic relationship:

$$F_z = \frac{F_{z2}}{2} + \frac{F_{z2}}{4} \left[ 3 \left( \frac{z - z_0}{z_m} \right) - \left( \frac{z - z_0}{z_m} \right)^3 \right] \quad [2-14]$$

$$z_0 = \frac{z_2 + z_3}{2} \quad [2-15]$$

$$z_m = \frac{z_2 - z_3}{2} \quad [2-16]$$

### 2.3.3 Re-Contact

If the pipe undergoes reloading after it is fully separated from the soil (Point 3), the soil resistance will increase slowly until it reaches Point 1. The soil resistance in this path is given by a cubic relationship similar to Eq. [2-14] as follows:

$$F_z = \frac{F_{z1}}{2} + \frac{F_{z1}}{4} \left[ 3 \left( \frac{z - z_0}{z_m} \right) - \left( \frac{z - z_0}{z_m} \right)^3 \right] \quad [2-17]$$

$$z_0 = \frac{z_1 + z_3}{2} \quad [2-18]$$

$$z_m = \frac{z_1 - z_3}{2} \quad [2-19]$$

Fig. 2-3 shows the main bounding loop of the P-y curve, as explained previously.

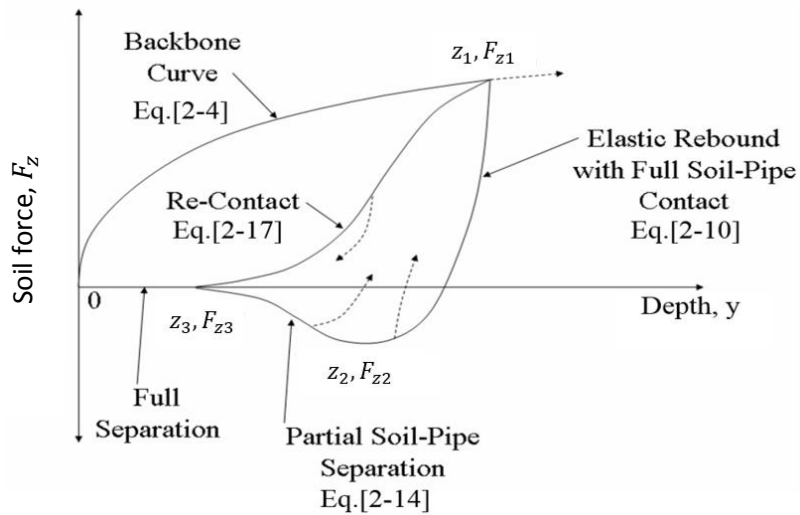


Fig. 2-3. Bounding loop description.

## 2.4 Arbitrary Loop

The main bounding loop in the previous section only explains the soil behaviour during extreme motion cycles (the pipe is always fully separated before reloading occurs). In reality, the reloading often occurs before the pipe is fully separated or reaches the maximum suction limit.

If the reversal occurs during Path 1-2 (elastic rebound) or Path 3-1 at certain arbitrary reversal point ( $z_{rb}, F_{zrb}$ ), the soil resistance is given as follows:

$$F_z = F_{zrb} + \frac{z - z_{rb}}{\frac{1}{k_o} + \chi \frac{z - z_{rb}}{(1 + \omega)F_{z1}}} \quad [2-20]$$

The parameter  $\chi$  is equal to 1 for reloading (i.e. reversal from Path 1-2) and -1 for unloading (i.e. reversal from Path 3-1). It should be noted that soil resistance given by Eq. [2-20] can exceed the value from the main bounding loop (Eqs. [2-10], [2-14], and [2-17]). In such condition, the load-displacement pattern should return to the main bounding loop.

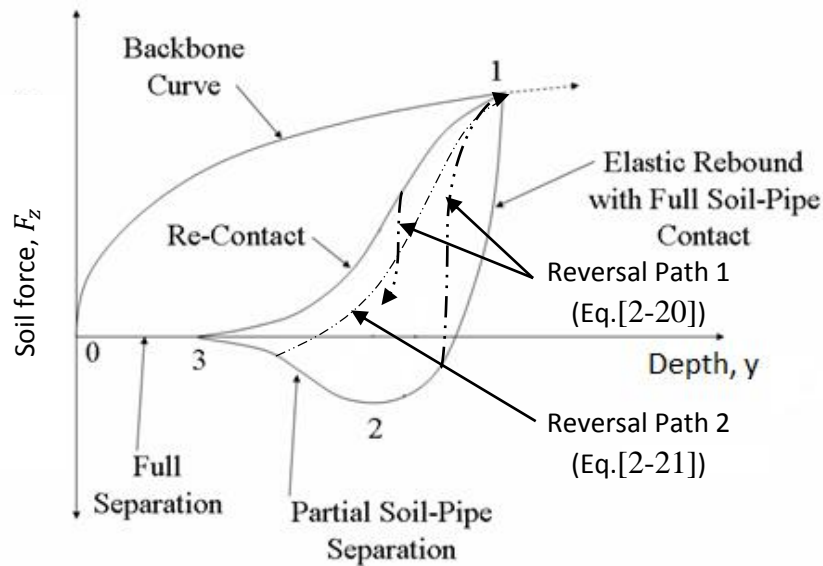


Fig. 2-4. Reversal paths from the main bounding loop.

If the reversal occurs during Path 2-3, the soil resistance is given by a modified version of Eq. [2-17] as follows:

$$F_z = \frac{F_{z1} + F_{zrb}}{2} + \frac{F_{z1} - F_{zrb}}{4} \left[ 3 \left( \frac{z - z_0}{z_m} \right) - \left( \frac{z - z_0}{z_m} \right)^3 \right] \quad [2-21]$$

$$z_0 = \frac{z_1 + z_{rb}}{2} \quad [2-22]$$

$$z_m = \frac{z_1 - z_{rb}}{2} \quad [2-23]$$



Fig. 2-4 shows the possible paths that can be taken if the reversal occurs in various points in the bounding loop. If the next reversal occurs during this path at a specific reversal point ( $z_r, F_{zr}$ ), the soil resistance is given by modifying Eq. [2-20] as follows:

$$F_z = F_{zr} + \frac{z - z_r}{\frac{1}{k_o} + \chi \frac{z - z_r}{(1 + \omega)F_{z1}}} \quad [2-24]$$

As stated before, the parameter  $\chi$  is defined by the nature of the next reversal ( $\chi=1$  for reloading and  $\chi=-1$  for unloading). This effectively will define an *arbitrary loop* in the force-displacement curve aside from the bounding loop. Fig. 2-5 shows an example of an arbitrary loop formed inside the bounding loop.

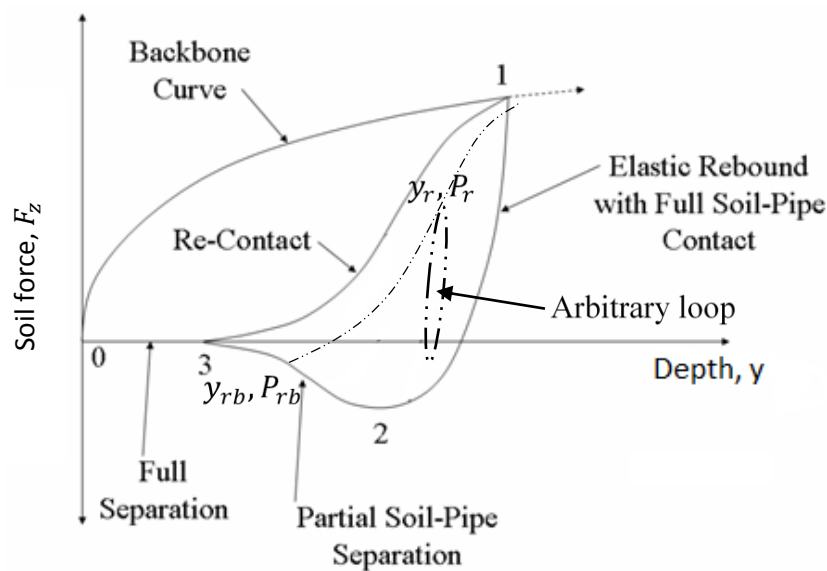


Fig. 2-5. Arbitrary loop in P-y curve.

## 2.5 Memory Parameters

The set of memory parameters is needed to determine the solution of the vertical pipe-soil interaction in each load step, and update it accordingly. As mentioned previously, vertical pipe-soil interaction is a path-dependent process; therefore, several memory parameters are required to integrate it with global riser analysis. The required parameters are as follow:

- a. Path identifier: The force-displacement curve consists of several unique paths. Therefore, it is critical to define a unique path identifier and updated it in each iteration. It is used to determine the path that will be taken in the next iteration.
- b. Bounding loop points: These consist of Point 1, Point 2, and Point 3 in the bounding loop, which define the characteristic of the curve.
- c. Reversal points: These consist of the reversal points from the bounding loop ( $z_{rb}, F_{zrb}$ ) and the latest known reversal points ( $z_r, F_{zr}$ ).
- d. Bounding loop soil resistance: It is used as the reference soil resistance if the current path enters the arbitrary reversal path, as mentioned in section 2.4. If the current soil resistance exceeds the reference resistance, the path is updated to follow the bounding loop path.
- e. Previous penetration depth,  $z_{i-1}$ : It is used to define the path of the current iteration together with the path identifier parameter.

In total, 16 memory parameters need to be defined in each iteration cycle. However, only path identifier and penetration depth are required to be updated and used regularly in each iteration. The rest of the memory parameters are used and updated if certain conditions are fulfilled. Further implementation of the vertical soil model is explained in CHAPTER 4.

## CHAPTER 3 LATERAL PIPE-SOIL INTERACTION

In the past, lateral soil interaction has been modelled using a simple friction coefficient (also known as the Coulomb model). This model is very simplified and is an unrealistic method to model pipe-soil interaction because it does not consider non-linearity of the soil force, especially in large lateral displacement situations. Several research projects have been conducted in the past to refine the pipe-soil model. They include the model developed by Verley ([6], [7]) and SAFEBUCK Joint Industry Program (SAFEBUCK JIP) [8]. The PONDUS software that developed by MARINTEK is one of the software that utilized the Verley's model. The SAFEBUCK JIP program is primarily concentrated on the lateral soil model during large displacement lateral buckling, and it examines the effect of the soil berm.

In this chapter, a non-linear soil model for cohesive soil (clay) is presented. The chapter addresses the mathematical models and the general behaviour of the force-displacement curve during lateral pipe-soil interaction. The mathematical model presented in this chapter serves as the theoretical basis for the new subroutine's formulation that will be explained in chapter 4.

### 3.1 General Model

The proposed lateral soil model contains two main components: friction component (Coulomb force) and passive soil force component. The model for passive soil force was developed by Verley and Sotberg [7] for sand, and by Verley and Lund [6] for the clay model. The mathematical model of the passive soil resistance is created using simple dimensional analysis methods fitted to large scale laboratory testing tools such as PIPESTAB [9] and AGA [10]. Both models have been incorporated in DNV-RP-F109 [11] as recommended soil models for pipelines design. The Verley model also was implemented inside the PONDUS program that was developed by MARINTEK [12].

The mathematical model that is explained here briefly is based on implementation of Verley's clay model inside the PONDUS program. For full details regarding model explanation, references should be made to Verley and Sotberg [6] and the PONDUS theory manual [12].

The coordinate system and force definition for the lateral soil model is defined in Fig. 3-1.

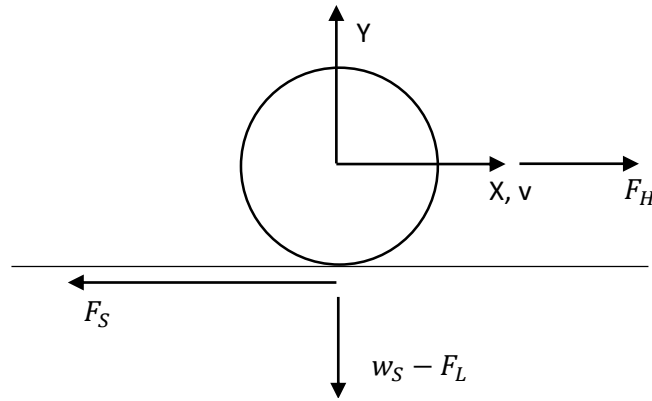


Fig. 3-1. Lateral pipe-soil model definition [12].

where  $F_s$  is soil force;  $F_L$  is lift force, and  $F_H$  is hydrodynamic force.

The total lateral displacement,  $v$ , can be divided into elastic and plastic contributions as follows:

$$v = v_e + v_p \tag{3-1}$$

where  $v_e$  is elastic displacement, and  $v_p$  is plastic displacement.

The soil force,  $F_s$ , in the elastic range, is defined by following equation:

$$F_s = k_s \cdot v_e \tag{3-2}$$

where  $k_s$  is the soil elastic stiffness.

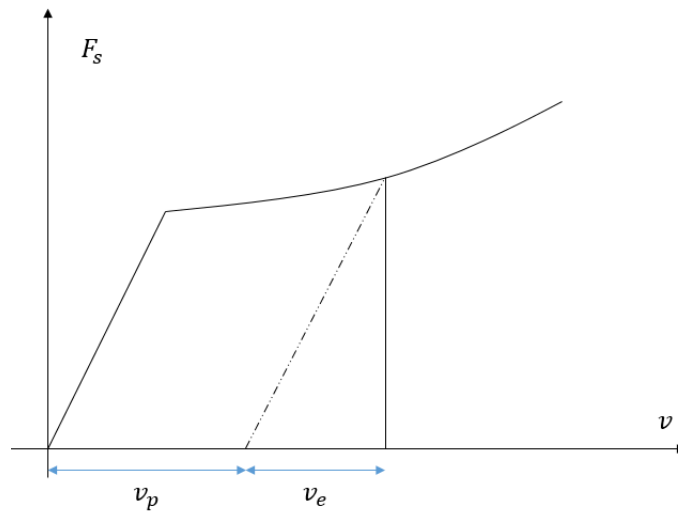


Fig. 3-2. Elastic and plastic displacement.

The soil resistance in the plastic range is defined as follows:

$$F_s = F_f + F_r \tag{3-3}$$

$$F_f = \mu(w_s - F_l) * \text{sgn}(\dot{v}) \quad [3-4]$$

$$F_r = D_s * \text{sgn}(\dot{v}) \quad [3-5]$$

$$\begin{aligned} \text{sgn}(\dot{v}) &= +1 \text{ if } \dot{v} > 0 \\ &= -1 \text{ if } \dot{v} < 0 \end{aligned} \quad [3-6]$$

where  $F_l$  = lift force =  $w_s$  if  $F_l > w_s$ ;

$F_s$  = plastic soil force = 0 if  $\mu(w_s - F_l) + D_s$ ;

$w_s$  = the submerged weight of the pipe;

$\mu$  = constant friction coefficient = 0.2 for clay;

$D_s$  = remaining force function.

The soil resistance consists of two components, as can be seen in Eq. [3-3]. The first component,  $F_f$ , is the pure friction component (Coulomb friction force), and the second component,  $F_r$ , is the soil remaining force [12] or passive resistance, which is a function of soil penetration, lift force, and displacement of the soil.

The transition from the elastic to plastic regime is then defined by the following equation [12]:

$$|k_s v_e| = (\mu(w_s - F_l) + D_s) \quad [3-7]$$

The transition from plastic to elastic occurs directly in the moment of load reversal.

During the plastic regime, the elastic displacement contribution can be derived from the relationship shown in Fig. 3-2 as follows:

$$v_e = \frac{F_s}{k_s} \quad [3-8]$$

### 3.2 Passive Resistance Model

In general, the passive resistance of the soil has four stages of development, as shown in Fig. 3-3. The stages as described by DNV are as follows [11]:

1. An elastic region where the lateral displacement is less than typically 2% of the diameter. The upper limit of the passive resistance in this stage is denoted as  $F_{R1}$ .
2. A region where significant lateral displacement may be experienced, up to half the pipe diameter for sand and clay soils in which the pipe-soil interaction causes an increase in the penetration and thus in the pipe-soil resistance. The upper limit of soil passive resistance is called breakout resistance,  $F_{R2}$ .
3. After breakout, the resistance and penetration decrease.
4. When displacement exceeds typically one diameter, the passive resistance and penetration may be assumed constant. The soil resistance at this stage is denoted as  $F_{R3}$ .

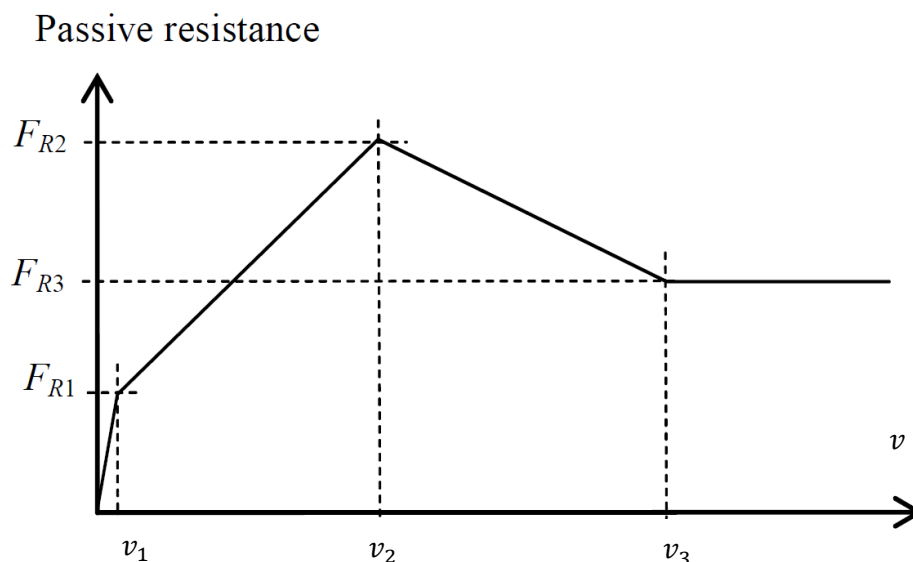


Fig. 3-3. Typical load-displacement curve for lateral soil resistance [11].

#### 3.2.1 Elastic Regime

The initial passive soil resistance is linear elastic and assumes no work is done. In this stage, the assumed pipe penetration does not change from the initial penetration into the soil. The initial penetration due to self-weight of the pipe on clay soil is defined as follows [11]:

$$\frac{z_i}{D} = 0.0071 \left( \frac{G^{0.3}}{K_c} \right)^{3.2} + 0.062 \left( \frac{G^{0.3}}{K_c} \right)^{0.7} \quad [3-9]$$

$$G = \frac{s_u}{D \cdot \gamma_s} \quad [3-10]$$

$$K_c = \frac{s_u \cdot D}{w_s - F_l} \quad [3-11]$$

where  $s_u$  is undrained shear strength of the clay;  $D$  is pipe diameter;  $w_s$  is pipe submerged weight per unit length; and  $F_l$  is the lift load.

The upper limit of the passive resistance is denoted as  $F_{R1}$  and defined as follows ([6], [11]):

$$F_{R1} = \frac{4.13K_c(w_s - F_l)}{G^{0.392}} \left(\frac{z_1}{D}\right)^{1.31} \quad [3-12]$$

where  $z_1$  is the initial penetration of the pipe into the soil. The upper limit for the lateral motion in the elastic regime,  $v_1$  is defined as 0.02 of pipe diameter by DNV [11] or  $(F_{R1}+F_f)/k_s$  by PONDUS [12].

The soil resistance in the elastic regime therefore can be found using the following equation:

$$F_R = k_s \cdot v \quad [3-13]$$

The elastic stiffness,  $k_s$ , for clay is typically 20-40 N/m [11].

### 3.2.2 Plastic Regime

If the lateral motion increases further, the passive soil resistance will enter the plastic regime. The soil penetration will increase due to accumulated work (energy) by lateral motion. The work in the plastic regime is defined as follows:

$$E = \int_0^t F_R ds \quad [3-14]$$

The total soil penetration,  $z_2$ , due to lateral motion in the plastic regime can be found as follows:

$$\frac{z_2}{D} = \left[ 0.12 \cdot S^{0.637} \xi^{0.32} \left(\frac{a}{D}\right)^{-0.25} \right], \quad \left(\frac{a}{D}\right) \geq 0.05 \quad [3-15]$$

$$\xi = \frac{E}{s_u \cdot D^2} \quad [3-16]$$

where  $a$  is the pipe oscillation amplitude in the lateral direction. If  $(a/D)$  is less than 0.05, then  $a/D=0.05$  [12].

The soil penetration in the plastic regime is limited by the following equations:

$$\left(\frac{z_2}{D}\right)_{max} = 1.1S \cdot G^{0.54} \left(\frac{a}{D}\right)^{0.17}, \quad \left(\frac{z_2}{D}\right) \leq 0.3, \quad \left(\frac{a}{D}\right) \geq 0.05 \quad [3-17]$$

Due to limitation of the data in the development of Verley's model, the upper limit of the soil penetration is defined as follows [6]:

$$z_{2max} = 0.3 \cdot D, \quad \left(\frac{z_2}{D}\right) > 0.3 \quad [3-18]$$

The peak of the soil resistance force in this stage (the breakout strength) is denoted as  $F_{R2}$  and can be found as follows [11]:

$$F_{R2} = \frac{4.13K_c(w_s - F_l)}{G^{0.392}} \left(\frac{z_2}{D}\right)^{1.31} \quad [3-19]$$

From Eqs. [3-19] and [3-15], it can be seen that the breakout strength will vary during the lateral motion. The maximum lateral motion, where the maximum breakout,  $v_2$ , occurs is defined as  $0.5D$  [11]. In the PONDUS model, the  $v_2$  was extended to  $0.75D$ .

The soil stiffness in the plastic regime can be found as a function of soil penetration, as shown below:

$$k_{z2} = \frac{(F_{R2} - F_{R1})}{v_2 - v_1} \quad [3-20]$$

From the equation, it easily can be seen that the soil stiffness in plastic regime is not constant and varies with an increase in soil penetration.

By assuming the linear relation between  $F_{R1}$  and  $F_{R2}$  during plastic deformation, the passive soil resistance therefore can be found as:

$$D_s = F_{R1} + k_{z2} \cdot (v - v_1) \quad [3-21]$$



Even though a linear relation is assumed, the passive soil resistance may show a non-linear result due to changing breakout strength during lateral motion.

### 3.2.3 After Breakout

If the pipe continues to move in the same direction after breakout, some horizontal resistance in addition to friction will present due to the soil mound being pushed ahead of the pipe [12]. The accumulated work is set to zero, and no work is considered in this stage. The soil penetration is reduced, accordingly, to the penetration associated with  $z_3$ . DNV recommends the value of  $z_3$  as half of the soil penetration at  $z_2$  until  $v = D$ , as defined below [11]:

$$z_3 = 0.5z_2^* \quad [3-22]$$

where  $z_2^*$  is the soil penetration at breakout.

In PONDUS, after soil breakout the force-displacement curve moves with distance of  $(v-v_2)$ . The value of  $z_3$  in PONDUS is also calculated with a different method by using Eq. [3-9].

The residual resistance,  $F_{R3}$ , is therefore defined as follows:

$$F_{R3} = \frac{4.13K_c(w_s - F_l)}{G^{0.392}} \left(\frac{z_3}{D}\right)^{1.31}$$

The calculation of the residual limit,  $v_3$ , is different in DNV and PONDUS. In DNV,  $v_3$  is set to be equal to  $1D$ , while in PONDUS the limit is calculated using the following expression:

$$v_3 = D \left( 0.6 \left( \frac{5.5}{\kappa} + 1 \right) + \frac{v_2}{D} \right) \quad [3-23]$$

where  $\kappa = \frac{\gamma_s D^2}{w_s}$ .

The slope of the passive soil force after breakout is then defined as follows:

$$k_{z3} = \frac{(F_{R2} - F_{R3})}{y_3 - y_2} \quad [3-24]$$

The passive soil resistance for in-between therefore can be found by modifying Eq. [3-21] by the appropriate slope, as follows:

$$D_s = F_{R2} + k_{z3} \cdot (y - y_3) \quad [3-25]$$

If the pipe still moves in the same direction after reaching  $z_3$ , the passive soil resistance is set equal to  $F_{R3}$  and soil penetration equal to  $z_3$ .

### 3.3 Berm Resistance

During large lateral displacement (typically higher than 1D), part of the soil will be dragged by the pipe, causing added soil resistance. This effect had been captured inside Verley’s model by means of residual soil resistance. However, Verley’s model does not capture the effect of soil berm that builds up at the end of every large displacement sweep. In each successive sweep, the soil in front of the pipe remoulded into a soil berm, as shown in Fig. 3-4.

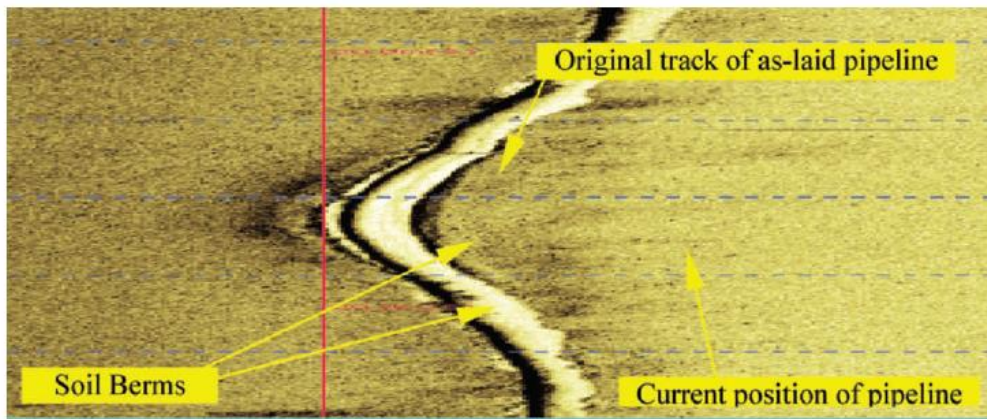


Fig. 3-4. Soil berm formation due to lateral movement [8].

As shown by SAFEBUCK’s result [8], the resistance due to soil berm can be very significant. The soil berm resistance is an important factor in lateral buckling design of pipeline. In the past, the Coulomb friction model was used to model the soil resistance due to complexity in berm formation. This approach will make the pipeline buckle easily and reduce the buckling loading. However this simple model is deemed unrealistic [8] for the lateral buckle problem, which is very sensitive to pipe-soil interaction.

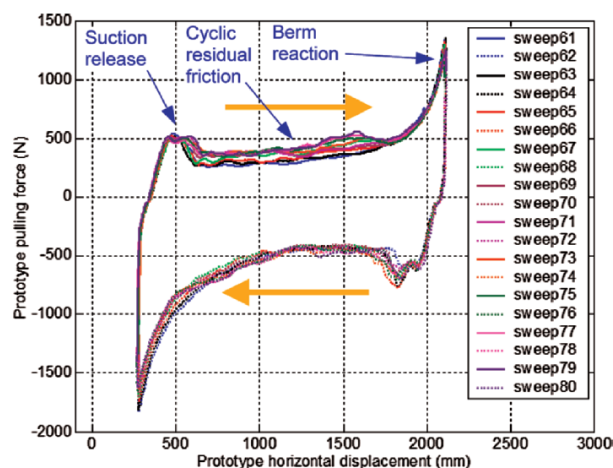


Fig. 3-5. Cyclic lateral force–displacement curve for large displacement [8].

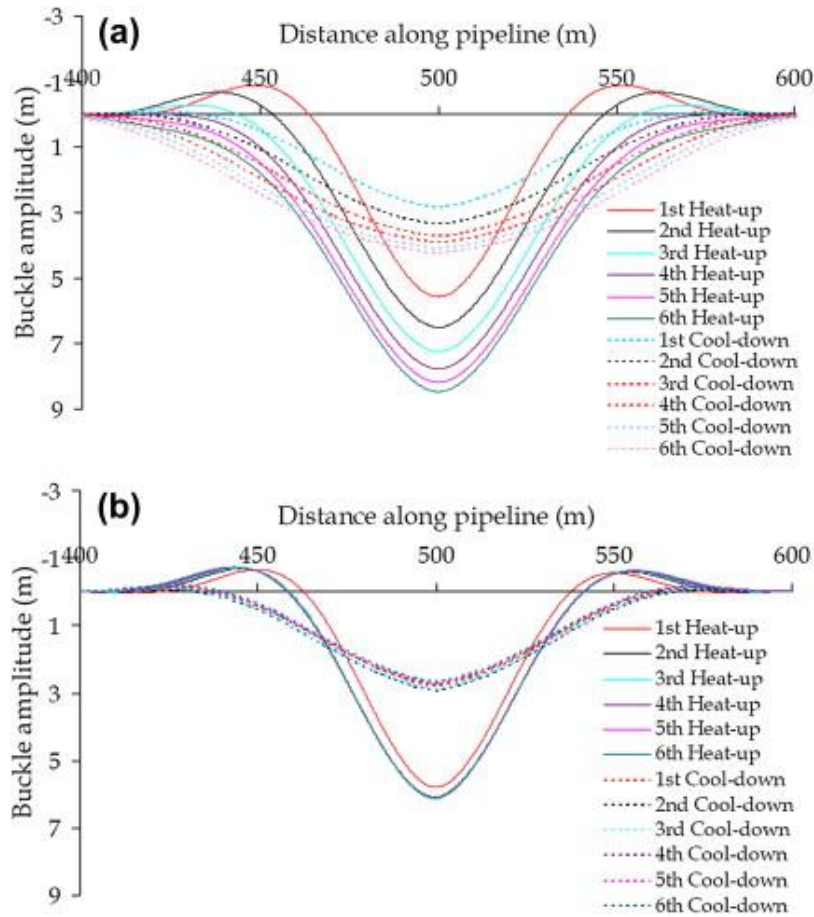


Fig. 3-6. Pipe buckle configuration: (a) without soil berm, and (b) with soil berm [2].

Fig. 3-6 shows the buckle configuration of pipelines with and without soil berm. It can be seen that with soil berm, the lateral deformation is arrested. If the soil berm is ignored, the soil resistance remains constants (equal to residual and friction force). Numerical modelling shows that this will cause the buckle to grow in amplitude with each cycle, and will result in underestimating the fatigue damage [13].

Some research has been conducted to formulate the soil berm resistance (e.g. SAFEBUCK [8] and IPT [14]) in a simple and easily implemented way. Both SAFEBUCK and IPT proposed that the soil berm resistance can be formulated as friction load. The SAFEBUCK program proposed that additional berm resistance,  $\Delta F_{berm}$ , can be added on top of residual soil resistance when during the berm build-up. The proposed value of  $\Delta F_{berm}$  is:

$$\Delta F_{berm} = 1.5F_v \tag{3-26}$$

where  $F_v$  is the vertical force acting on the force. The number of the sweep that is required to achieve this maximum berm resistance is five cycles (typically) [8].

### 3.4 Soil Resistance Cycles

In reality, the offshore pipeline will be subjected to wave loading and current, which can be cyclic in a given time range. Therefore, the soil model must be able to accommodate the change of load directions to fully model the pipe-soil interaction. The reversal assumptions differ greatly in soil model used, between DNV and PONDUS; this difference is explained below.

#### 3.4.1 DNV Model

If the reversal occurs at the elastic regime, no change in the curve is made, and the passive soil resistance can be found as shown in Eq. [3-13]. However, if the reversal occurs in the plastic regime at point  $v_{rev}$ ,  $F_{rev}$ , the origin of the force-displacement curve is shifted by  $v_{rev} - F_{rev}/k_s$ . The passive soil resistance therefore can be calculated using this new curve from here on. In the event of reversal, the force-displacement from the plastic regime also is shifted directly to the elastic regime. The current penetration is treated as initial penetration in the next cycle. The typical load reversal scenario of the DNV model can be shown in Fig. 3-7.

#### 3.4.2 PONDUS Model

If the reversal occurs in the elastic regime or lower than  $v_2$ , no change is required in the curve origin. In the event of reversal occurring at reversal point  $v_{rev}$ ,  $F_{rev}$ , which is larger than  $v_2$ , the curve origin must be moved by distance of  $(v_{rev} - v_2)$ . The current penetration is maintained, but no change in elastic limit ( $F_{R1}$ ) is necessary. If the current displacement had passed the elastic regime but not reached the new plastic limit, the elastic limit would be maintained as the passive soil force. The typical reversal scenario in the PONDUS model can be seen in Fig. 3-8 and Fig. 3-9.

Comparison of Fig. 3-7 and Fig. 3-9 reveals distinct differences between both models that will result in a different soil force history after several cycles. These differences are described further in chapter 5.

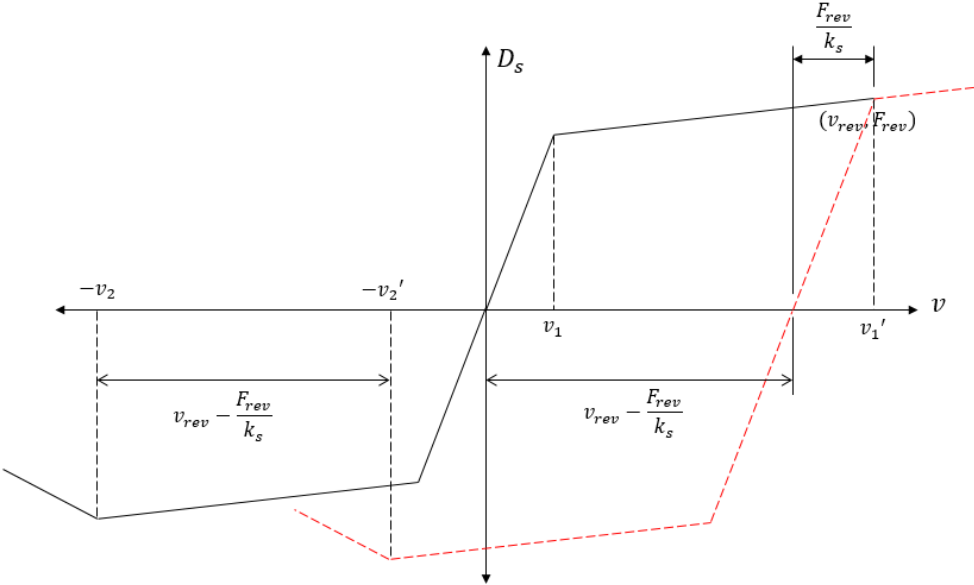


Fig. 3-7. Sketch of typical reversal scenario in DNV Model.

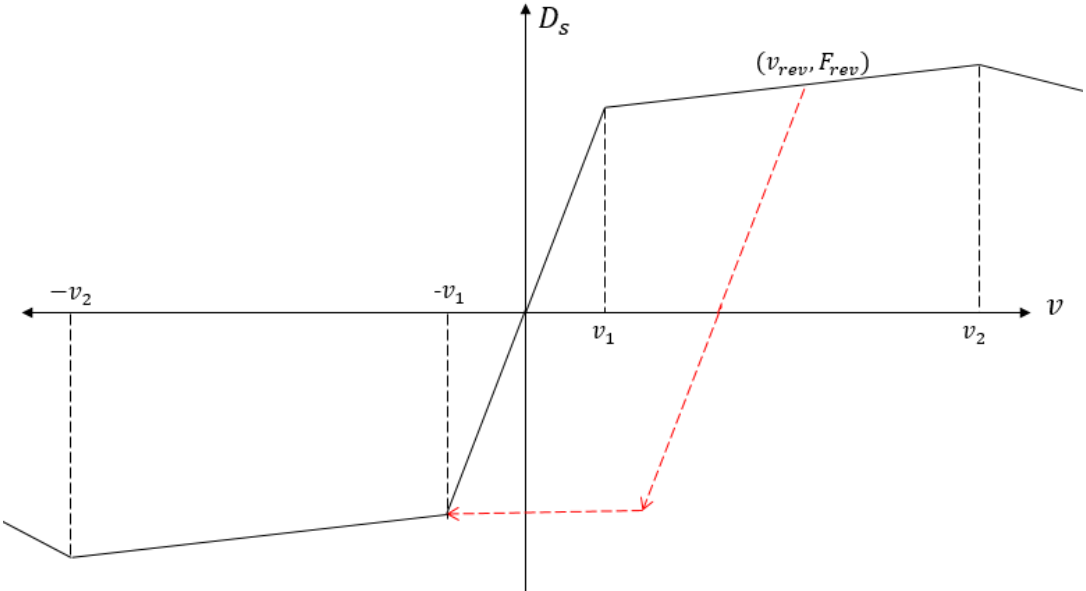


Fig. 3-8. Sketch of typical reversal scenario based on PONDUS mode for  $v_{rev} < v_2$ .

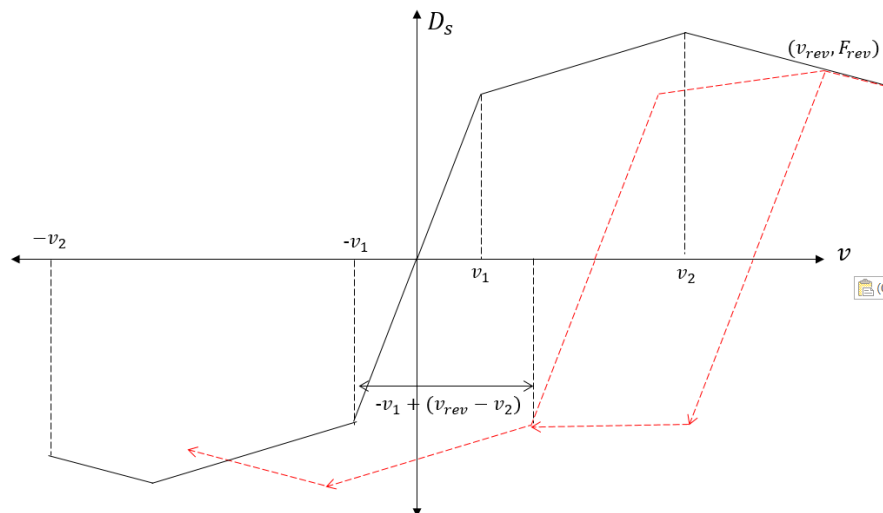


Fig. 3-9. Sketch of typical reversal scenario based on PONDUS model for  $v_{rev} > v_2$ .

### 3.5 Memory Parameters

As in the case of the vertical soil model, the lateral soil model also needs several memory parameters to describe the soil resistance in time-domain analysis. Definition of the memory parameters in the lateral model becomes quite complex because the force-displacement curve is changing in every time step. Several types of memory parameters are required:

- Path identifier: A unique number that identifies the path currently taken in the force-displacement curve. It is used to determine how to calculate soil resistance force.
- Previous load step results: This includes penetration, soil force, and applied vertical force obtained in previous load steps.
- Reversal points: The point (displacement, soil force) at which last known reversal occurs.
- Curve definition: This includes the definition of characteristic points such as  $(F_{R1}, v_1)$  and  $(F_{R2}, v_2)$  in every load step. The values are updated during reversal or other specified conditions.

The total number of memory parameters needed depends upon how the soil model is implemented. In this thesis, soil models from DNV, PONDUS, and SAFEBUCK are used; therefore, 36 memory parameters are needed. A large number of parameters are reserved for curve definition of the three soil models. The memory parameters are implemented as work arrays which are updated in every load step. Details about the implementation of the lateral soil models are presented in the following chapter.

## CHAPTER 4 FORMULATION AND IMPLEMENTATION

Previous chapters in this thesis discussed the mathematical models of vertical and lateral non-linear soil interaction. This chapter will present the formulation of those models into the FORTRAN language to create new subroutines. The subroutines then will be integrated inside a SIMLA structural/finite element model to achieve complete pipe-soil interaction analysis.

The vertical soil model that is used as the basis for this thesis is the non-linear model developed by Aubeny et al. [1]. For the lateral model, both the DNV [11] and PONDUS [12] model are incorporated. Furthermore, the lateral model also includes the berm resistance model based on SAFEBUCK JIP's result [8] to obtain accurate soil behaviour for lateral buckle analysis.

The FORTRAN 90/95 compiler was used throughout the programming step. The lateral soil model and vertical soil model were named DNVMODEL-Y and AUBENY-Z, respectively.

Both subroutines can be executed alone or in conjunction with the SIMLA structural model to solve pipe-soil interaction problem. Even though both of them are non-linear soil models, they are developed from different research efforts and assumptions, and therefore are not meant to be used together. Other soil models must be used along with one of them during the analysis of pipe-soil interaction. Examples of such analyses are presented in chapter 5.

### 4.1 Lateral Soil Model (DNVMODEL-Y)

#### 4.1.1 General Process

The general process of the DNVMODEL-Y is best described in the flowchart shown in Fig. 4-1. The subroutine has three main inputs: the lateral displacement,  $v$ ; model selection case, IOP; and load step number, LSNUM. The user-defined parameters are grouped in the INPUT ARRAY. The OPTION ARRAY contains information regarding various analysis option that can be chosen. The WORK ARRAY contains specific information that is needed to execute the simulation in every load step or iteration.

Table 4-1 List of PATHCARD in Lateral Soil Model

PATH ID	PATHCARD Description	Notes
0/15	Elastic regime, positive/negative loading	
20/21	Extended elastic regime	Only for PONDUS model
12/121	Breakthrough build-up, positive/negative loading	
13/131	After breakthrough, positive/negative loading	
14	New curve definition, reversal	

PATH ID	PATHCARD Description	Notes
99/98	Berm resistance model, positive/negative loading	Only for Berm Model

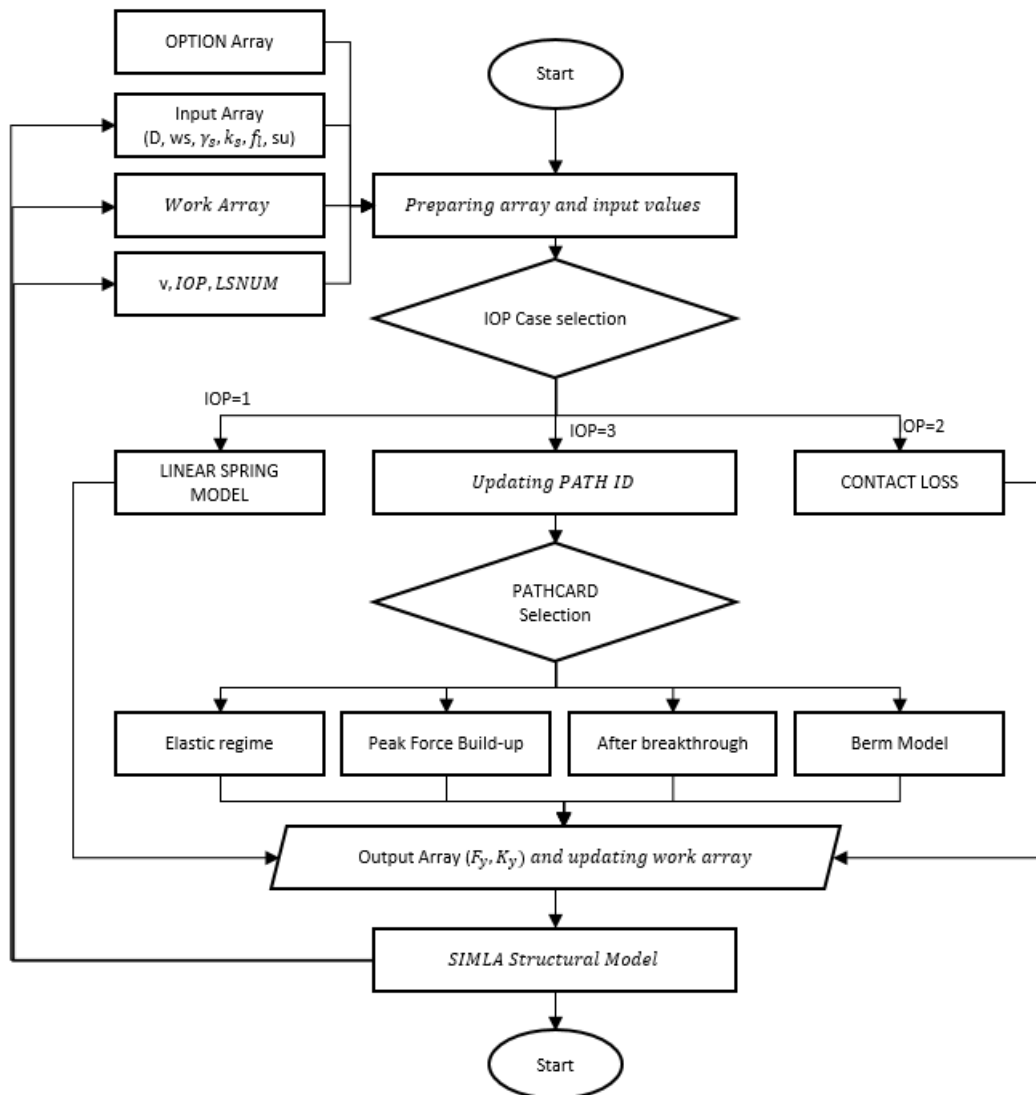


Fig. 4-1. General process flowchart of DNVLATERAL-Y.

As described in chapter 3, the lateral soil model is a very path-dependent process. Therefore, to easily formulate the lateral soil model, a unique identifier known as PATH was used. This identifier directs the calculation to correct PATH-specific routines called PATHCARD. In total, there are 6 PATHCARD routines with 11 PATH identifiers that describe specific physical characteristic of the model, as can be seen in Table 4-1. In each of these cards, the PATH identifier can be updated accordingly to switch to a different PATHCARD to simulate change in the soil model.

The OPTION array in DNVMODEL-Y contains three parameters. The first parameter, OPT1, defines the algorithm to be used to calculate the penetration during residual action,  $z_3$ . The



second parameter, OPT2, governs the activation of the berm model. The last parameter, OPT3, is used to let the user choose the non-linear soil model. Currently, the models based on DNV criteria (OPT3=1) and PONDUS criteria (OPT3=2) can be selected. Both models can be used in conjunction with the berm model.

The WORK array contains the memory parameters described in CHAPTER 3. The WORK array have 36x1 dimension, corresponding to the amount of needed memory parameters.

The outputs of each of the PATHCARD routines are lateral soil force,  $F_y$ , and soil stiffness,  $K_y$ . The results are then sent to SIMLA as input to the equilibrium iteration of the pipe-soil model.

For a more detailed explanation regarding the input/output of the subroutine, refer to the manual of the subroutine in APPENDIX C.

#### 4.1.2 IOP Case

In reality, the pipelines on the seabed can be lifted off the seabed due to hydrodynamic loads or other factors. Therefore, the subroutine must model this behaviour correctly. By inputting IOP=2, the subroutine will simulate the Contact Loss model. This model will give zero soil force and soil stiffness as the results while resetting the entire work array. In the event of re-contact, the model will treat the soil as never having been disturbed before (virgin soil).

The subroutine also can model the lateral pipe-soil interaction using the linear spring method by assigning IOP=1. By using this model, the soil force and stiffness will be given as follows:

$$F_y = k_s \cdot v \quad [4-1]$$

$$K_y = k_s \quad [4-2]$$

where  $k_s$  and  $v$  are soil stiffness and lateral displacement, respectively.

The linear spring model is generally useful in initializing equilibrium at the start of pipe-soil simulation.

#### 4.1.3 Elastic Model

The elastic model of the lateral soil model is calculated using PATHCARD 0 and PATHCARD 15. The calculation of the soil force and elastic stiffness in this PATHCARD is as follows:

$$F_{y_i} = F_{y_{rev}} + k_s \cdot (v_i - v_{rev}) \quad [4-3]$$

$$K_y = k_s, \quad \text{if } v_i \geq v_{i-1} \quad [4-4]$$

where  $v_i$  lateral displacement in current iteration;  
 $v_{rev}, F_{y_{rev}}$  last known reversal points (start values are zero);  
 $k_s$  user-defined soil stiffness.

From this PATHCARD, the simulation can branch directly into the plastic regime if the DNV Model is selected (OPT3=1) or the extended elastic regime if the PONDUS model is selected (OPT3=2).

The limit of the elastic regime is defined as follows:

$$v_1 = \pm \frac{(0.2(w_s - f_L)) + F_{R1}(z_l)}{k_s} \quad [4-5]$$

where  $F_{R1}()$  passive soil resistance elastic limit as function of penetration (Eq. [3-12]);  
 $z_l$  initial penetration (Eq. [3-9]).

In the extended elastic regime (PATH=20 and only in PONDUS model), the soil force is taken as equal to the elastic limit:

$$F_{y_i} = (0.2(w_s - f_L)) + F_{R1}(z_l) \quad [4-6]$$

and the soil stiffness is set to zero.

In the extended elastic regime, the penetration is assumed to increase with the mechanism detailed in the following section.

#### 4.1.4 Plastic Regime

The plastic regime is identified by PATHCARD 12 and 121 for positive and negative loading, respectively. At the start of the simulation, the current iteration's passive soil resistance ( $D_s$ ) is calculated using the penetration known from previous iterations:

$$D_{s_i} = \frac{(F_{R2}(z_{i-1}) - F_{R1}(z_l))}{v_2 - v_1} \cdot (v_{p_i} - v_1) \quad [4-7]$$

$$D_{s_{i-1}} = F_{y_{i-1}} - 0.2(w_s - f_L) \quad [4-8]$$

where  $F_{R1}, F_{R2}$  passive soil resistance force's limit as function of soil penetration;  
 $v_1, v_2$  characteristic lateral displacement limit for elastic and plastic regime;

$v_{p_i}$  current iteration plastic displacement.

The plastic displacement for the current iteration is assumed can be found as follows:

$$v_{p_i} = v_i - \frac{0.2w_s}{k_s} \quad [4-9]$$

The slope of soil passive resistance in the current iteration can be calculated as follows:

$$\frac{\partial D_s}{\partial v_p} = \frac{D_{s_i} - D_{s_{i-1}}}{v_{p_i} - v_{p_{i-1}}} \quad [4-10]$$

The incremental energy therefore can be calculated using the trapezoidal rule:

$$\Delta E = 0.5(D_{s_i} - D_{s_{i-1}})(v_{p_i} - v_{p_{i-1}}) \quad [4-11]$$

The energy gained from previous soil penetration can be calculated by back substituting Eq. [3-15] as follows:

$$E_{fac} = \left( 0.12 \cdot S^{0.637} \left( \frac{a}{D} \right)^{-0.25} \right)^{\frac{1}{0.32}} \quad [4-12]$$

$$E_{i-1} = S_u D^2 \left( \frac{z_{i-1}}{D} \right)^{0.32} \cdot \frac{1}{E_{fac}} \quad [4-13]$$

The total work performed in the current iteration is therefore:

$$E_i = E_{i-1} + \Delta E \quad [4-14]$$

The soil penetration can be found using Eq. [3-15] by inputting the total work in the current iteration:

$$\frac{z_i}{D} = \left[ 0.12 \cdot S^{0.637} \left( \frac{E_i}{S_u D^2} \right)^{0.32} \left( \frac{a}{D} \right)^{-0.25} \right] \quad [4-15]$$

By knowing the soil penetration at the current iteration, the remaining soil forces at the current load step (Eq. [4-8]) then can be updated to give correct values. However, due to penetration developments resulting from Verley's model, the soil penetration is limited to  $0.3D$ . The amplitude of the oscillation is taken as the distance between the current lateral displacement and the previous displacement where the velocities changed sign.

The incremental soil force in the lateral direction can be calculated as:

$$\Delta F_y = (-0.2\Delta F_L + \Delta D_s) \cdot \text{sgn}(\dot{v}_i) \quad [4-16]$$

The soil passive resistance is defined to be the function plastic soil displacement only and can be expressed as follows:

$$\Delta D_s = \frac{\partial D_s}{\partial v_p} \Delta v_p \quad [4-17]$$

$\frac{\partial D_s}{\partial v_p}$  is the slope of the soil remaining force and can be calculated using Eq. [4-10] at every load step. The incremental plastic soil displacement,  $\Delta v_p$ , can be found by rearranging Eq. [3-1] as follows:

$$\Delta v_p = \Delta v - \frac{\Delta F_s}{k_s} \quad [4-18]$$

By combining Eqs. [4-17] and [4-18], the incremental soil force then can be expressed:

$$\Delta F_s = \frac{f}{1+f} k_s \Delta v - \frac{1}{1+f} (0.2\Delta F_L) \quad [4-19]$$

where  $f = \frac{\partial D_s}{\partial v_p} \frac{1}{k_s} \text{sgn}(\dot{v}_i)$ .

The soil force and stiffness at the current iteration therefore can be found using the following equations:

$$F_{y_i} = F_{y_{i-1}} + \Delta F_s \quad [4-20]$$

$$K_y = \frac{(F_{R2}(z_{i-1}) - F_{R1}(z_I))}{v_2 - v_1} \quad [4-21]$$

The limit of the plastic regime is defined as 0.5D if the DNV model (OPT3=1) is selected or 0.75D if the PONDUS model is selected (OPT3=2). From this PATHCARD, the regime can move to the residual force model (PATHCARD 13/131) if displacement is larger than the plastic limit, or back to the elastic model (PATHCARD 15) if the load is reversed.

#### 4.1.5 Residual Model

The residual force model includes the after breakout model and residual force model. The PATHID for this PATHCARD is 13 and 131. The residual force is calculated using the following expression:

$$F_{R3} = \frac{4.13K_c(w_s - F_l)}{G^{0.392}} \left(\frac{z_3}{D}\right)^{1.31} \quad [4-22]$$

where  $z_3$  is soil penetration after breakthrough. The DNV recommends the value to be  $0.5z_2^*$ , where  $z_2^*$  is the soil penetration in the event of breakout. The PONDUS model set the value back to the initial penetration ( $z_1$ ) due to the self-weight. The user can choose between these options by assigning OPT1=1 or OPT1=2 in the subroutine.

The residual force is activated when lateral displacement is larger than  $v_3$ . The  $v_3$  again differs between DNV and PONDUS model. The DNV recommends the value as  $1D$ , while for PONDUS the value can be found using the following expression:

$$v_3 = D \left( 0.6 \left( \frac{5.5}{\kappa} + 1 \right) + \frac{v_2}{D} \right) \quad [4-23]$$

where  $\kappa = \frac{\gamma_s D^2}{w_s}$ .

If the lateral displacement is larger than  $v_3$ , the soil force and penetration is set to be constant and equal to  $F_{R3}$  and  $z_3$ , while the stiffness is zero.

Between  $v_2$  and  $v_3$ , the soil force and penetration are calculated in the after breakout model.

#### 4.1.5.1 After Breakout – DNV Model

In the DNV model, the soil force after breakout is calculated as follows:

$$F_{y_i} = F_y^* + \frac{(F_{R3} + F_f) - F_y^*}{v_3 - v_2} (v_i - v_2) \quad [4-24]$$

where  $F_f$  Coulomb friction force =  $0.2(w_s - f_l)$ ;

$F_y^*$  peak soil force.

The soil penetration is found by assuming a linear relationship between  $z_2$  and  $z_3$ :

$$z_i = z_2 + \frac{z_3 - z_2}{v_3 - v_2} (v_i - v_2) \quad [4-25]$$

The soil stiffness immediately after breakout can be found using a simple expression:

$$K_{y_i} = \frac{F_{R3} - F_{R2}}{v_3 - v_2} \quad [4-26]$$

#### 4.1.5.2 After Breakout—PONDUS Model

In the PONDUS model, calculation of soil force and penetration is slightly more complex compared to the DNV model. After breakout, the origin of the force-displacement curve in the PONDUS model moved with the distance of  $v_0=(v-v_2)$ , therefore changing the  $F_{R2}$  in every load step.

In every new load step, the peak force is updated based on the last known penetration. The slope of the remaining force function is calculated as follows:

$$\frac{\partial D_s}{\partial v_p} = \frac{F_{R3} - F_{R2}(z_{i-1})}{v_3 - v_2} \quad [4-27]$$

The new soil remaining force,  $D_s$ , is calculated using Eq. [4-27] and Eq. [4-19]:

$$D_{s_i} = F_{r2} + \frac{f}{1+f} k_s (v_i - v_{i-1}) \quad [4-28]$$

$$f = \frac{\partial D_s}{\partial v_p} * \frac{1}{k_s} \quad [4-29]$$

The soil penetration is then calculated using the updated soil remaining force by the following expression:

$$z_i = \left( \frac{|D_{s_i}|}{4.13D \cdot s_u \cdot G^{-0.392}} \right)^{\frac{1}{1.31}} \quad [4-30]$$

The total soil force at the current load step can be calculated using Eq. [4-20] after updating the soil remaining force with the correct penetration. The soil stiffness in every load step then can be found using the following expression:

$$K_{y_i} = \frac{F_{R3} - F_{R2}}{v_3 - v_2} \quad [4-31]$$

Fig. 4-2 shows the movement mechanism of the force-displacement curve in the PONDUS model. Notice that the curve becomes flatter with every load step, while the peak soil force,  $F_{R2}$ , approaches the residual force,  $F_{R3}$ .

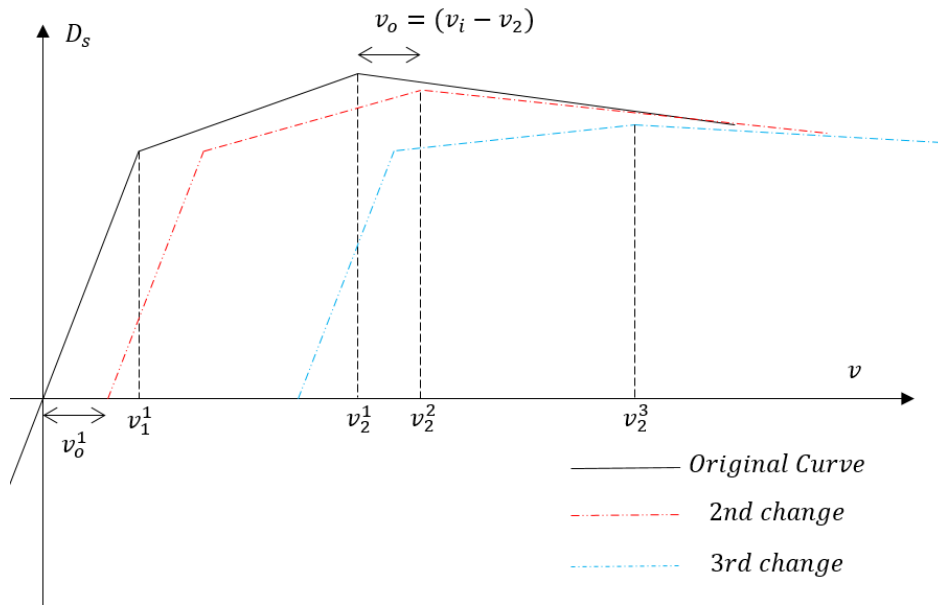


Fig. 4-2. Force-displacement movement after breakout in PONDUS model.

#### 4.1.6 Berm Resistance Model

The berm resistance model used in DNVMODEL-Y is based on the research of SAFEBUCK JIP. In line with the SAFEBUCK JIP’s result [8], additional soil resistance due to soil berm is added on top of the residual soil force. The author recommends that the berm model be used in conjunction with the DNV model instead of the PONDUS model due to fixed  $v_3$  criteria used in the DNV model. The additional berm resistance,  $\Delta F_{berm}$ , is calculated using the following expression:

$$\Delta F_{berm} = 1.5(w_s - F_l) \tag{4-32}$$

The maximum berm resistance therefore can be calculated as follows:

$$F_{berm_{max}} = (F_{R3} + F_f) + \Delta F_{berm} \tag{4-33}$$

This maximum berm resistance is reached after a number of sweeps in each direction. In the lateral model, the number of sweeps to reach maximum berm resistance,  $N_{max}$ , can be defined by the user. If the number of cycles is less than  $N_{max}$ , the added resistance is linearly interpolated between residual force and maximum berm resistance.

The incremental berm resistance therefore can be calculated:

$$f_{berm} = \frac{1}{N_{max}} N_{rev} \tag{4-34}$$

$$\Delta F_y = \frac{\Delta F_{berm} \cdot f_{berm}}{v_{rev} - v_{berm}} (v_i - v_{berm}) \quad [4-35]$$

where  $N_{max}$  number of cycles to reach maximum berm resistance;

$N_{rev}$  number of reversals that already occurred in current iteration;

$v_{rev}$  last known reversal point;

$v_{berm}$  start point of berm model.

Defining the  $v_{berm}$  is the key assumption in this model. In this thesis, the  $v_{berm}$  is defined as half the distance between  $v_{rev}$  and  $v_3$ , as expressed below:

$$v_{berm} = 0.5(v_{rev} + v_3) \quad [4-36]$$

The soil resistance and stiffness therefore can be calculated:

$$F_{y_i} = (F_{R3} + F_f) + \Delta F_y \quad [4-37]$$

$$K_{y_i} = \frac{\Delta F_{berm} \cdot f_{berm}}{v_{rev} - v_{berm}} \quad [4-38]$$

The berm resistance model is only activated if OPT2 is larger than zero. If it is larger than zero, the value inputted by the user will be defined as the  $N_{max}$ .

## 4.2 Vertical Soil Model (AUBENY-Z)

### 4.2.1 General Process

The vertical soil model subroutine developed in this thesis is named AUBENY-Z and is based on the research conducted by Aubeny et al. [1]. The general process of the subroutine can be seen in Fig. 4-3. The main inputs of the subroutine are the bottom contact point z-coordinate,



IOP, and LSNUM. The z-coordinate is defined positive downward (penetrating the soil). The IOP is the linear or non-linear modelling selection, while LSNUM is the load step number.

The user-defined parameters are stored in the INPUT ARRAY. The subroutine has a 16x1 WORK ARRAY, which consists of the memory parameters needed to model the vertical pipe-soil interaction. The output is stored in the OUTPUT ARRAY and consists of the vertical soil force and stiffness for a given vertical penetration. As in the lateral soil model, the subroutine consists of several PATHCARD routines which are defined by unique PATH identifier. There are eight PATHCARD in total—the description can be seen in Table 4-2. The PATH identifier is updated in each iteration and can be changed accordingly if the current iteration fulfills the requirement to switch to another PATHCARD.

Table 4-2 PATHCARD Description for Vertical Soil Model

<b>PATH ID</b>	<b>PATHCARD Description</b>
0	Backbone curve/virgin penetration
12	Elastic rebound
121/122	Reversal during elastic rebound
23	Partial separation
231	Reversal during partial separation
30	Full separation
31	Re-contact

The output of the subroutine is the soil force ( $F_z$ ) and soil stiffness at the given penetration,  $z$ , which is collected in the OUTPUT array. At the end of each load step, the WORK array and OUTPUT array are updated.

It is worth noting that at this study, trench width is assumed to be  $w/D=1$ . The effect of trench width on the bearing capacity of the soil is ignored in this model.

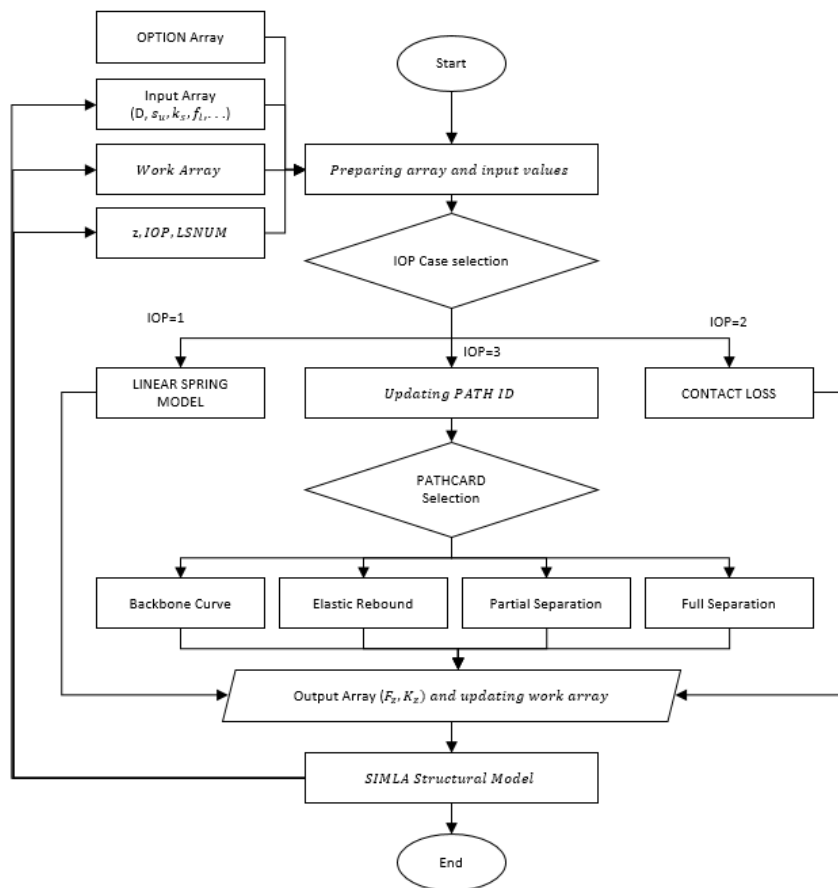


Fig. 4-3. Vertical soil model (AUBENY-Z) flowchart.

#### 4.2.2 Linear Model

AUBENY-Z includes two main models: the linear model and the non-linear model. The linear model is used if input parameter IOP=1. The calculation of the soil force in this model is linear elastic, which is given by the following expression:

$$F_z = k_s \cdot z \tag{4-39}$$

where  $k_s$  is user-defined elastic soil stiffness. The soil stiffness in the linear model is given by the following equation:

$$k_z = k_s \tag{4-40}$$

#### 4.2.3 Main Bounding Loop

The main bounding loop of the force-displacement curve consists of the backbone curve, elastic rebound, partial/full separation, and re-contact. The full sequence in the subroutine in terms of PATHID is 0-12-23-30-31.

The soil resistance during virgin penetration of the soil is modelled in PATHCARD 0. The calculation of the soil force is as follows:

$$F_{z_i} = a \left( \frac{z_i}{D} \right)^b (s_u + s_g z_i) \cdot D \quad [4-41]$$

where  $z_i$  is the soil penetration at the current load step.

The soil stiffness is found using the derivative of Eq. [4-41]:

$$K_{z_i} = a \cdot b \cdot \frac{z_i}{D} (s_u + s_g z_i) \cdot D + a \left( \frac{z_i}{D} \right)^b s_g D \quad [4-42]$$

If  $z_i < z_{i-1}$ , the reversal occurs and the PATH ID is updated from 0 to 12 and enters the elastic rebound path. The soil force and penetration from the previous load step (i-1) is considered as the re-contact point (Point 1). Other bounding loop points are calculated at this load step based on Point 1 and user-defined parameters as described in chapter 2.

The soil force at the current load step in PATHCARD 12 is calculated as follows:

$$F_{z_i} = F_{z_1} + \frac{z_i - z_1}{\frac{1}{k_o} + \chi \frac{z_i - z_1}{(1 + \omega) F_{z_1}}} \quad [4-43]$$

where  $\chi = -1$  for unloading and  $\chi = 1$  for reloading. The soil stiffness is then calculated using the derivation of Eq. [4-43] as shown by the following expression:

$$K_{z_i} = \frac{1}{A} + \chi \frac{(z_1 - z_i)}{((1 + \omega) F_{z_1}) A^2} \quad [4-44]$$

$$A = \frac{1}{k_o} + \chi \frac{(z_i - z_1)}{((1 + \omega) F_{z_1})} \quad [4-45]$$

If the pipe continues to move upward after the first reversal and passes the suction limit (Point 2), the path will enter the partial separation path. The PATHID therefore will be updated from 12 to 23.

The soil force and stiffness during partial separation is calculated using the following expression:

$$F_{z_i} = \frac{F_{z_2}}{2} + \frac{F_{z_2}}{4} \left[ 3 \left( \frac{z_i - z_0}{z_m} \right) - \left( \frac{z_i - z_0}{z_m} \right)^3 \right] \quad [4-46]$$

$$K_{z_i} = \frac{F_{z2}}{4} \left[ \frac{3}{z_m} - \frac{3(z_i - z_0)^2}{z_m^3} \right] \tag{4-47}$$

The path will enter the full separation path if the penetration is less than  $z_3$ . The PATHID also is updated from 23 to 30. During full separation, soil force and stiffness in the OUTPUT array is zero.

The re-contact of the pipe and the soil is identified by PATHID 31. In the re-contact PATHCARD, the soil force is calculated as follows:

$$F_{z_i} = \frac{F_{z1}}{2} + \frac{F_{z1}}{4} \left[ 3 \left( \frac{z_i - z_0}{z_m} \right) - \left( \frac{z_i - z_0}{z_m} \right)^3 \right] \tag{4-48}$$

The soil stiffness contribution is then determined:

$$K_{z_i} = \frac{F_{z1}}{4} \left[ \frac{3}{z_m} - \frac{3(z_i - z_0)^2}{z_m^3} \right] \tag{4-49}$$

Fig. 4-4 shows the force-displacement curve output in terms of PATHCARD sequence.

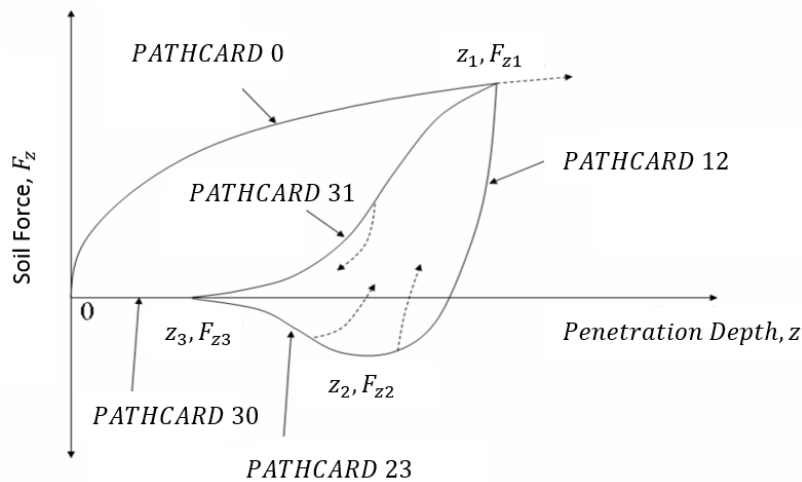


Fig. 4-4. PATHCARD sequence during main bounding loop in AUBENY-Z.

#### 4.2.4 Arbitrary Loop

If the reversal occurs during elastic rebound (PATHCARD 12), the PATHID will be updated from 12 to 121 and enter PATHCARD 121. The soil force and penetration from the previous load step therefore is defined as the reversal point at the bounding loop ( $F_{zrb}, z_{rb}$ ).

The soil force in this path is given as follows:

$$F_{z_i} = F_{z_{rb}} + \frac{z_i - z_{rb}}{\frac{1}{k_o} + \chi \frac{z_i - z_{rb}}{(1 + \omega)F_{z_1}}} \quad [4-50]$$

The soil stiffness during this path is the same as given by Eq. [4-44]. If the reversal occurs again during this path, the PATHID is updated from 121 to 122. PATHCARD 121 and 122 therefore create a small bounding loop if the pipe movement does not progress further than the last known main bounding loop reversal point.

If the reversal occurs during full separation, the PATHID is updated from 23 to 231. The soil force is calculated by the following expression:

$$F_{z_i} = \frac{F_{z_1} + F_{z_{rb}}}{2} + \frac{F_{z_1} - F_{z_{rb}}}{4} \left[ 3 \left( \frac{z_i - z_0}{z_m} \right) - \left( \frac{z_i - z_0}{z_m} \right)^3 \right] \quad [4-51]$$

The soil stiffness at PATHCARD 231 is then calculated:

$$K_{z_i} = \frac{F_{z_1} - F_{z_{rb}}}{4} \left[ \frac{3}{z_m} - \frac{3(z_i - z_0)^2}{z_m^3} \right] \quad [4-52]$$

Further reversals in PATHCARD 231 will lead back to the loop of PATHCARD 121-122. Fig. 4-5 shows the PATHCARD sequence that formed the arbitrary loop in AUBENY-Z.

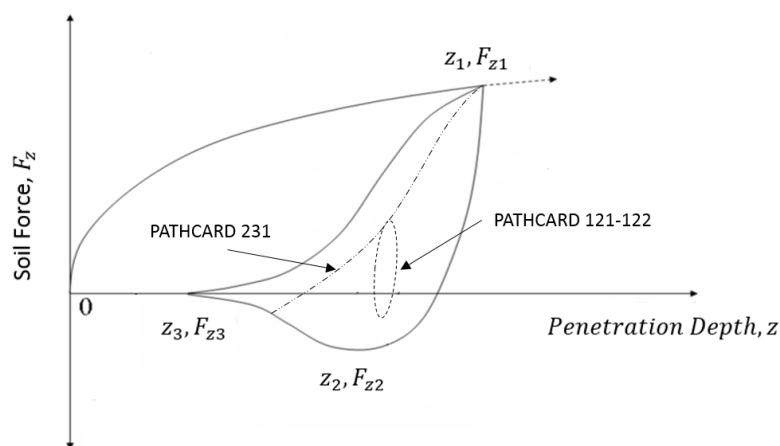


Fig. 4-5. Sequence of arbitrary loop in AUBENY-Z.

### 4.3 SIMLA Implementation

As mentioned before, the new soil model subroutines are implemented inside SIMLA finite element software. Both subroutines are considered as one of the material models and are intended to be used together with the CONT126 element type.

The communication between SIMLA and the subroutines is accomplished primarily through the WORK array. The WORK array stores critical parameters that are needed to calculate the soil force and stiffness, and is updated in every load step. Because SIMLA is a non-linear structural model, each load step has several force unbalance (equilibrium) iteration steps. In every iteration step, the last known work array from the previous load step is copied to the subroutine. The subroutine then calculates the soil force and stiffness based on this work array. At the end of equilibrium iteration, the work array finally is updated with the new values. Fig. 4-6 shows the communication flowchart of the soil models and SIMLA.

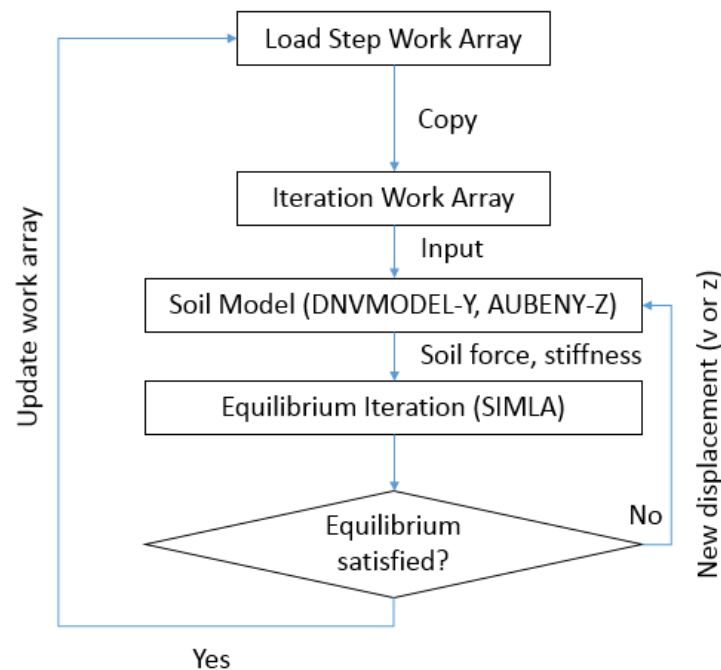


Fig. 4-6. Communication flowchart between soil subroutines and SIMLA.

It is important to mention that even though both soil subroutines are based on non-linear theory, at this stage of development they are not meant to be used together. Further research is required to ensure that both models can work together correctly. Those activities are not part of the scope of this thesis.

The SIMLA manual, which explains the input of the soil subroutines inside SIMLA, can be seen in APPENDIX C.

## CHAPTER 5      VALIDATION OF MODELS

Validation of a new engineering program/software is a very important part of the development process. The program should be able to produce correct physical behaviour and other assumptions that serve as the basis of the program. Therefore, in this thesis, this chapter is dedicated to the validation procedure that is used to calibrate and validate the subroutine's results.

Two validation methods are used in this thesis. The first validates by comparing the subroutine results with existing works such as the PONDUS program. The second gives prescribed displacements as inputs to the subroutines and validates the force-displacement curve. Both stand-alone subroutine results and SIMLA pipe-soil analyses are validated.

### 5.1 Related Software

This section serves as a simple introduction to some of the related software packages that have been used in the validation process.

- PONDUS Software

PONDUS software is FEM-based software with 2D elements. It typically is used for pipeline in seabed conditions. The software is developed by MARINTEK and feature non-linear, time-dependent lateral pipe-soil interaction. The lateral soil model in PONDUS software uses a soil model developed by Verley for both clay [6] and sand models [7]. The PONDUS software is primarily used to calibrate the lateral soil subroutine, DNVMODEL-Y.

- SIMLA Software

SIMLA is a special-purpose computer tool for engineering analysis of offshore pipelines during design, installation, and operation [15]. SIMLA is an advanced 3D FEM software that can model pipe-soil interaction using hyperelastic or elastoplastic material. The current SIMLA version incorporates the PONDUS soil model; however, it is not fully functional, which is one of the reasons the PONDUS model is included in DNVMODEL-Y.

In this thesis, the SIMLA software is used to model the pipe-soil interaction with specified contact elements. The DNVMODEL-Y and AUBENY-Z are integrated inside the SIMLA and used to solve the pipe-soil interaction.

The SIMLA software is capable of static and dynamic analysis in the time domain. Five modules are contained in SIMLA software, and every module uses a standardized database. The schematic of the software is shown in Fig. 5-1.

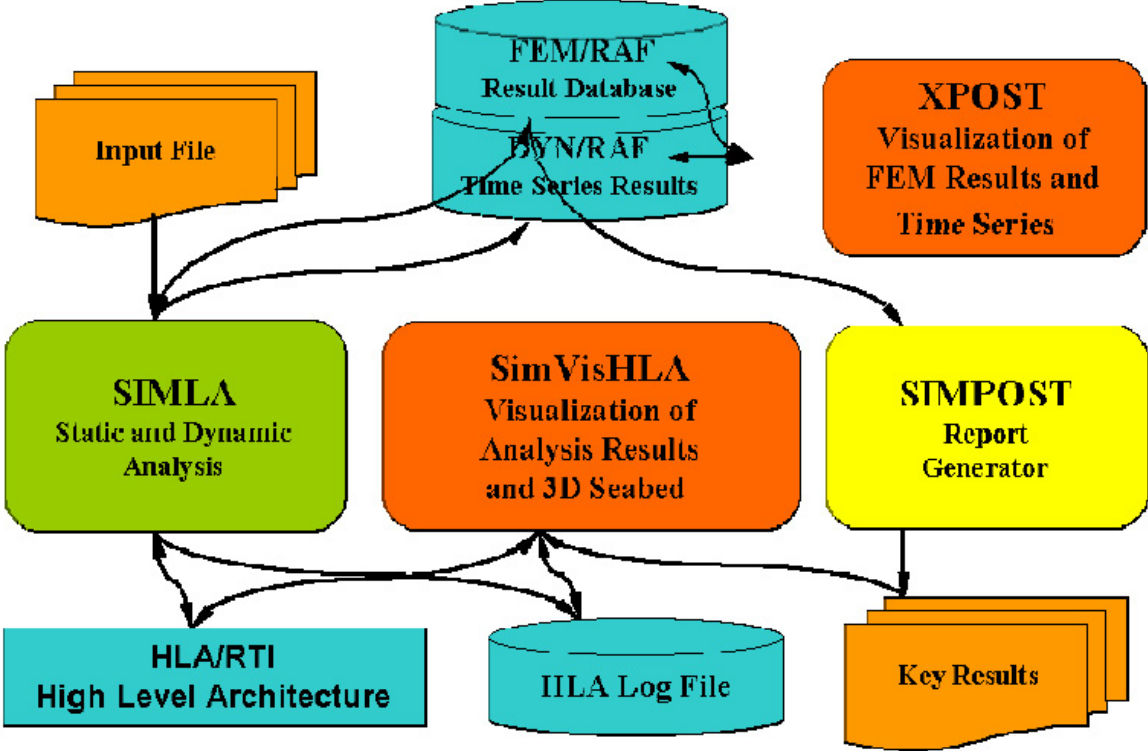


Fig. 5-1. SIMLA program schematic [16].



## 5.2 PONDUS Comparison

### 5.2.1 Case Description

To compare the results of DNVLMODEL-Y and PONDUS software, it is necessary to create the analysis in PONDUS and use the displacement outputs as the prescribed displacement load in DNAMODEL-Y. Two analysis cases have been developed for the validation procedure. The first case is the case of small lateral displacement without any breakout; the second case is large displacement. The input files that are used in the PONDUS analysis can be seen in APPENDIX A.

The soil parameters that are included in the analysis are described in Table 5-1. The pipe used in PONDUS and DNVMODEL-Y has a diameter of 0.2032 m and thickness of 0.01 m. Hydrodynamic loads are considered in the PONDUS analysis; however, the lift load effect in the soil model is neglected.

As described in chapter 4, the subroutine contains PONDUS-mode, which utilizes similar methods for soil force and penetration calculation as PONDUS software, as mentioned in section 4.1. Therefore, the subroutine should produce similar results to PONDUS, given the same displacement history, to validate the program.

Dynamic analysis used in the PONDUS analysis with Fig. 5-2 shows lateral displacement of the pipe over time for both analysis cases. This displacement history is used as input for the DNVMODEL-Y. Other input parameters (i.e. LSNUM, IOP) for the subroutines are adjusted accordingly to ensure correct soil behaviour.

Table 5-1 PONDUS Test Case Soil Parameters

Parameter	Value
Soil shear strength, $S_u$	800 Pa
Shear strength gradient, $S_g$	0
Soil elastic stiffness, $K_s$	65000 N/m <sup>2</sup>
Soil friction factor, $\mu_s$	0.2
Soil submerged weight, $\gamma_s$	18000 N/m <sup>3</sup>

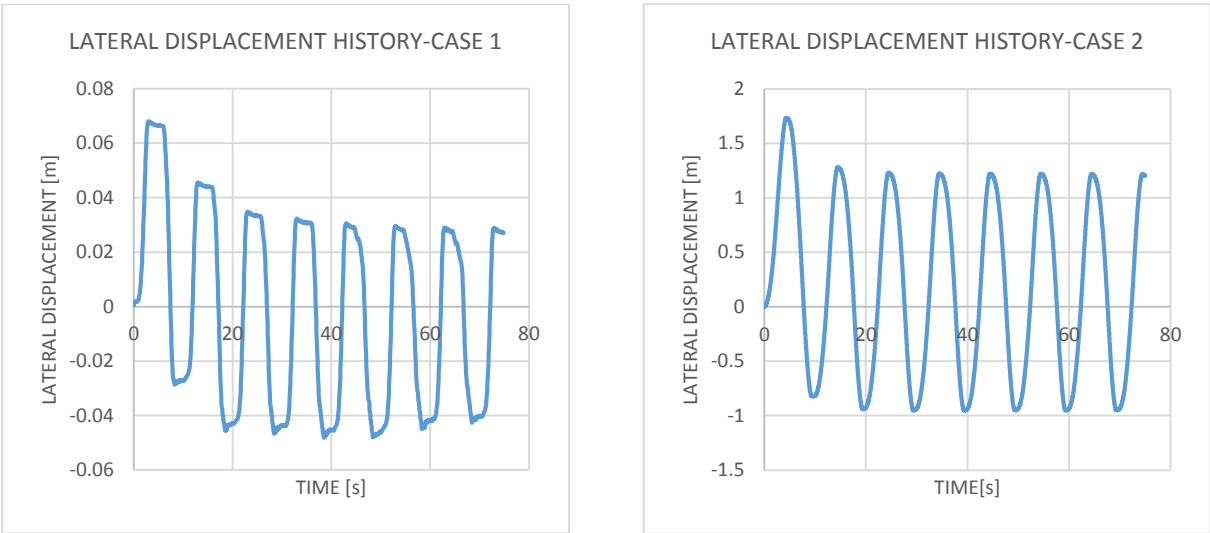


Fig. 5-2. Forced displacement time history for PONDUS test case.

5.2.2 Case 1 Results and Discussion

It is not clearly evident from Fig. 5-2, but many small vibrations are present in the displacement history. The small vibrations can be seen quite clearly in the soil force history in Fig. 5-4 because small reversals in displacement can cause big changes in the soil resistance.

From the soil force history, it can be seen that the DNVMODEL-Y replicates the soil force history from PONDUS quite well. The PONDUS result shows significant reversals in soil force, more than observed in the displacement history. The cause of this is unknown, but it is likely related to the calculation algorithm implemented inside PONDUS. The DNVMODEL-Y algorithm dictates that the soil reversal cycles equal the displacement history. This results in less ‘jagged’ results in the DNVMODEL-Y.

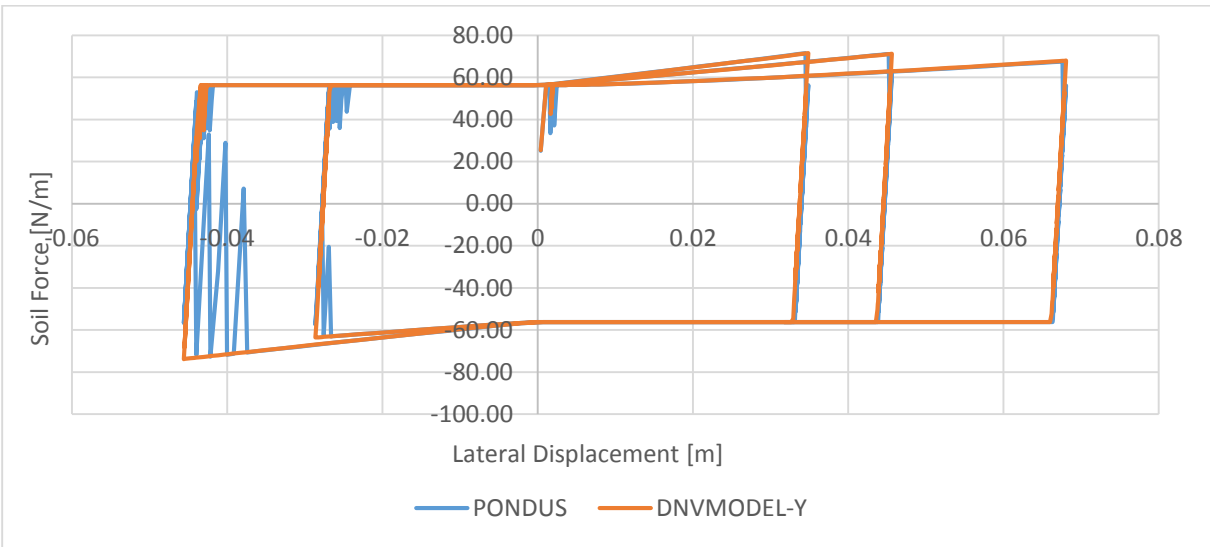


Fig. 5-3. Force-displacement curve for PONDUS Case 1.

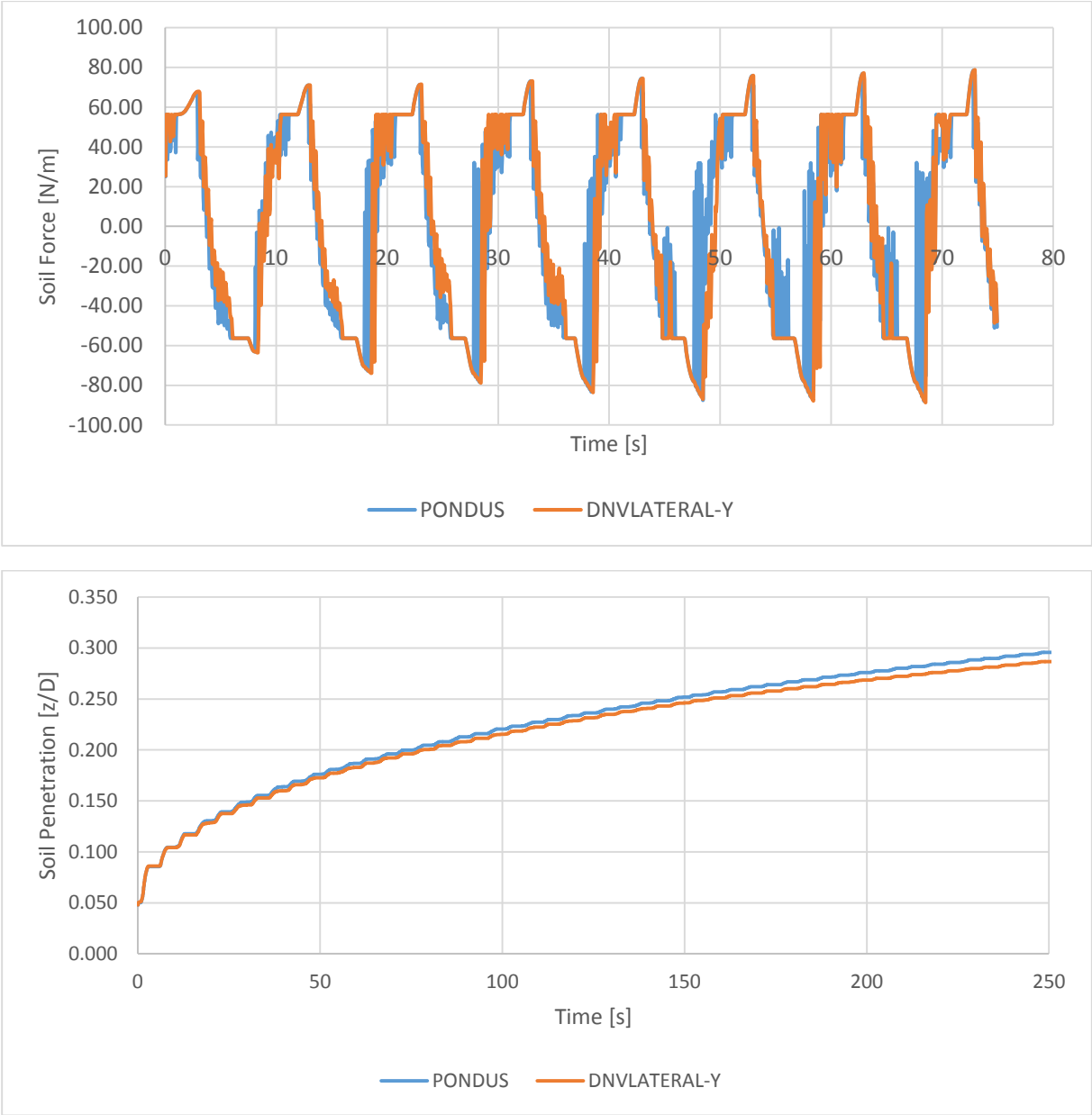


Fig. 5-4. Soil force history (top) and penetration history (bottom) for Case 1.

In terms of soil penetration development, the DNVMODEL-Y results show less penetration over time compared to those given by PONDUS. The possible cause of this is the presence of additional soil reversal cycles observed in the PONDUS results. Because soil force reversal can affect the penetration development, the penetration in PONDUS can grow quicker compared to DNVMODEL-Y. However, this difference is quite small, with a maximum observed difference of 3%. This also explains why the peak force in both software packages are very similar.

Fig. 5-3 shows the force-displacement curve from PONDUS and DNVMODEL-Y, which is the most important aspect to be compared. The curves are almost identical to each other, with the results from DNVMODEL-Y presenting a smoother curve. This result, with consideration of

other results, illustrates that the subroutine is correct in modelling small displacement pipe-soil interactions.

### 5.2.3 Case 2 Results and Discussion

Case 2 demonstrates the pipe-soil interaction under large displacement. The pipe is oscillating with approximately 1 m amplitude. This case also features fewer small vibrations compared to Case 1.

The results from both models show almost identical soil force and penetration histories (see Fig. 5-6). The breakout resistances in both models are identical, and the behaviours for the models are closely matched. Results for maximum penetration at breakout are identical for the models. However, slight differences in penetration history are seen for the after-breakout condition.

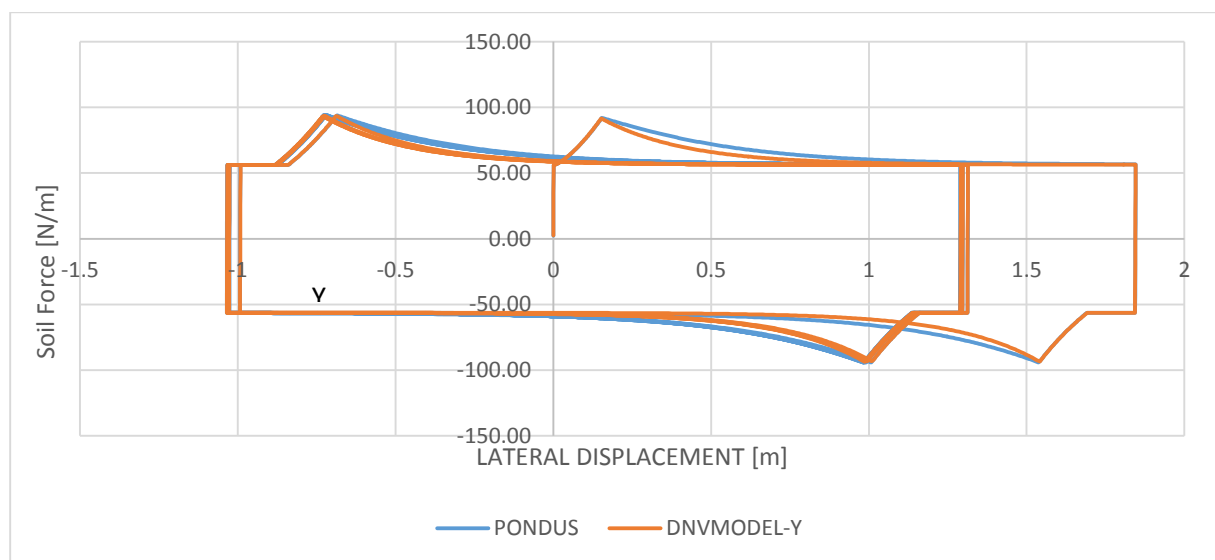


Fig. 5-5. Force-displacement curve for PONDUS Case 2.

Fig. 5-5 shows the force-displacement curve for Case 2. After breakout, DNVMODEL-Y is observed to give slightly lower soil force compared to PONDUS. This is caused by the differences in soil force and penetration calculation method after breakout in the DNVMODEL-Y and PONDUS programs. The observed maximum difference is approximately 10% for soil force after breakout between both models. Despite these differences, the results from DNVMODEL-Y show that the subroutine can produce accurate soil behaviours and patterns as given by PONDUS.

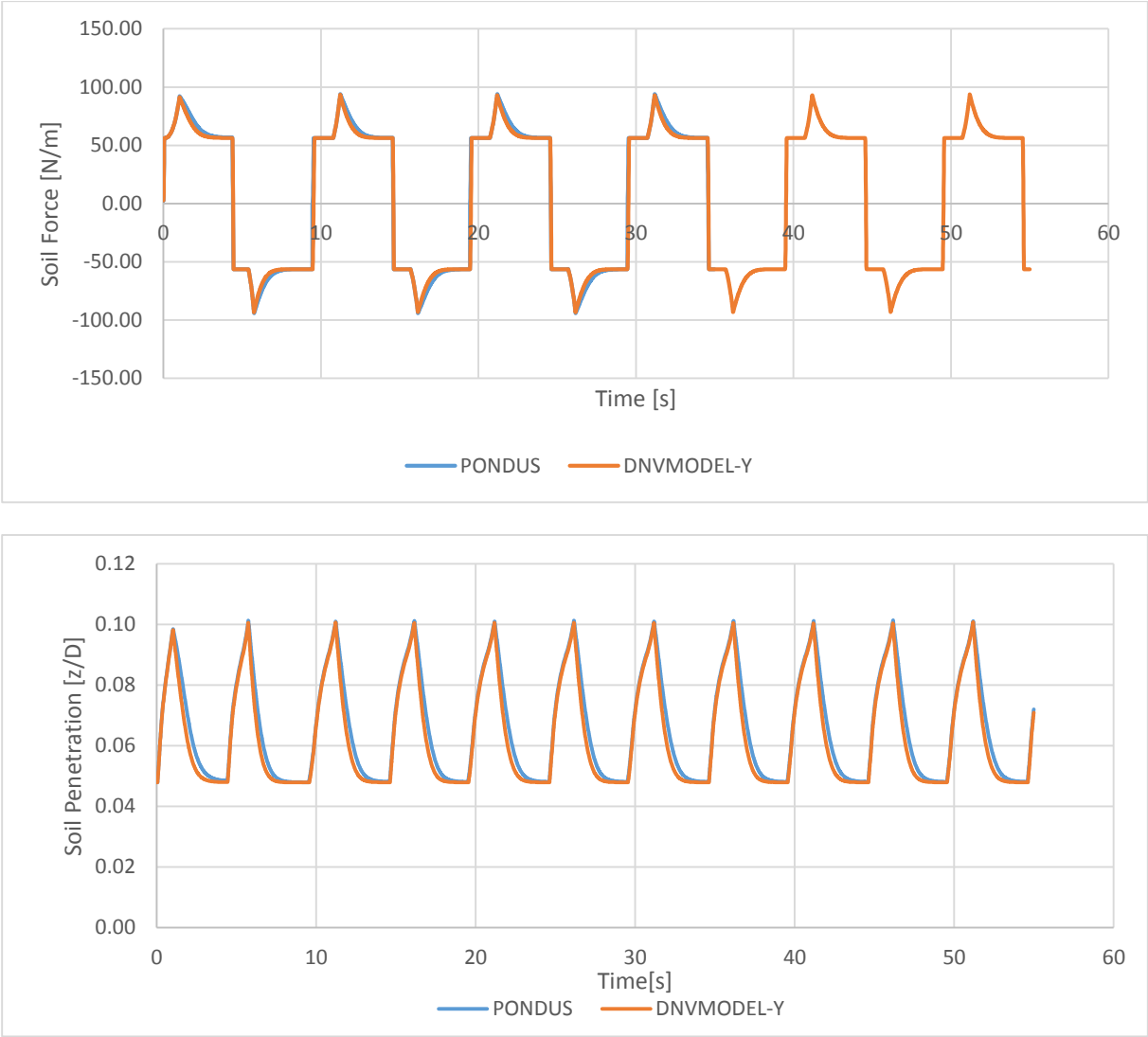


Fig. 5-6. Soil force history (top) and penetration history (bottom) for Case 2.

### 5.2.4 Validation Conclusions

From results presented in the previous sections, one can conclude that the DNVMODEL-Y can produce correct behaviours of soil in small and large lateral displacements without lift load. Some differences are observed in both cases, but these differences are quite small and unavoidable due to differences in calculation algorithms. Both models also produce identical peak force and maximum penetration, which is the most important aspect for pipe-soil penetration.

Because these results validate the methods of soil penetration development, the conclusion can be partly extended to the DNV-mode of the subroutine because they use the same methods.

### 5.3 DNV-PONDUS Mode Comparison

#### 5.3.1 Case Description

These test cases were performed to validate the analysis results of the DNV-mode of DNVMODEL-Y using prescribed displacement loads. Comparison with the PONDUS-mode also illustrated differences in behaviour between the modes.

The test cases consist of two different harmonic forced displacement cases. The first case is a small amplitude (0.1D) displacement case, and the second one is a large amplitude (1.5D) displacement case. The displacement history used in the analysis is presented in Fig. 5-7.

The pipes used in both modes have a diameter of 0.2032 m and a thickness of 0.01 m. The soil parameters used in the analysis are shown in Table 5-1.

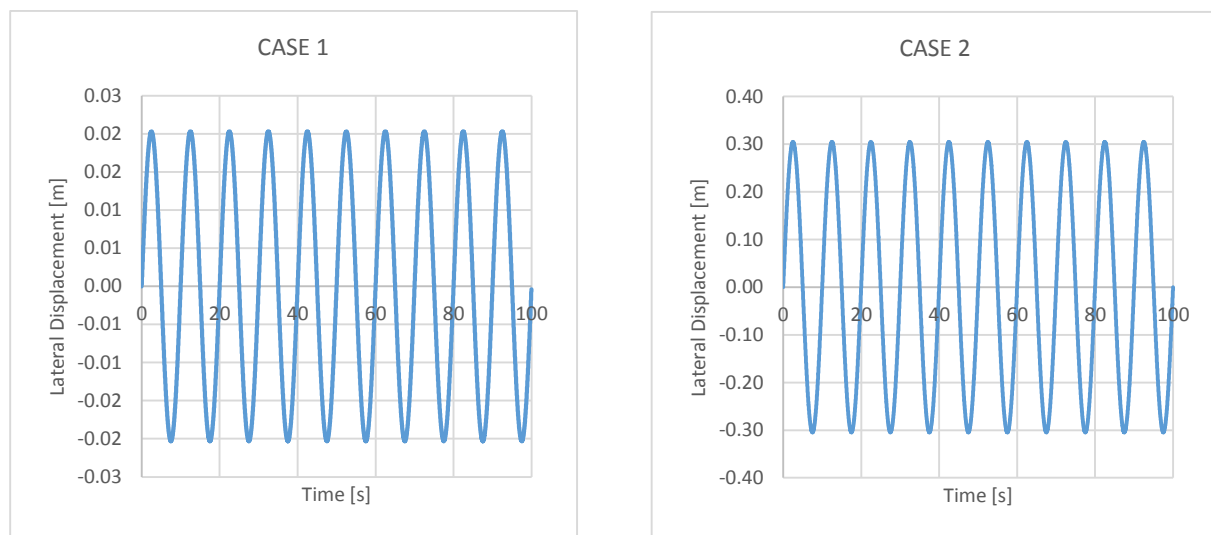


Fig. 5-7. Forced displacement time history for DNV test case.

#### 5.3.2 Case 1 Result and Discussion

The results for both analysis modes are shown in Fig. 5-8. From the figure, it can be seen that the DNV-mode gives higher soil force compared to the PONDUS-mode over time. The primary reason for this difference is the different assumptions of characteristic limit. The DNV model does not have ‘elastic force extension’, as seen in the PONDUS model. In each reversal, the remaining soil force ( $D_s$ ) directly enters the plastic range after passing the elastic limit. The DNV also uses the penetration in reversal point as the initial penetration, therefore increasing the soil force further in each cycle. From penetration history, it can be seen that penetration develops much quicker in the DNV-mode compared to the PONDUS-mode.

Fig. 5-9 shows clearly that the DNV-mode has an increasing trend, while the PONDUS-mode gives the same pattern for each cycle. After a few cycles, the soil force from the DNV-mode

can be twice that from the PONDUS-mode. If maximum allowed penetration is reached, the soil force stops increasing, forming a closed loop in the force-displacement curve.

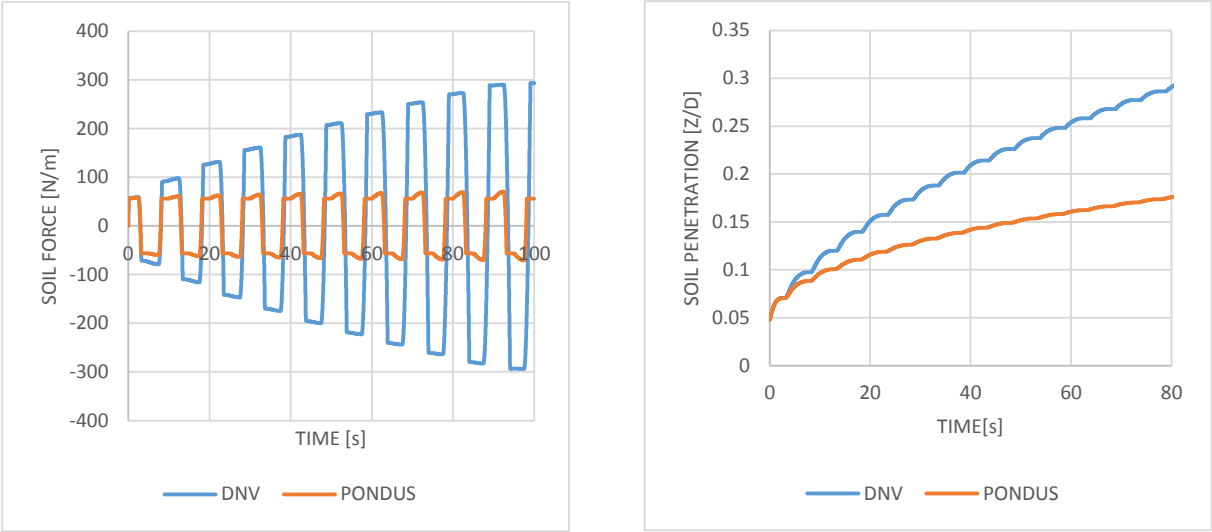


Fig. 5-8. Result comparison of DNV and PONDUS analysis mode for small displacement, DNV Case 1.

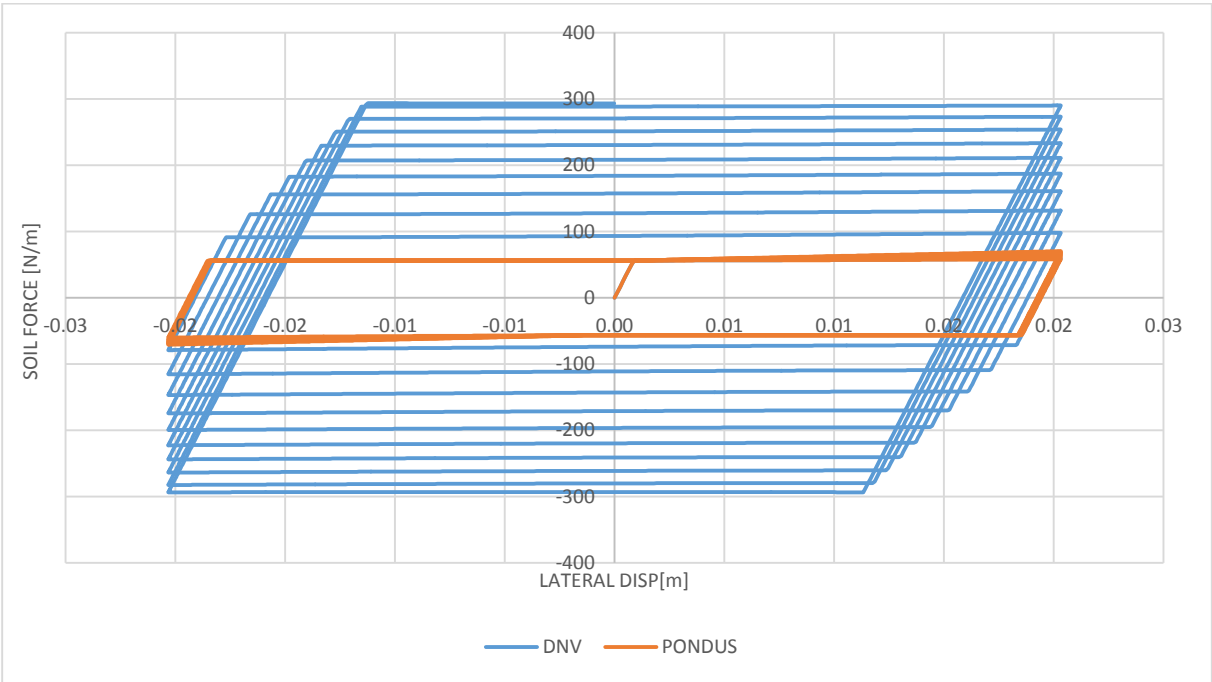


Fig. 5-9 Force-displacement curve for DNV Case 1.

### 5.3.3 Case 2 Results and Discussion

The analysis results for Case 2 are presented in Fig. 5-10 and Fig. 5-11. The results show key differences between both models. In penetration development, the DNV-mode gives a sharp decrease in penetration after the pipe breakout. Conversely, the PONDUS-mode results show a

very gradual decrease in penetration. Looking at the soil force history, the DNV-mode gives lower peak resistance and flat residual force compared to PONDUS-mode results.

Three factors cause these differences. The first factor relates to the breakout limit. The DNV model has  $0.5D$  as the breakout limit instead of the limit of  $0.75D$  used in the PONDUS model. This lower limit in the DNV model causes the DNV model to have a lower peak soil force in each cycle due to a shorter plastic regime.

The second factor is regarding the residual limit,  $v_3$ . The DNV model has fixed criteria for the start of residual soil force, which is  $1D$ . The PONDUS model residual limit depends on the submerged weight of the pipe and moves over time (see section 3.4) if the displacement is larger than  $0.75D$ . This causes the DNV-mode to reach the residual limit faster than the PONDUS-mode, which gives the flat curve shown in Fig. 5-10.

The third factor is due to the difference in calculating the penetration after breakout between the two modes. DNV-mode uses linear interpolation between breakout penetration,  $z_2$ , and residual penetration,  $z_3$ . The PONDUS uses a specialized method as described in chapter 4. This makes the penetration in DNV-mode decrease faster than in PONDUS-mode.

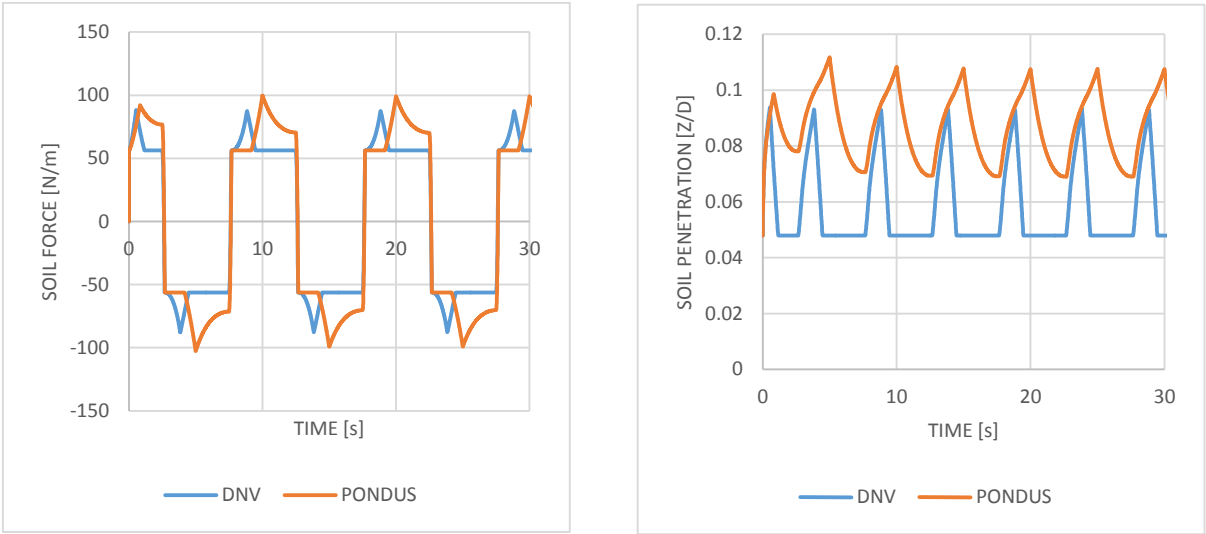


Fig. 5-10. Result comparison of DNV and PONDUS model for Case 2.



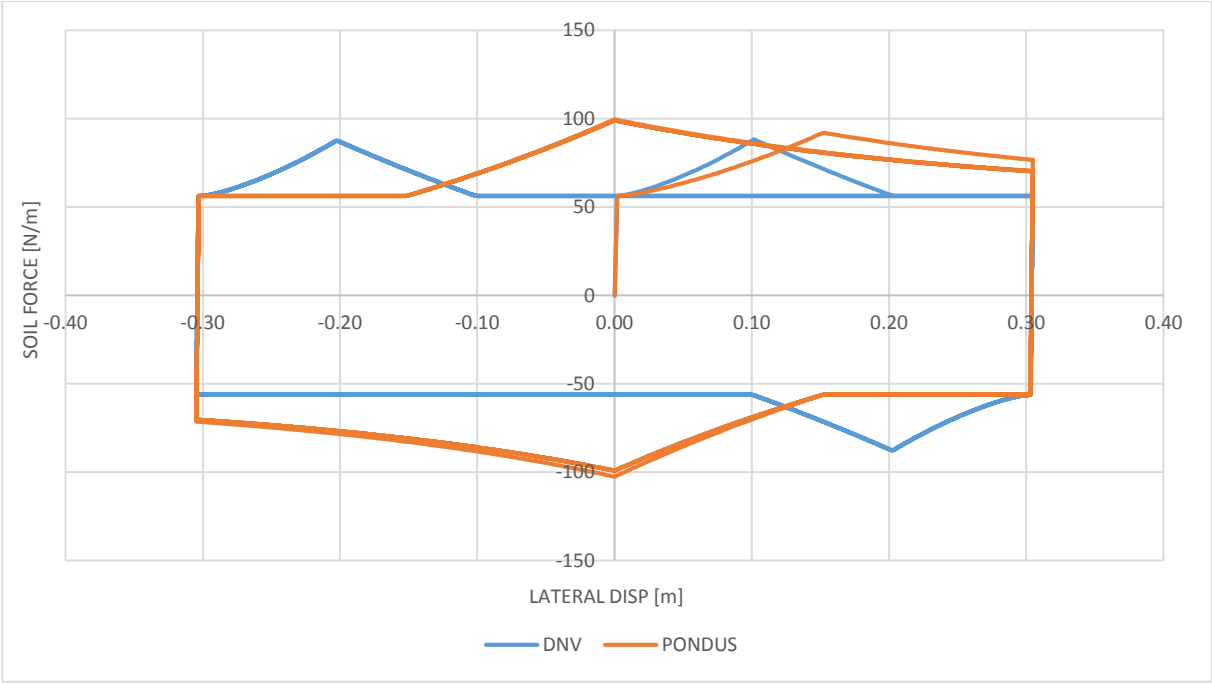


Fig. 5-11. Soil force vs. lateral displacement from DNV and PONDUS models for Case 2.

5.3.4 Validation Conclusion

The results from DNV Case 1 and Case 2 show the differences between DNV and PONDUS-mode from the subroutine DNVMODEL-Y. Despite some significant differences in both models, the DNV-mode produces the expected soil force pattern and behaviour. Therefore, it can be concluded that the DNV-mode is validated for the given assumptions and can be used for solving the pipe-soil interaction.

## 5.4 Breakout Force Comparison

### 5.4.1 Case Description

The breakout soil force calculated by the method developed by SAFEBUCK JIP [8] is used for the comparison models in this section. Because SAFEBUCK methods require the penetration to be known, the initial penetration model developed by Verley [6] is used as the input. The breakout soil forces calculated by PONDUS-mode and DNV-mode are compared with these SAFEBUCK models.

The soil parameters used in the analysis are listed in Table 5-2 (very soft clay). The pipe is subjected to a harmonic large amplitude (1.5D) prescribed displacement load

The pipe used in the analysis has a diameter of 0.2032 m and thickness of 0.01 m. Each test case has a different soil strength,  $s_u$ , between 0.8 and 4 kPa (very soft clay).

Table 5-2 Soil Parameters for Analytical Test Cases

Parameter	Value
Soil shear strength, $S_u$	800 Pa
Shear strength gradient, $S_g$	0
Soil elastic stiffness, $K_s$	65000 N/m <sup>2</sup>
Soil friction factor, $\mu_s$	0.2
Soil submerged weight, $\gamma_s$	18000 N/m <sup>3</sup>

### 5.4.2 Results and Discussion

Fig. 5-12 shows how much the penetration develops with varying soil strength. It can be seen that penetration development has an inverse relationship with soil strength. With increasing soil strength, the penetration at breakout is more limited to initial penetration due to soil becoming harder to penetrate. Harder soil also means that the breakout resistance does not develop much and becomes closer to the elastic limit.

Fig. 5-13 compares breakout resistance computed using different models. Breakout resistance from the SAFEBUCK model using breakout penetration of the DNV-model is included as a reference.

The figure shows that for low initial penetration (i.e. hard soil), the models give similar breakout resistances. In softer soil, the results from the DNV-model and PONDUS-model are inside the range of the SAFEBUCK model results. If the initial penetration is used in the SAFEBUCK

model, it will give lower values compared to other models because the soil cycles increase the penetration significantly. The problem with using the SAFEBUCK model is that it does not specify a method to calculate the penetration development and therefore is limited to use the initial penetration only. If actual breakout penetration (based from PONDUS method) is used, the figure shows that it can give higher breakout resistance compared to the other two models.

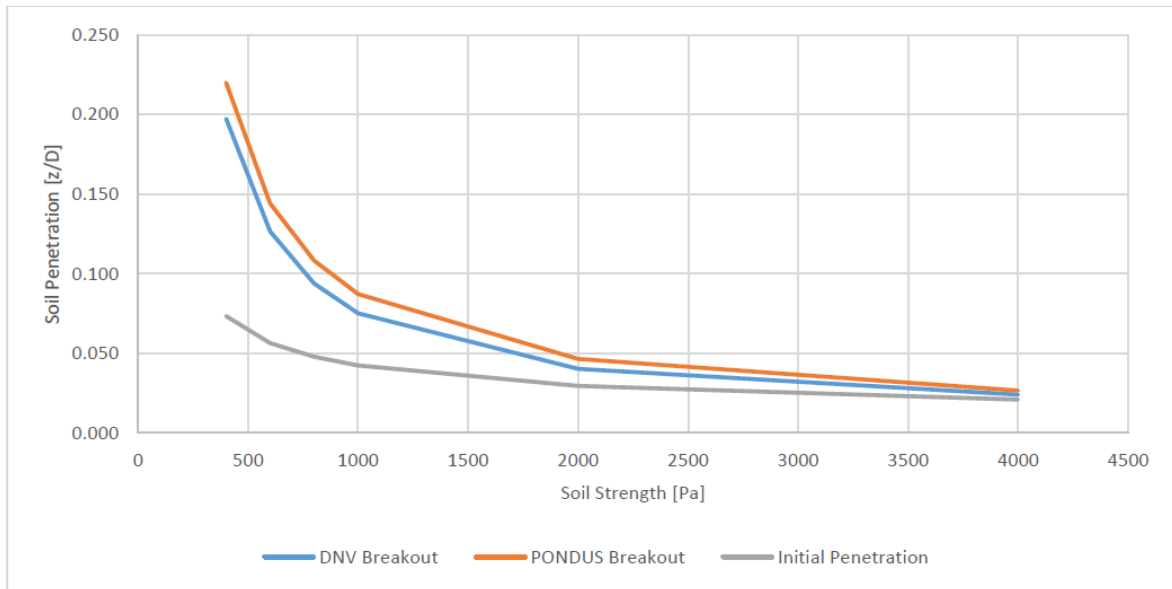


Fig. 5-12. Comparison of breakout penetration and initial penetration between models.

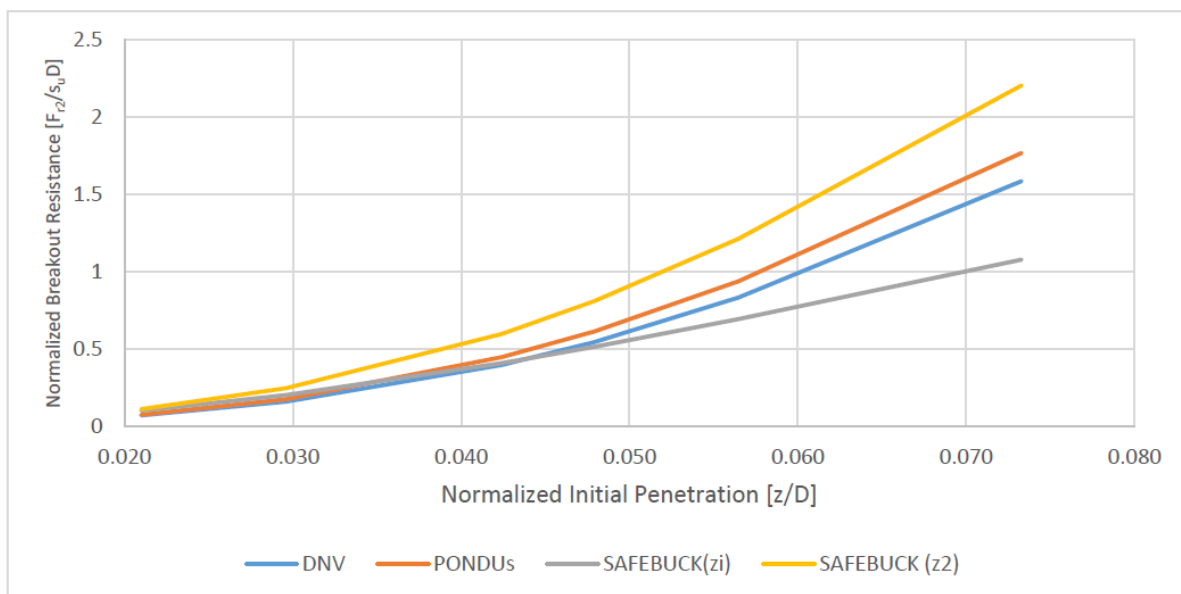


Fig. 5-13. Comparison of breakout resistance between different models.

## 5.5 DNV-BERM RESISTANCE MODEL

### 5.5.1 Case Description

This test case was conducted to demonstrate the berm resistance model for large displacement, which is programmed into the lateral model. The test case consists of a large amplitude harmonic forced displacement load, as shown in Fig. 5-14. The berm resistance model is combined with the DNV lateral model. The number of cycles needed to reach maximum berm resistance is defined as five cycles. The berm resistance at the end of every cycle is assumed to be linearly increasing until it reaches the defined maximum berm resistance. The pipe used in the test case has a diameter of 0.2032 m and a thickness of 0.01 m. The soil parameters are given in Table 5-1.

### 5.5.2 Results

The results of the analysis are illustrated in Fig. 5-15. The results show that the lateral model can capture the berm effect during large displacement. The berm resistance is linearly increasing starting from half the distance between the start of residual force and the next reversal point. The maximum berm resistance in each cycle is a fraction of the maximum possible berm resistance, which is 307 N/m. In each successive cycle, this fraction is increased linearly until the defined number of cycles. It is worth mentioning that results show two distinct berm resistance cycles. However, the maximum possible berm resistance is not changed.

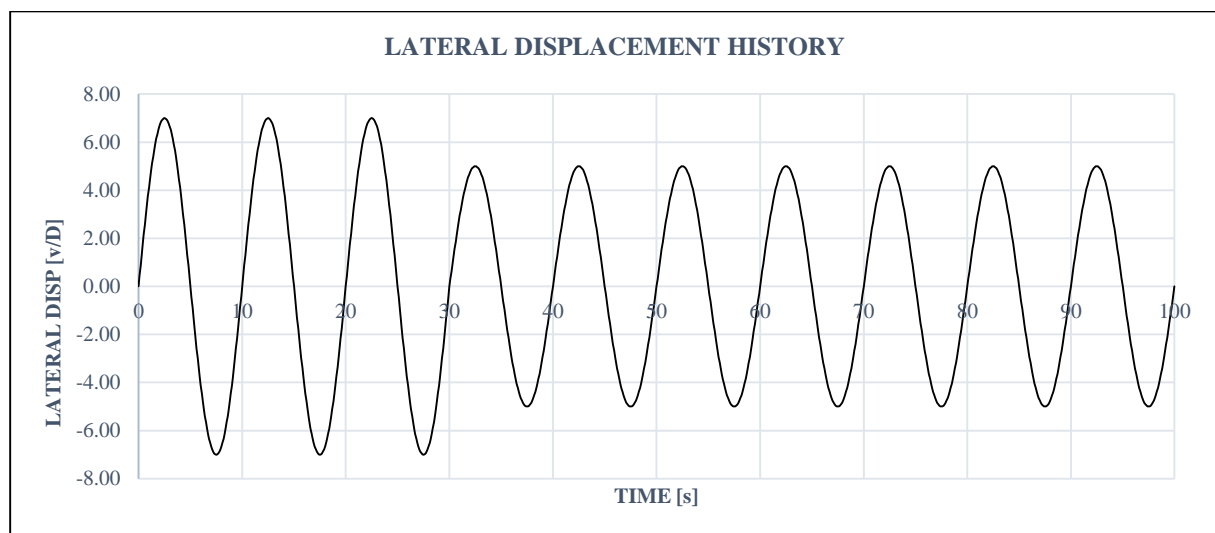


Fig. 5-14. Lateral displacement history for berm resistance test case.

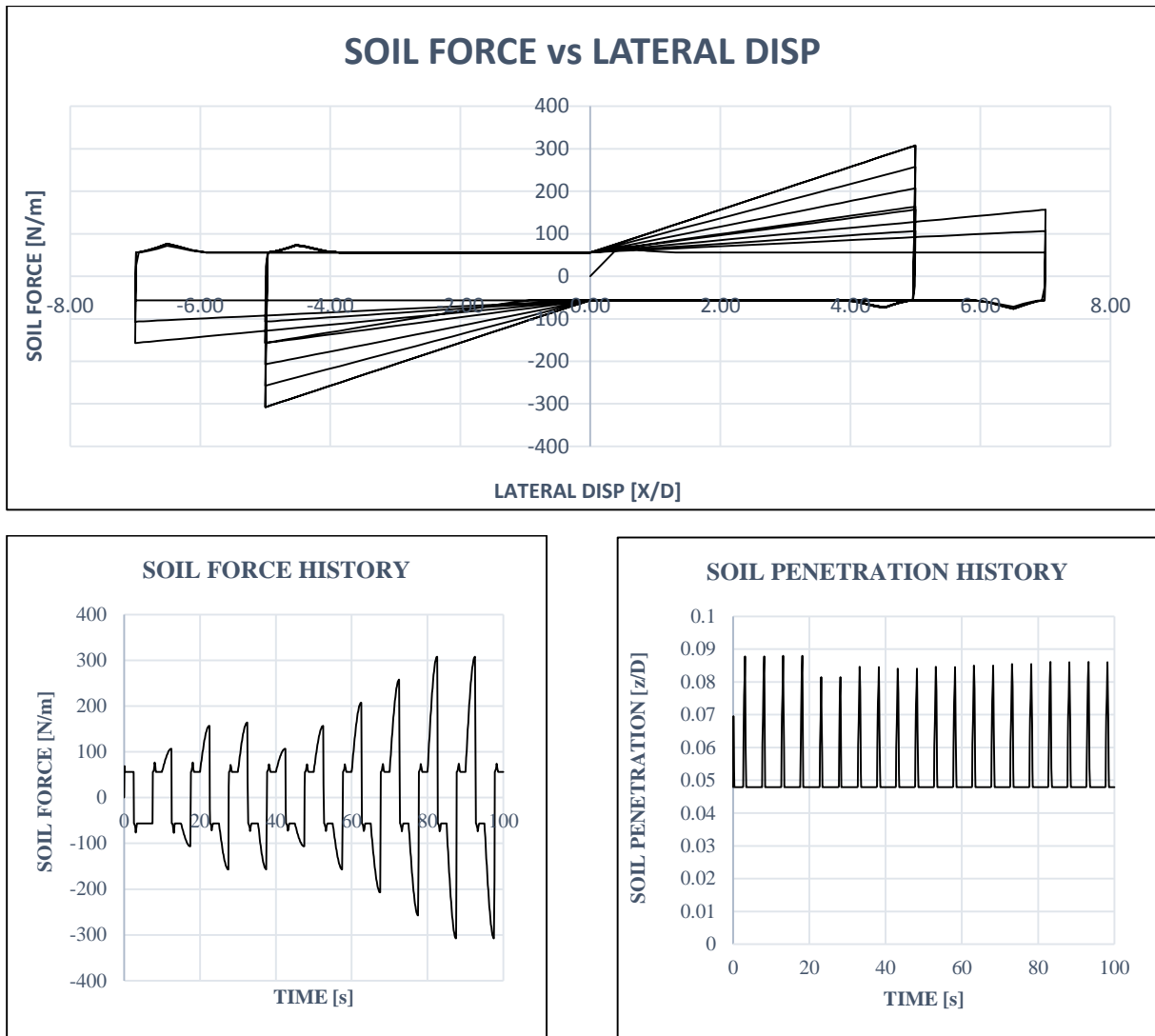


Fig. 5-15. Results of berm resistance model for large amplitude lateral displacement.

## 5.6 SIMLA Integration Validation

This section is focused on validating the results of SIMLA with integrated non-linear soil models (DNVMODEL-Y and AUBENY-Z). Up until now, the validation has been accomplished via stand-alone subroutines. Therefore, it is important to demonstrate that the subroutine integration is working correctly and producing results as expected.

The SIMLA model used in the validation tests can be seen in Fig. 5-16. The model consists of one element of 2 m length that is subjected to a prescribed harmonic displacement in the horizontal and vertical directions. The amplitude of displacement is 1D and 0.2D for lateral and vertical displacement motion, respectively. The soil parameters used in this validation are presented in Table 5-3.

Table 5-3 Soil Parameters for SIMLA Integration Validation

Parameter	DNVMODEL-Y	AUBENY-Z
Soil shear strength, $S_u$	800 Pa	800 Pa
Shear strength gradient, $S_g$	0	0
Soil elastic stiffness, $K_s$	65000 N/m <sup>2</sup>	65000 N/m <sup>2</sup>
Soil friction factor, $\mu_s$	0.2	0.2
Soil submerged weight, $\gamma_s$	18000 N/m <sup>3</sup>	18000 N/m <sup>3</sup>
Suction factor, $f_{suc}$	-	0.203
Asymptote factor, $w$		0.433
Separation point factor, $\psi$		0.661
Backbone curve factor 1, $a$		6.73
Backbone curve factor 2, $b$		0.29

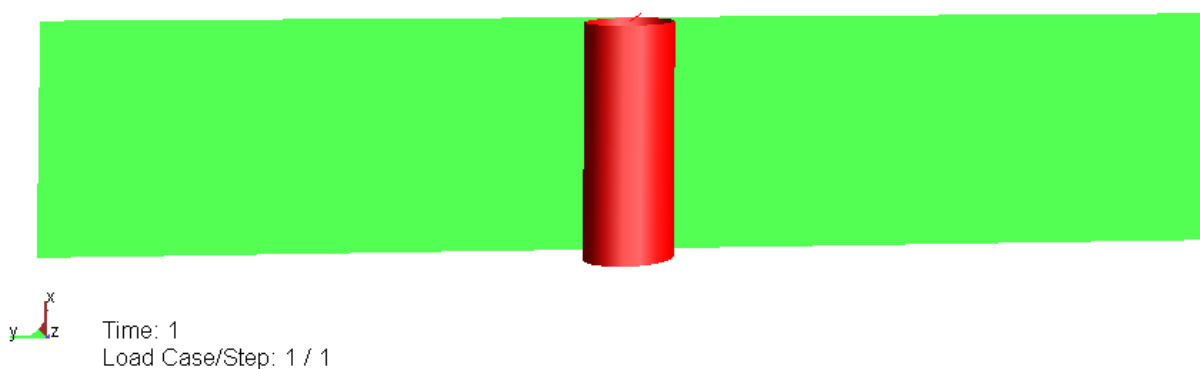


Fig. 5-16. SIMLA model used in the validation tests.

Fig. 5-17 and Fig. 5-18 show the force-displacement curves from the results. The curves are on top of each other, therefore proving that the SIMLA integration is successful and able to produce the same result as the analytical solution. However, it is observed that the result is quite sensitive to the time increment used in the analysis. A longer time increment can cause undesirable results, such as lower breakout resistance or strange behaviour in the non-linear model. Therefore, careful consideration regarding the time increment is needed during pipe-soil interaction analysis.

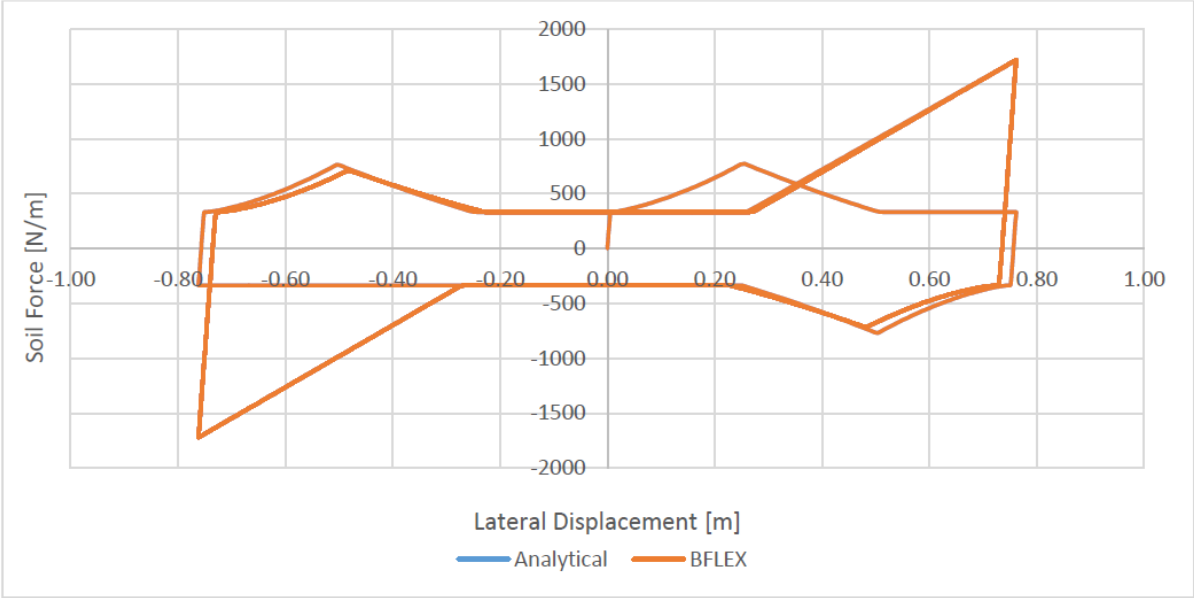


Fig. 5-17. Force-displacement curve of lateral motion from analytical solution and SIMLA.

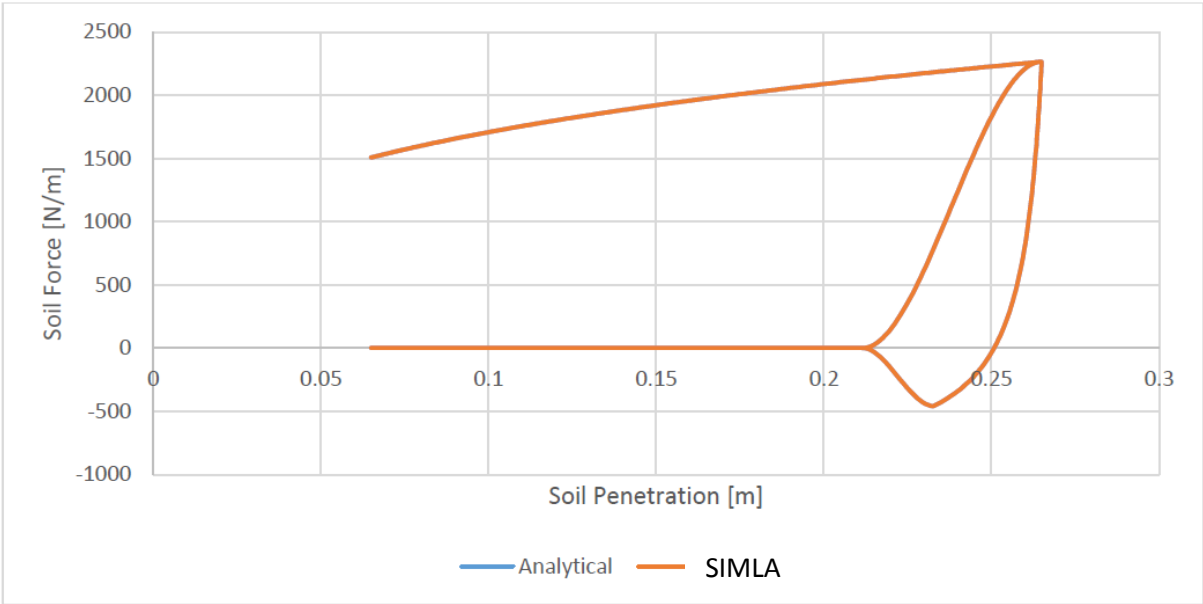


Fig. 5-18. Force-displacement of vertical motion from analytical solution and SIMLA.

## CHAPTER 6 APPLICATION OF PROGRAMS

This chapter discusses the application of the soil subroutines, DNVMODEL-Y and AUBENY-Z, in conjunction with the SIMLA structural model for solving pipe-soil interaction problems. First, the finite element model that was used in the analysis will be described. The description will cover the general description of the model and various constants and parameters appearing in this chapter.

Several analysis cases regarding soil stiffness and strength sensitivity have been performed to study the effects of pipe-soil interactions. However, this chapter focuses on pipeline walking analysis and SCR analysis due to their importance in practical design. Comparison with the linear/Coulomb model in solving the interaction problem is also addressed in this chapter.

### 6.1 Model Description

#### 6.1.1 Lateral Pipe-Soil Model

A pipeline with a length of 200 m is considered in every case analysis presented in this chapter. The pipe has a diameter of 0.508 m and thickness of 0.025 m. The pipe is subjected to an initial strain of varying magnitude in addition to self-weight. The purpose of the initial strain is primarily to simulate expansion and contraction of the pipeline due to thermal cycling (see section 6.4). The seabed is modelled as a flat surface with a uniform depth of 100 m. The seabed model has a length of 300 m and width of 46 m. No wave load is applied in any case presented.

The pipe is modelled using the PIPE element type in SIMLA. Two PIPE element types are used in the analysis: PIPE31 element type is used to model purely elastic behaviour, while PIPE 33 is used to model elastoplastic material [16]. Both of them assume constant axial strain and torsion. In the case of analyses using elastoplastic material, a stress-strain curve is defined (section 6.4).

To model pipe-soil interaction, a contact element is necessary to connect the pipe element with the soil element. The contact element type used in SIMLA, CONT126, is a 3D seabed contact element [16]. The lateral soil model subroutine, DNVMODEL-Y, is connected to this contact element to simulate lateral soil resistance and stiffness during pipe-soil interaction simulation.

The pipe is divided into several elements, with every element having length of 1 m. The seabed element has a size of 1x4 m and is described in a separate input file. The sketch of the finite element model of the pipe and seabed is shown in Fig. 6-1. The pipe is fixed at both ends, in all directions except vertical.



The sea model is divided into several elements of 20 m x 20 m size. The reason for such a large element size is primarily due to the fact that waves and current are not considered in the analysis. The sea element type in SIMLA is called SEA150 and is defined to have a density of 1024 kg/m<sup>3</sup>.

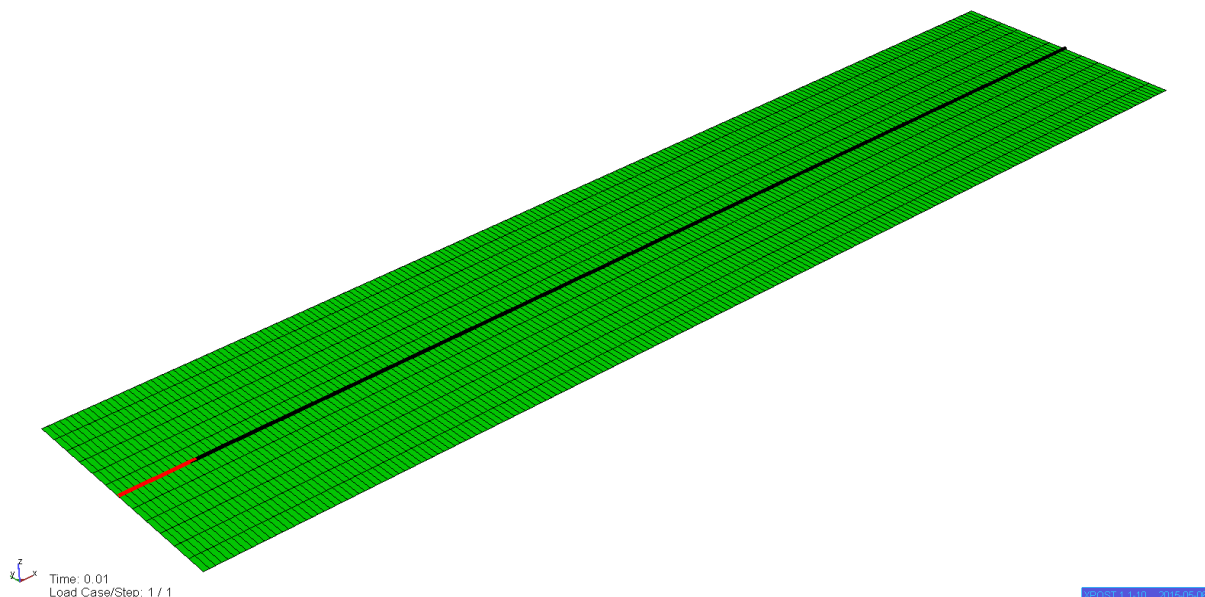


Fig. 6-1. Sketch of finite element model of the pipe and the seabed.

The model is subjected to both static and dynamic analysis. The static analysis is used primarily in the initialization stage. The initialization stage is used to create the pipe's lateral imperfection and therefore to enable lateral buckling. The imperfection is created by loading the pipe laterally with artificial loads in the centre of the pipe in the positive y-direction. The magnitude of the load is small (1 kN) to avoid entering the plastic range of the lateral soil model in the initialization stage accidentally. The dynamic analysis is used in the main part of the analysis after imperfection is created. The initial strain load is used in the dynamic analysis and is stepped over time in the form of a sine function. This is used to create a smooth expansion and contraction along the pipeline to simulate the thermal cycling. A period of 40 s is primarily used in the analysis to provide a smooth loading of the pipeline. Fig. 6-2 shows the typical strain load factor over time that is used through most of the analysis.

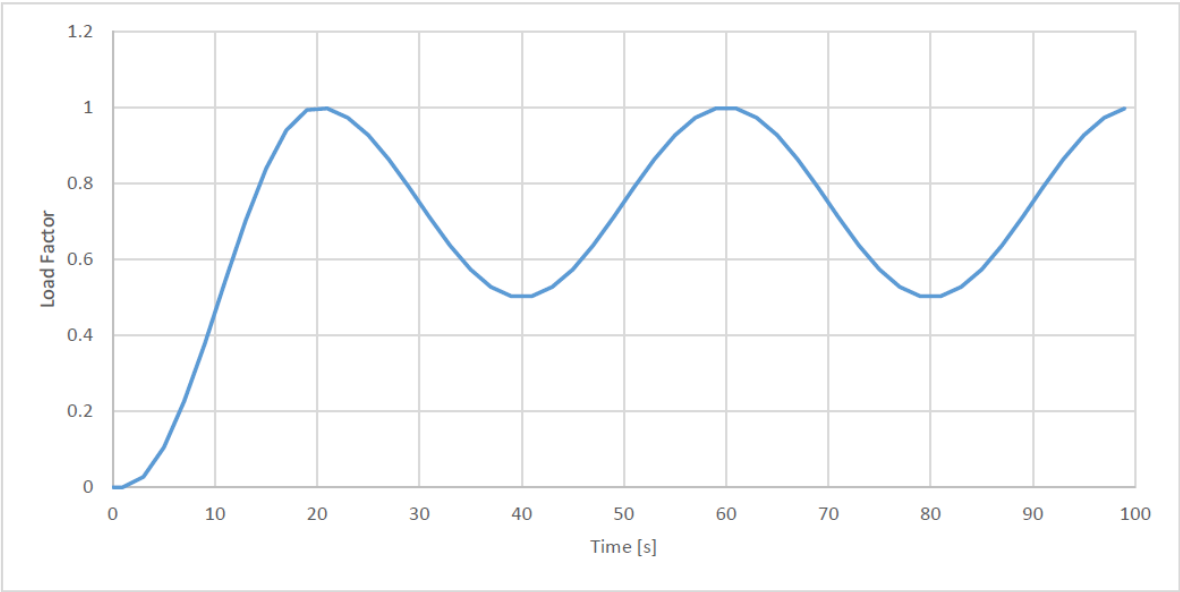


Fig. 6-2. Typical load factor history for lateral pipe-soil interaction.

The lateral pipe-soil subroutine, DNVMODEL-Y, only covers the lateral soil model. However, even in lateral pipe-soil interaction problems, a material model is needed to simulate the axial and vertical pipe-soil interaction. SIMLA has two options available for this: EPCURVE model and HYCURVE model.

EPCURVE is a material model that is used to model elastoplastic material behaviour with kinematic/isotropic hardening. HYCYRVE is used to model hyperelastic (non-linear elastic) material behaviour [16]. The EPCURVE model is typically used to model Coulomb friction force, and therefore is chosen to model the axial pipe-soil interaction. The HYCURVE is selected to model the pipe-soil interaction in the vertical direction. Fig. 6-3 shows the EPCURVE model that is used in the analysis.

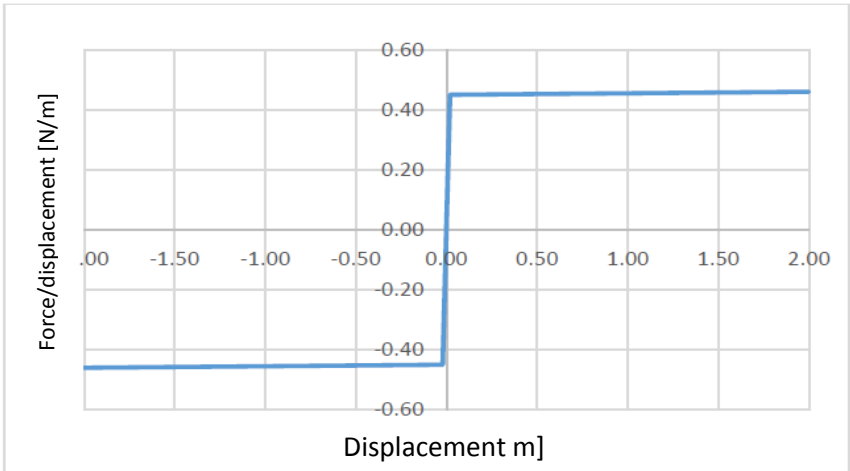


Fig. 6-3. Typical EPCURVE model for axial pipe-soil interaction.

### 6.1.2 Vertical Pipe-Soil Model

A steel catenary riser (SCR) in 1000 m water depth is used in the analysis. The SCR is subjected to forced harmonic motion at the top end (hang-off) point to simulate the riser's movement. The pipe is modelled using the elastic PIPE31 element type with the specification as described in Table 6-1.

The pipe is divided into elements with size of 1 m, while the seabed elements have a size of 1x100 m. In SCR analysis, lateral motion is considered very small; therefore, a wide element size can be used for the seabed. The contact between riser and soil at the touchdown point (TDP) is modelled using the CONT126 element type. The sea-surface is modelled using the SEA150 element type with a size of 30x200 m. The origin of the z-coordinate is located at the sea-surface with a positive direction upward.

The configuration of the SCR is shown in Fig. 6-4.

The EPCURVE material type with 0.45 friction coefficient is chosen to model pipe-soil interaction in the axial and lateral directions.

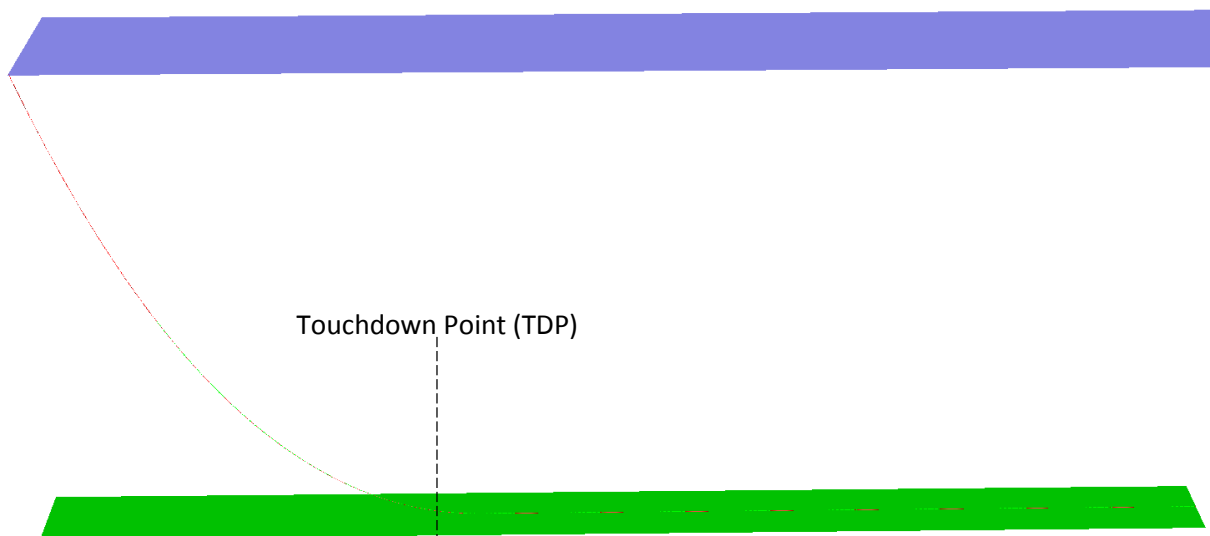


Fig. 6-4. SCR model for vertical pipe-soil interaction for 20 m water depth.

The pipe end at the seabed is fixed in all directions while the hang-off point is modelled as a hinge. The catenary shape is formed by moving one of the pipe ends vertically using static analysis. The linear soil model is used during static analysis with equivalent soil stiffness. The equivalent soil stiffness is calculated as shown in Fig. 6-5.

After the catenary shape is formed, the riser is analysed dynamically while it is subjected to forced harmonic displacement in the vertical direction. The non-linear soil model, AUBENY-Z, is activated during the dynamic analysis.

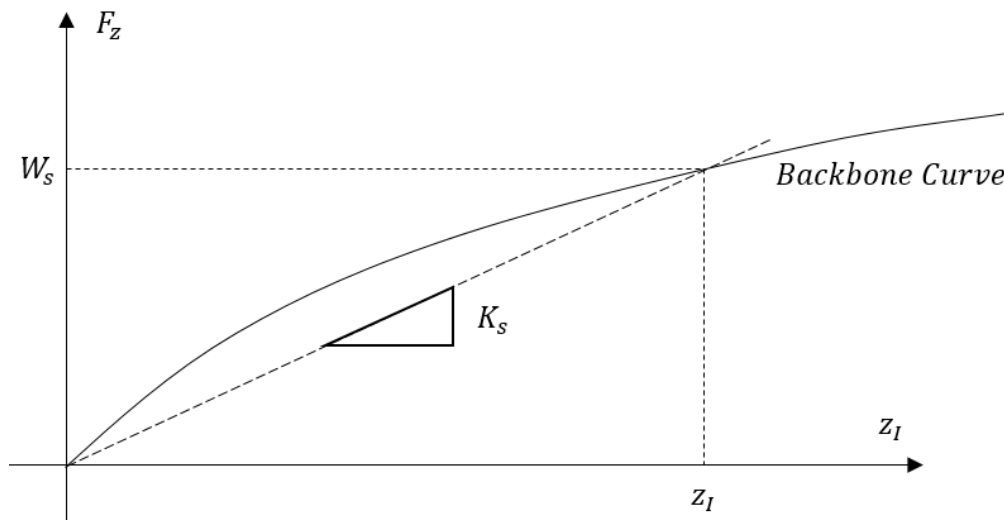


Fig. 6-5. Vertical soil stiffness calculation.

### 6.1.3 Constants

This section will describe the various constants that are used in all of the analyses presented. The details of the descriptions are provided in Table 6-1, unless noted otherwise. For SCR-soil interaction problems, the soil parameters are based on data interpreted by Aubeny et al. [1] from Dunlap et al. [3] data, which are described in Table 6-2.

Table 6-1 List of Constants

Parameter	Description	Value	Unit
$E_s$	Elastic steel modulus	200	[GPa]
$G$	Shear modulus	80	[GPa]
$D$	Pipe outer diameter	0.508	[m]
$th$	Pipe thickness	0.025	[m]
$EI$	Bending stiffness	224.847	[MN/m <sup>2</sup> ]
$EA$	Axial stiffness	7702	[MN]
$\sigma_y$	Yield stress	350	[MPa]
$m_d$	Dry mass	302.3	[kg/m]
$m_s$	Submerged mass	94.35	[kg/m]
$\rho_w$	Seawater's density	1024	[kg/m <sup>3</sup> ]
$\rho_s$	Steel's density	7850	[kg/m <sup>3</sup> ]

Parameter	Description	Value	Unit
$k_s$	Soil elastic stiffness	65000	[N/m <sup>2</sup> ]
$s_u$	Soil undrained strength	800	[Pa]
$s_g$	Soil strength gradient	0	[Pa/m]
$\mu_a$	Axial Coulomb friction factor	0.45 (minimum)	-
h	Water depth: Lateral model Vertical model	100 1000	[m]

Table 6-2 List of Soil Parameters for Vertical Pipe-Soil Interaction

Parameter	Description	Value
A	Backbone curve coefficient	6.73
b	Shear modulus	0.29
$k_o/c$	Unload initial stiffness	660
$\omega$	Unload large deflections	0.433
$f_{suc}$	Unload tension limit/suction factor	0.203
$\psi$	Soil-riser separation	0.661

## 6.2 Elastic Soil Stiffness Sensitivity

### 6.2.1 Case Description

The finite element model that is described in section 6.1 is used in this sensitivity analysis. The soil stiffness of  $65 \text{ kN/m}^2$  is defined as high soil stiffness, while elastic soil stiffness of  $1 \text{ kN/m}^2$  is defined as low soil stiffness. Analysis cases with high and low soil stiffness are called Case 1A and Case 1B, respectively. The pipeline is subjected to a maximum strain load of 0.005 and minimum strain load of 0.0025 stepped in sine shapes over time. The non-linear soil model used is the DNV-model without added berm resistance. An elastic material is used for the pipe elements. These test cases are used to demonstrate the effect of elastic soil stiffness on the buckling shape of the pipeline and soil resistance force. The case descriptions are given in Table 6-3.

Table 6-3 Case Description for Elastic Soil Stiffness Sensitivity Analysis

Case Name	Ks	Soil Model	Strain Load
Case 1A	$65000 \text{ N/m}^2$	DNV	0.005 – 0.0025
Case 1B	$1000 \text{ N/m}^2$	DNV	0.005 – 0.0025

### 6.2.2 Results and Discussion

The shape of the pipeline after undergoing lateral buckling for different values of elastic soil stiffness is presented in Fig. 6-6. From the figures, it is apparent that the formation of the pipeline after lateral buckling depends significantly on the pipe-soil interaction. In the case of high elastic soil stiffness, the pipeline is subjected to high elastic stiffness and lateral soil force. This prevents the pipeline from deforming significantly during early buckle formation, and forces the strain load to distribute along the pipeline instead of being focused on the centre of the pipeline (imperfection region). The distribution of the loads then formed three half-sine waves with increasing strain, as shown in the figure. In low elastic soil stiffness, the centre of the pipeline easily enters the plastic range of the soil and then breakout. This cause the pipeline deformation to be concentrated on the middle of the pipeline (imperfection area).

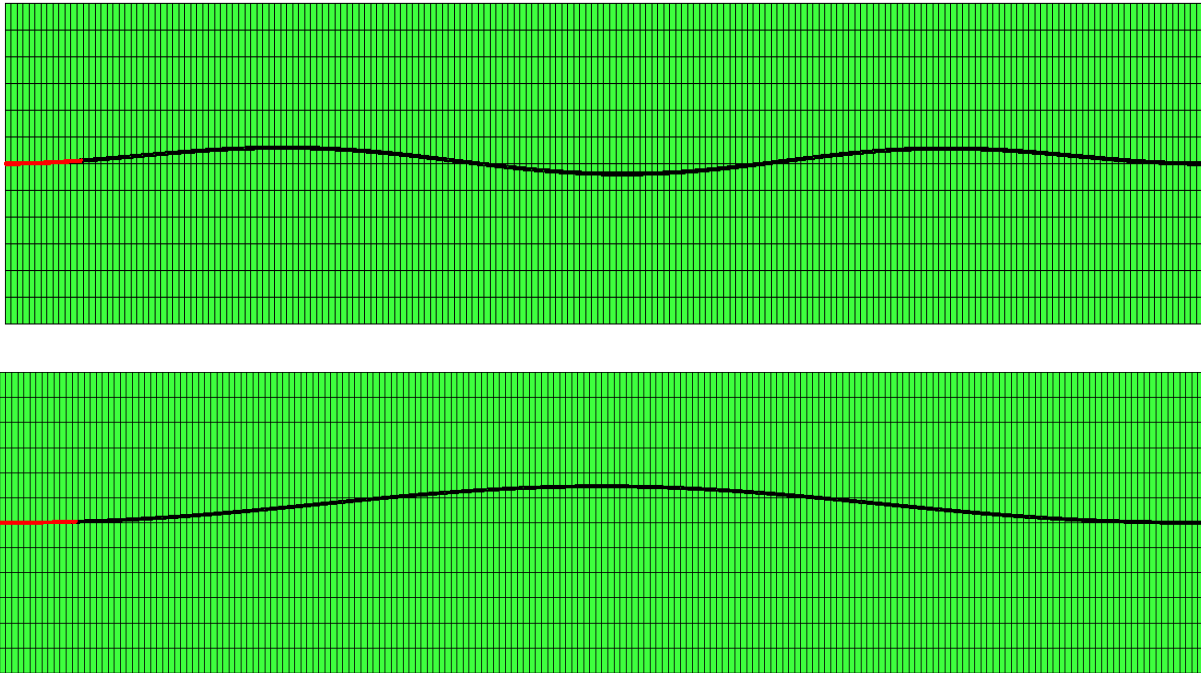


Fig. 6-6. The shape of pipeline after lateral buckling with high (top) and low (bottom) soil stiffness.

Fig. 6-7 shows the force-displacement curve of soil force for Case 1A and Case 1B. In Case 1A, the soil stiffness has sufficient plastic deformation, which increases the soil penetration as well as the lateral soil force compared to Case 1B. The maximum peak force ( $F_{R2}$ ) in Case 1A is approximately 950 N/m, which is twice the maximum peak force in Case 1B. In Case 1B, the elastic regime is very wide and causes insignificant plastic deformation before breakout. The soil resistance in Case 1B is effectively flat, and is generally equal to  $F_{R1}$ . It is also worth noting that the centre of the pipeline in Case 1A only moved 1.3 m compared to 8.8 m in Case 1B.

A significant difference also can be seen in the bending moment distribution. Fig. 6-8 shows the bending moment history at the centre of the pipeline. The maximum bending moment in Case 1A is 1.25 kN/m, while in Case 1B it is 2.6 kN/m. Case 1B produces a higher peak bending moment due to higher curvature compared to Case 1A.

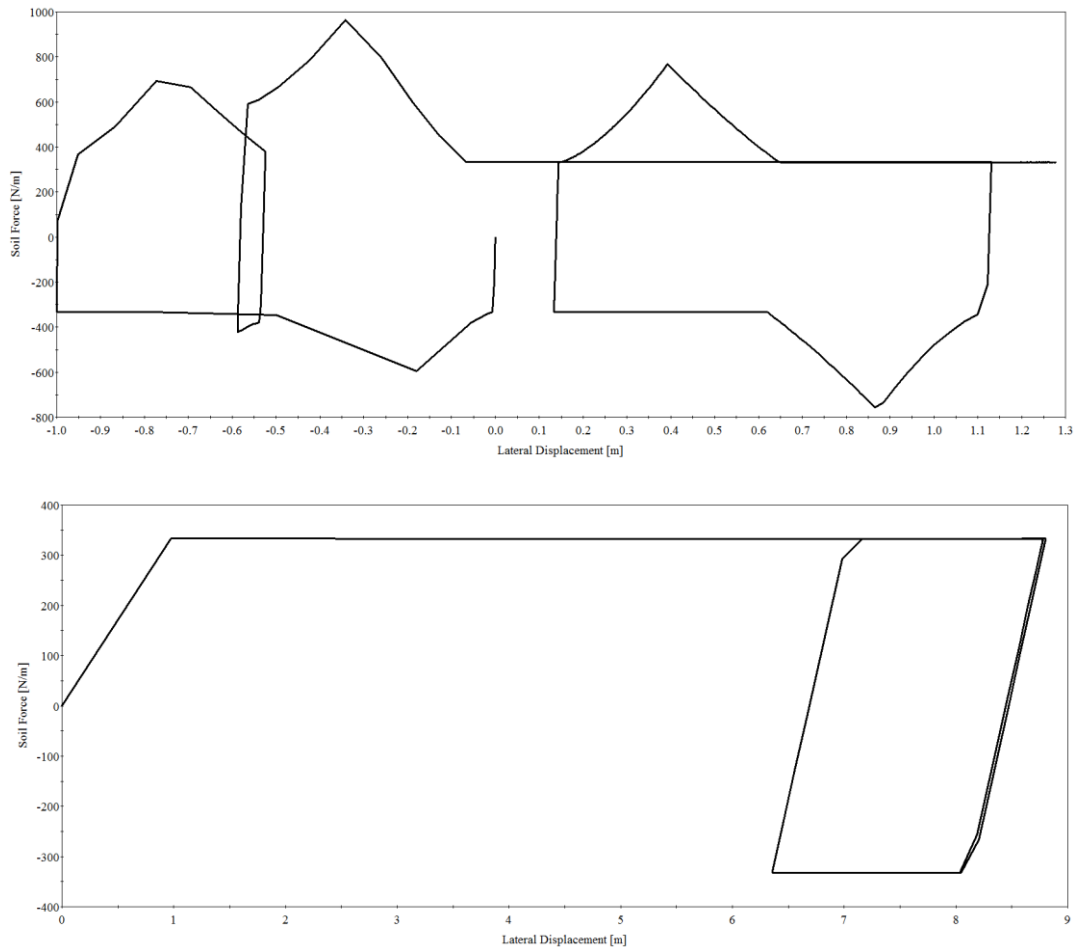


Fig. 6-7. Force-displacement curve for Case 1A (top) and Case 1B (bottom).

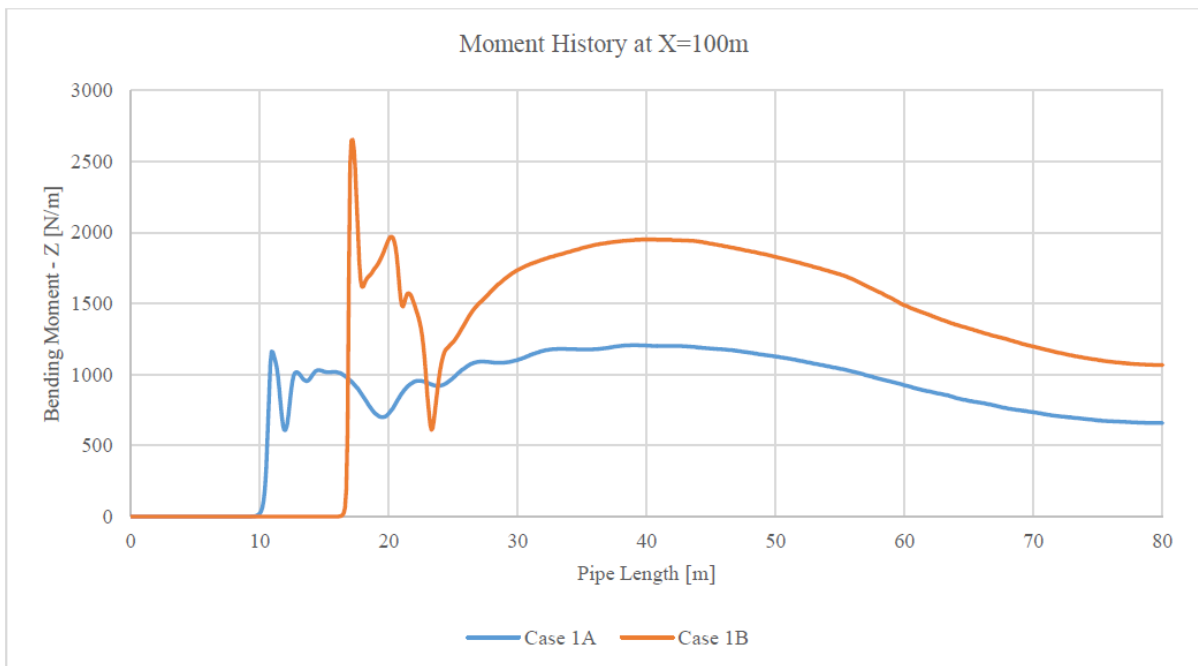


Fig. 6-8. Bending moment history at the centre of pipeline for Case 1A and Case 1B.



### 6.3 “Heavy” and “Light” Pipe

#### 6.3.1 Case Description

Several test cases have been developed to study the behaviour differences between “heavy” and “light” pipe. Classification of the pipe is determined from non-dimension parameter  $S$  as follows:

$$S = \frac{w_s}{S_u D} \quad [6-1]$$

where the pipe classified as light if  $S < 1$  and heavy if  $S > 1$ .

The finite element model used in this tests is described in section 6.1. Both the DNV model and PONDUS model are used as the non-linear soil models. The pipe is subjected to varying strain load of 0.005–0.0025 in all test cases. No wave load is considered in this case. Elastic material is used for the pipe element model.

#### 6.3.2 Results and Discussion

The results of the analysis are presented in Fig. 6-9. With increasing value of  $S$ , the peak soil resistance force also increases. This is because the non-dimensional  $S$  parameter describes the penetration resistance of the soil. A high value of  $S$  means that the pipe easily penetrates the soil (increases the initial penetration of the pipe) and that the pipe is considered to be a ‘heavy’ pipe. This will result in high soil resistance in the lateral direction, especially near the breakout limit. By plotting the soil force in non-dimensional form ( $F_s/W_s$ ), the equivalent Coulomb friction factor for the breakout resistance can be derived. If the pipe is very ‘heavy’, the equivalent Coulomb friction factor can even exceed one.

It is also easy to see that the PONDUS model gives generally higher breakout resistance compared to the DNV model. The reason for this is that the plastic/breakout limit of the PONDUS model is higher compared to that of the DNV model (0.75D in PONDUS). This allows the pipe to dig deeper into the soil and, in turn, causes higher lateral soil resistance.

It is also important to point out that the buckled shape of the pipeline has two different distinct types based on magnitude of lateral displacement, as shown in Fig. 6-6. In the high  $S$ -value region, the pipeline is buckled in ‘snaking’ form, as shown in Fig. 6-6. This is caused by high soil resistance in this region. In the low  $S$ -value region, the pipeline will buckle in one long arch and produce a very high and concentrated lateral displacement. The boundary between these two buckling shapes is approximately  $S=1.5$ .

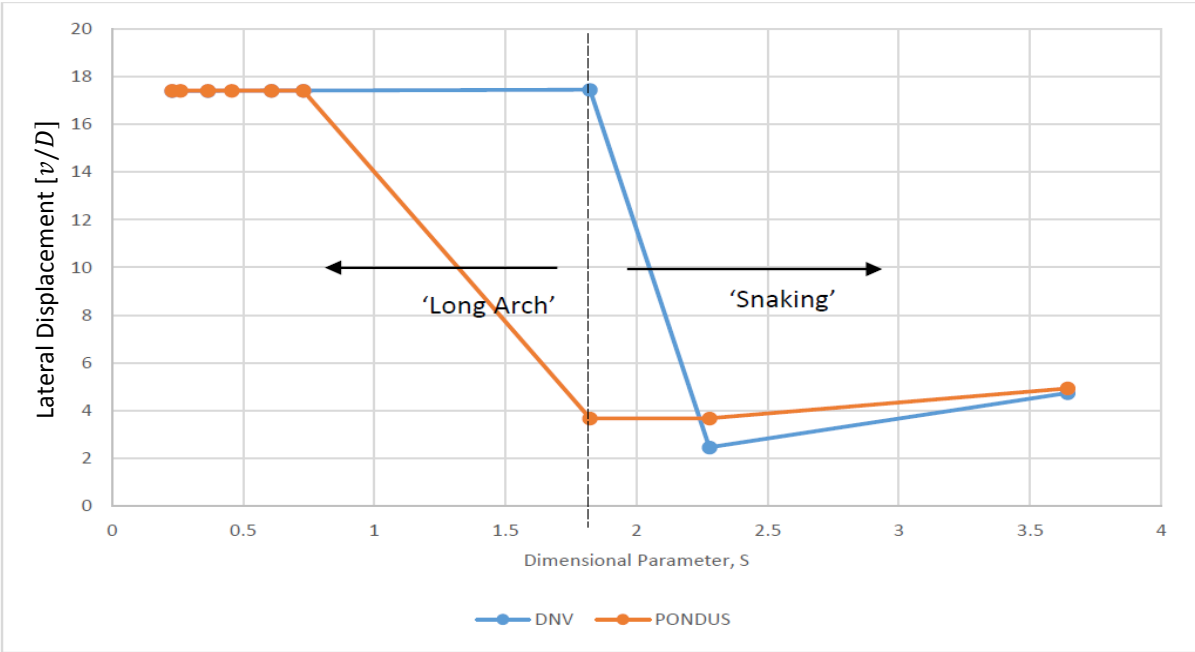
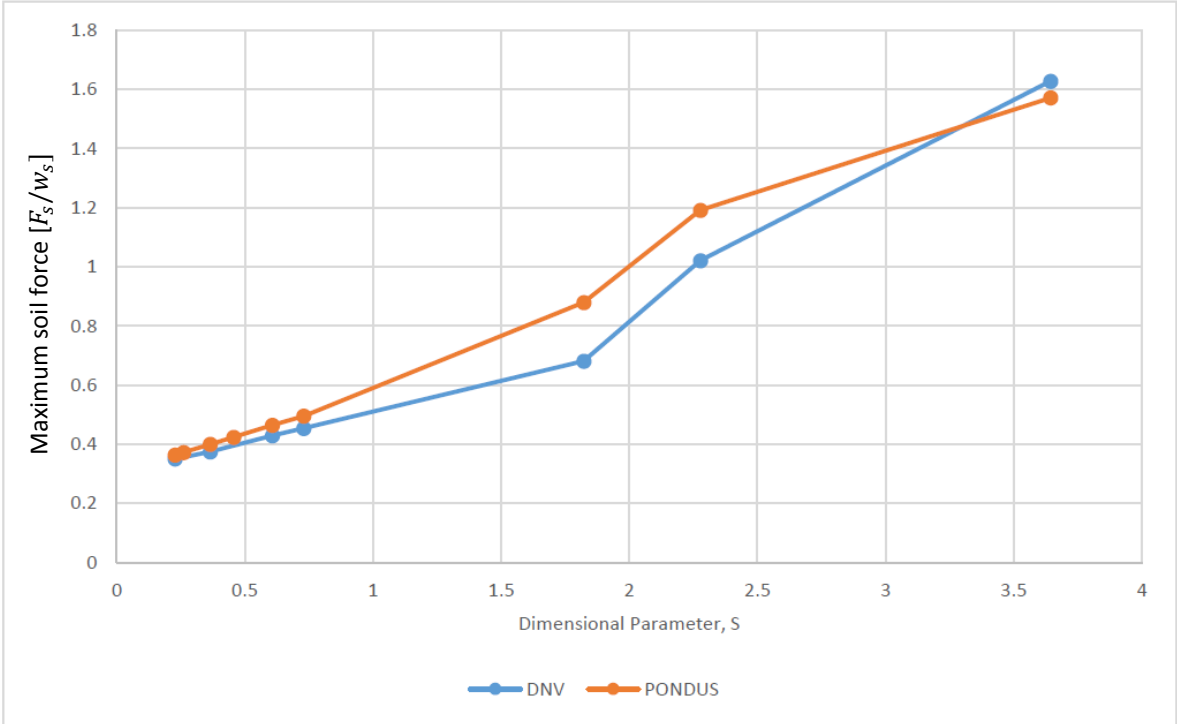


Fig. 6-9. Non-dimensional soil force (top) and lateral displacement (bottom) vs. non-dimensional parameter S.

## 6.4 Pipeline Walking

### 6.4.1 Introduction

Up until this point, elastic material was used as the pipe material model to focus on soil resistance force. However, elastic material is not a realistic choice to study the lateral pipe-soil interaction (i.e. pipeline walking). Pipeline walking is a term to describe an increase of lateral displacement after a cycle of heating and a cool-down period. This phenomenon is very important in pipeline design because it can accumulate to cause axial displacement of the entire pipeline, leading to potential failure at tie-ins or risers [17].

The pipeline walking is usually caused by thermal cycling along the pipeline, causing the pipeline to expand and contract. In the cooling-down period, the pipeline cannot return to the original position due to pipe-soil interaction, therefore causing a shift to the pipeline's original position. This shift is called 'walking', and it can be measured every cycle to find the walk/cycle ratio. The walk/cycle ratio is a key element in investigating the pipeline walking phenomenon. An example of pipeline walking is shown in Fig. 6-10. In this thesis, the effect of thermal cycling is handled by considering the strain load cycling in the entire pipeline to simulate the expansion and contraction.

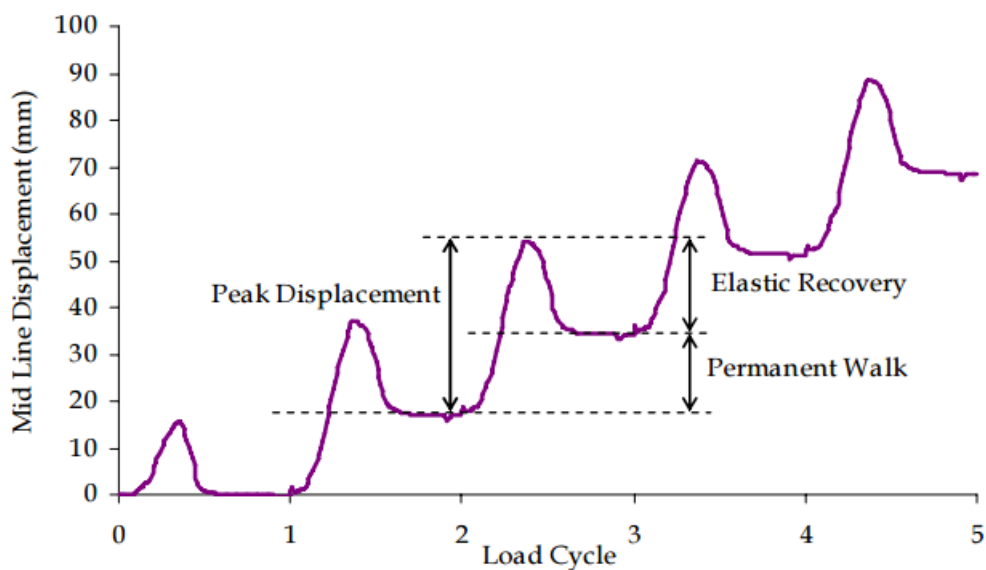


Fig. 6-10. A typical curve of lateral displacement development of pipeline under thermal cycling [17]. Pipe-soil interaction is a critical element of the pipeline walking phenomenon. The soil resistance in the lateral direction is a governing parameter of how much the pipeline will walk in every cycle. As described before, the Coulomb friction model is typically used to model pipe-soil interaction. In the following section, the PONDUS model and the Berm model will be used in addition to the Coulomb model to study the effect of each model in pipeline walking analysis.

### 6.4.2 Case Description

The finite element model described in section 6.1 will be used as a basis for the pipeline walking analysis. Elastoplastic material is used for the pipe element to accurately model the pipe behaviour. The stress-strain curve of the material model is shown in Fig. 6-11.

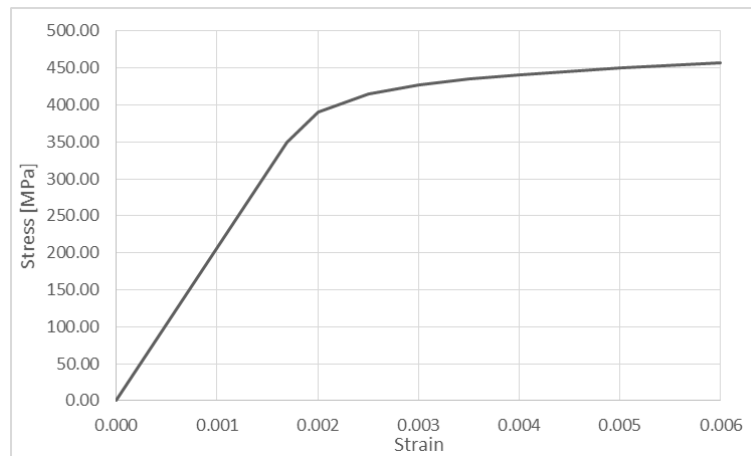


Fig. 6-11. Stress-strain curve for elastoplastic material model.

Several test cases with different strain load amplitudes were developed to study the pipeline walking phenomenon. Table 6-4 lists the analysis case that was studied. The soil models used in the analysis are Berm model, PONDUS model, and Coulomb friction model. Each model is subjected to the same strain load for each case, therefore totalling 18 analysis cases. The Berm model is coupled with the DNV model and had been set to reach maximum in only one cycle to reduce analysis time. The Coulomb model is defined to have a 0.45 friction coefficient.

Table 6-4 List of Cases for Pipeline Walking Analysis

Case Name	Strain Load
Case 2A	0.001 – 0.0005
Case 2B	0.0025 – 0.00125
Case 2C	0.005 – 0.0025
Case 2D	0.0075 – 0.00375
Case 2E	0.01 – 0.005
Case 2F	0.0125 – 0.0063

### 6.4.3 Results and Discussion

In general, the buckled form of the pipeline is the combination of long arch and snaking type, which is shown in Fig. 6-12. This is because elastoplastic material is used in the analysis instead of elastic material. From Table 6-4, it can be seen that all cases except 2A are higher than the elastic limit of the pipe. This causes the centre of the pipe to yield and therefore concentrates all the displacement in the centre. However, due to high soil stiffness, the displacement is distributed along the pipeline during early buckling formation which caused the deformed shape as seen in Fig. 6-12. It is worth mentioning that the lateral displacement of the pipeline moved in negative y-direction.

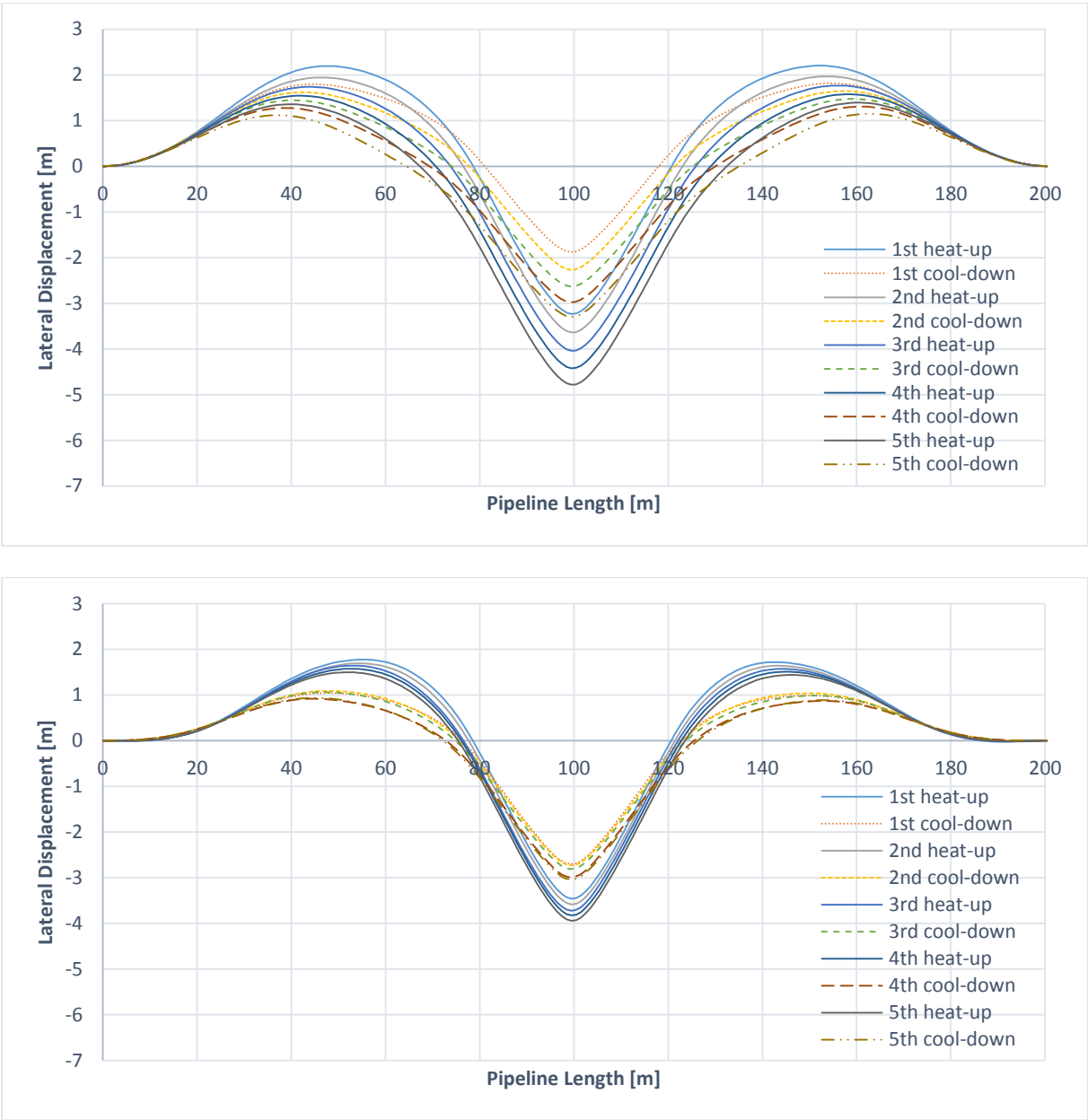


Fig. 6-12. Buckled form of pipeline for Case 2C with Coulomb Model (top) and Berm Model (bottom)

Regarding pipe-soil interaction, it is observed that the pipe behaviour differs according to the soil model used in terms of lateral displacement growth. Fig. 6-12 shows that the buckle grows very fast in Coulomb model compared to the results from Berm model. In Berm model the lateral displacement growth is restricted by the soil berm due to high soil resistance. This results are in-line with results obtained by Bruton et al. [2] and confirm that the Berm model is working correctly.

Fig. 6-13 shows the lateral displacement in the middle of the pipeline. The figures demonstrates that walk/cycle from the Coulomb model is the highest and increasing with each cycles. The results from the Berm model shows the displacement is constrained by the soil berm.

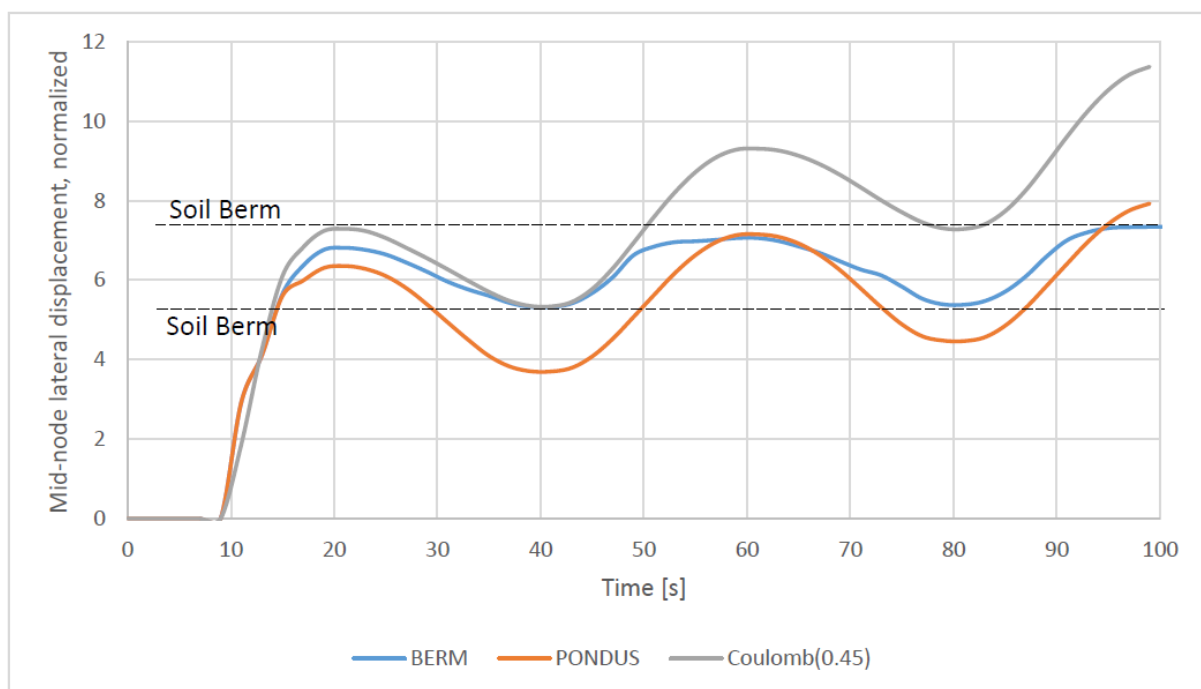


Fig. 6-13. Mid-node displacement, normalized against diameter, for various soil models from Case 2C.

The PONDUS model result shows that the displacement growth is higher compared to the Berm model due to unaccounted soil berm effect. The growth, however, is still considerably lower compared to the result from the Coulomb friction model. It is worth mentioning that the PONDUS model has an inherent 0.2 Coulomb friction factor, giving the Coulomb model more than twice the friction force of PONDUS. Fig. 6-13 shows that the friction force has less effect in reducing the buckle growth.

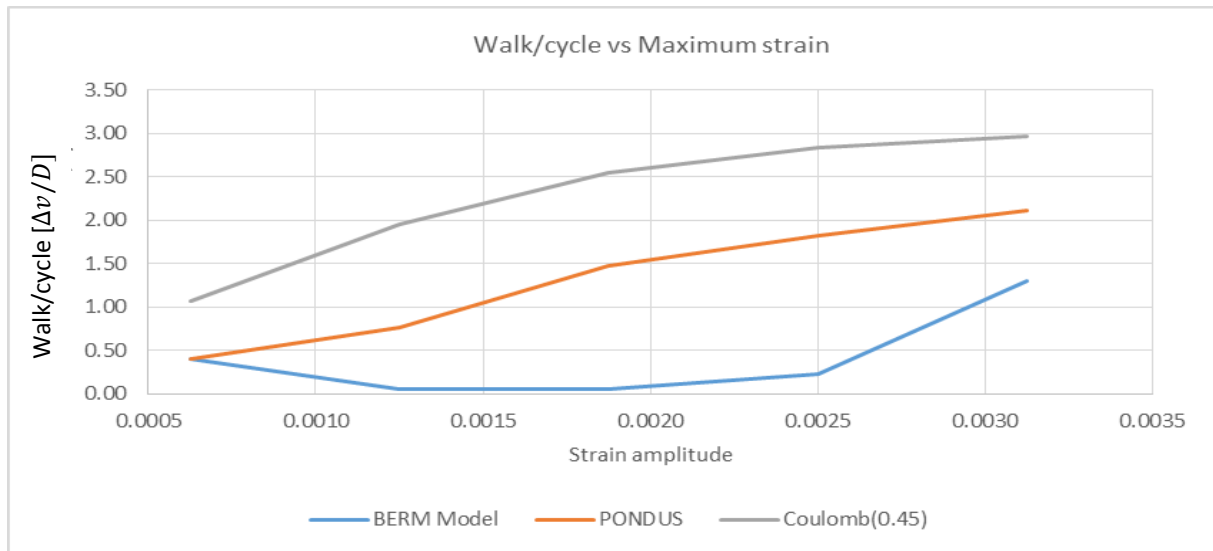


Fig. 6-14. Walk/cycle, normalized against diameter, in the centre of pipeline vs. strain load amplitude.

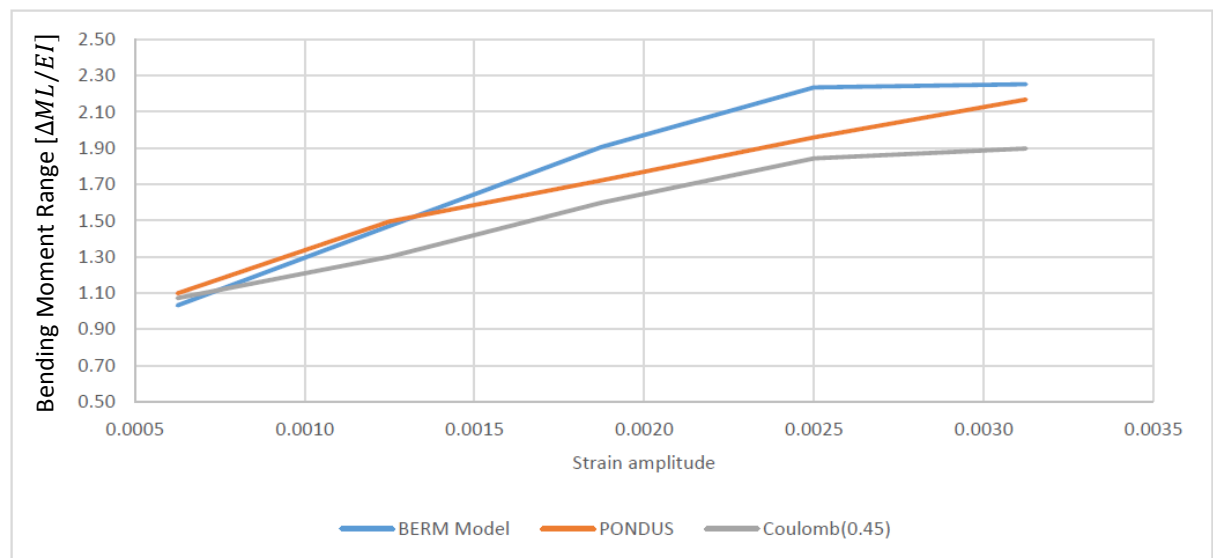


Fig. 6-15. Bending moment range in the centre of the pipeline versus strain load amplitude

Fig. 6-14 shows the overall results of the analysis regarding walk/cycle. The results show an increasing trend of walk/cycle ratio across all models, which is expected. The Coulomb model results show a very high walk/cycle compared to the other two models due to lower lateral soil force. The PONDUS model provides moderate results, and the Berm model gives the lowest results of all.

Fig. 6-15 shows the range of the bending moment in the centre of the pipeline. The trend is in-line with the walk/cycle results, with the Berm model expectedly providing the highest bending moment compared to the other two due to higher soil resistance. Fig. 6-16 shows two other peak moment regions beside the centre of the pipeline. The figure shows that the soil berm

resistance gives higher moment variation not only in the middle region of the pipeline compared to the results from Coulomb model.

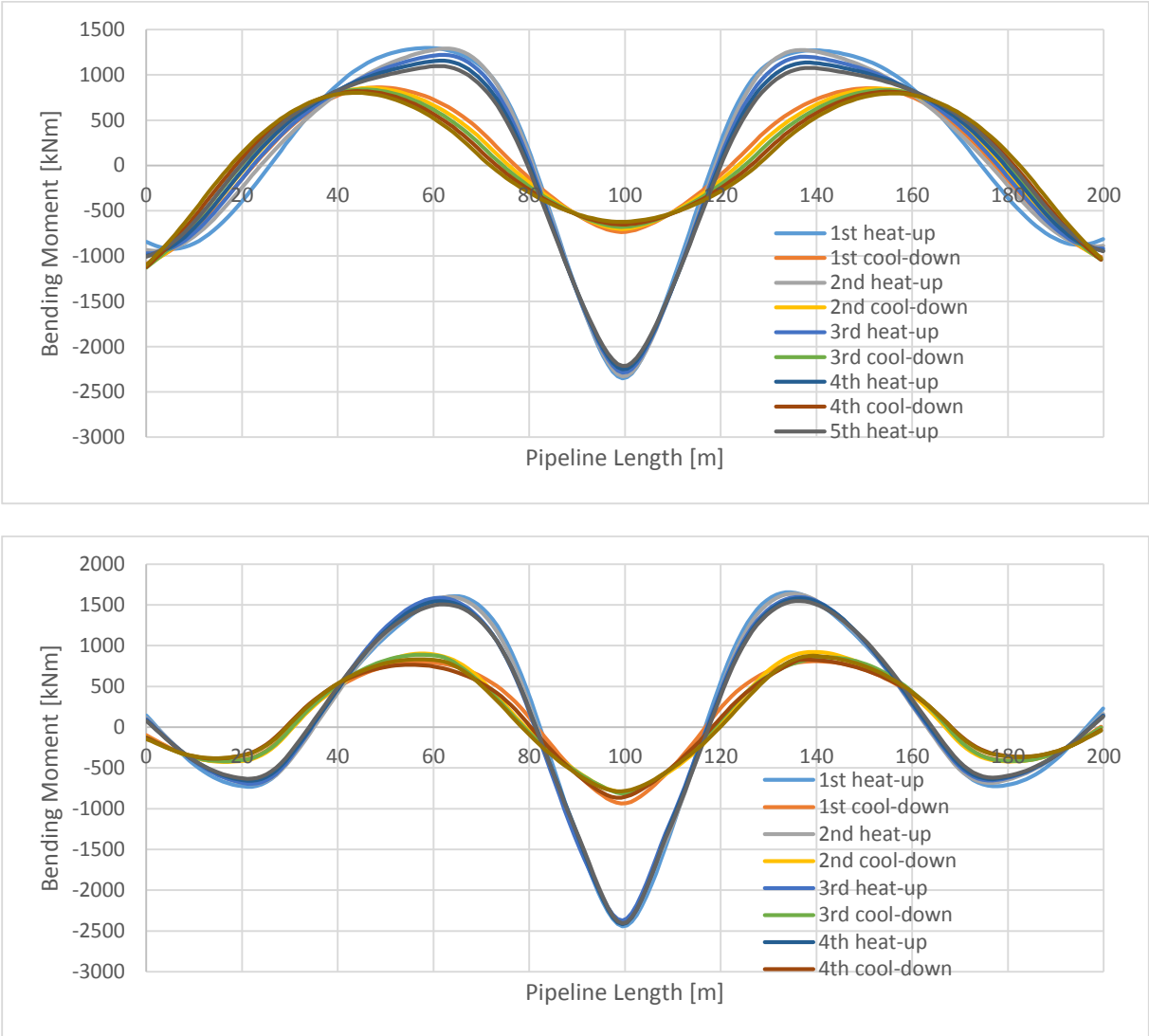


Fig. 6-16. Moment distribution along the pipeline for Case 2C with Coulomb model (top) and Berm model (bottom).

In pipeline design, fatigue of the pipe due to pipeline walking is a very important design consideration. Observation of Fig. 6-15 and Fig. 6-16 reveals that non-linear pipe-soil interaction gave a higher moment range compared to the Coulomb friction model. This result means that use of the Coulomb model can cause underestimation of the fatigue damage of the pipeline, leading to potential failure. In addition, the Coulomb model also gave higher walk/cycle results compared to the other two models, which can lead to over-design of the tie-in regions. These two design flaws are undesirable and can be avoided by using a more accurate soil model as described in this chapter.



## 6.5 Coulomb Friction Model

### 6.5.1 Case Description

As mentioned in previous sections, the Coulomb friction model is a typical method that is used to model pipe-soil interaction. It has the advantage of simplicity and is easy to implement. As can be seen in section 6.4.3, it fails to consider many important aspects such as breakout of the pipe and soil berm build-up that can lead to incorrect design. However, the Coulomb model is still an attractive choice for preliminary design, especially if detailed geotechnical data are not present. Therefore, it is important to understand in detail the effect of using the Coulomb model compared to a non-linear soil model.

In this section, several Coulomb models with friction coefficient of 0.2 to 1.5 will be considered and compared with Case 2C (Berm model and PONDUS) from Table 6-4. The purpose of this study is to determine which friction coefficient gives comparable results (walk/cycle, moment) to the Berm and PONDUS models.

### 6.5.2 Results and Discussion

The lateral displacement for various Coulomb friction factors can be seen in Fig. 6-18. The results show that for low friction coefficient ( $\mu < 0.4$ ), the lateral displacement moves toward the positive y-direction, following the imperfect shape. For higher friction coefficient, the displacement shifts toward the negative y-direction due to higher soil resistance force, in line with Berm and PONDUS model results.

It is interesting to point out that with high friction coefficient, some of the pipeline segment is lifted out of the seabed, as shown in Fig. 6-17. The middle region does not move much, and there are two lifted lateral displacement concentration points instead of one. This is caused by the very high soil force, which effectively acts like a wall and causes the pipeline to move upward and lose contact with the soil. This sort of behaviour is not seen in the Berm and PONDUS models.

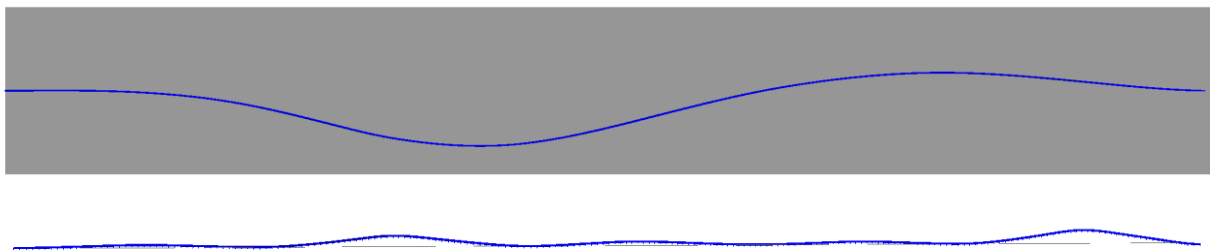


Fig. 6-17. Lifted pipeline segment with high friction coefficient ( $\mu > 0.9$ ). Displacement is scaled 3x.

With respect to bending moment, friction coefficients in the range of 0.4–0.9 are observed to give reasonable results. If the friction is too low or too high, the behaviour of the pipe will become erratic, and it can lose contact with the soil. The summary of the results of moment distribution are provided in Fig. 6-19.

From all the results, one can conclude that the Coulomb model is a very simplified model and cannot model the pipe-soil interaction correctly. If, during the analysis, the friction coefficient used is too low, the pipe will have negligible soil resistance and in turn, higher walk/cycle ratio and over-design possibility. If the friction is too high, the soil will act like a wall and the pipeline will be lifted out of the seabed, which gives inaccurate behaviour. Care must be taken by the user if the Coulomb model is used to avoid inaccurate behaviour.

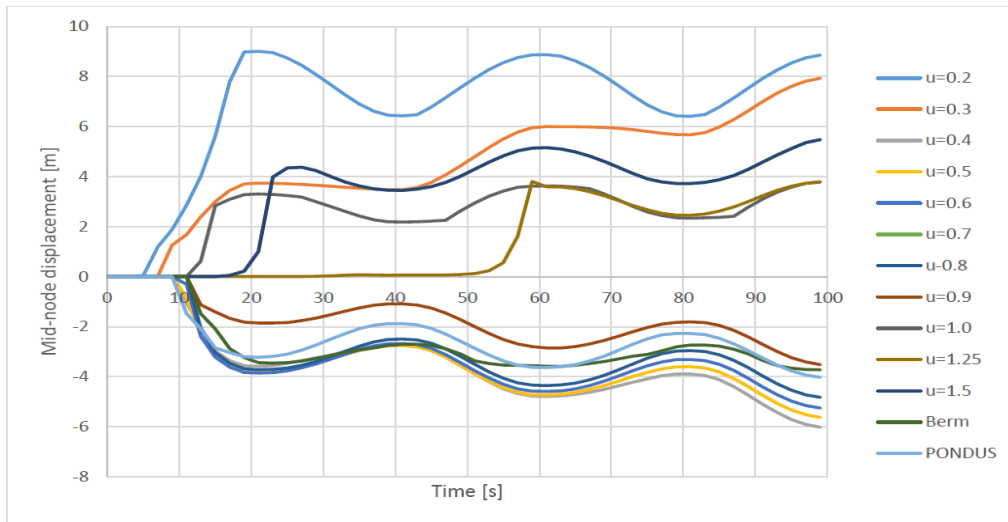


Fig. 6-18. Lateral displacement in the centre of the pipeline for various friction coefficients.

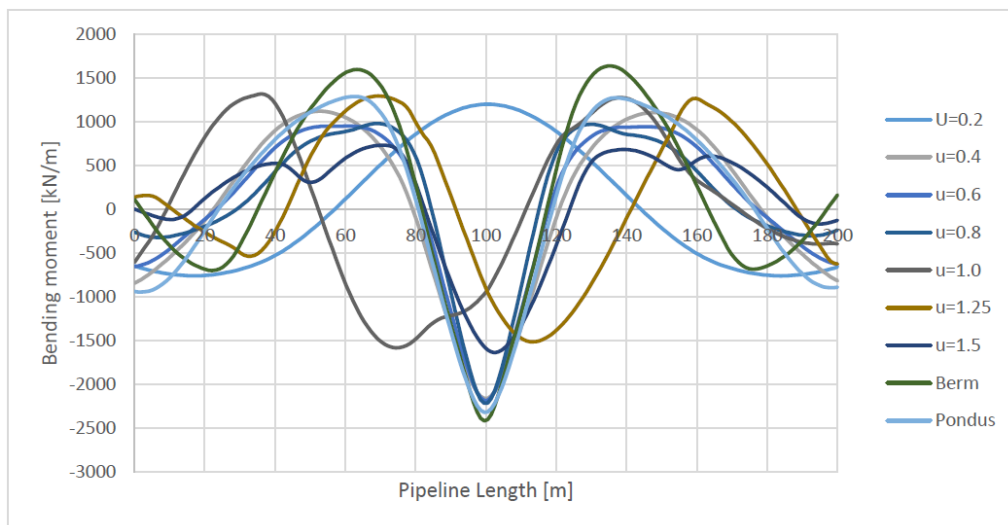


Fig. 6-19. Moment distribution along the pipeline for various friction coefficients.

## 6.6 SCR Analysis

### 6.6.1 Introduction

This section will demonstrate the effect of the non-linear soil model in steel catenary riser (SCR) analysis. The FEM model of the SCR, as described in section 6.1.2, is used in this section. The water depth used in this section is 1000 m. Several sensitivity analysis cases have been studied regarding soil strength, suction force, and heave motion to study the effects in the SCR-soil interaction.

### 6.6.2 Static Configuration

Fig. 6-20 shows the effective tension and bending moment along the horizontal coordinate for the static position. The maximum effective tension is 1.42 MN and is located at the hang-off point, while the minimum tension is 0.5 MN. The maximum bending moment is 402.7 kNm and is located approximately 848.3 m from the hang-off point. The touchdown point is located approximately 934 m from the hang-off point.

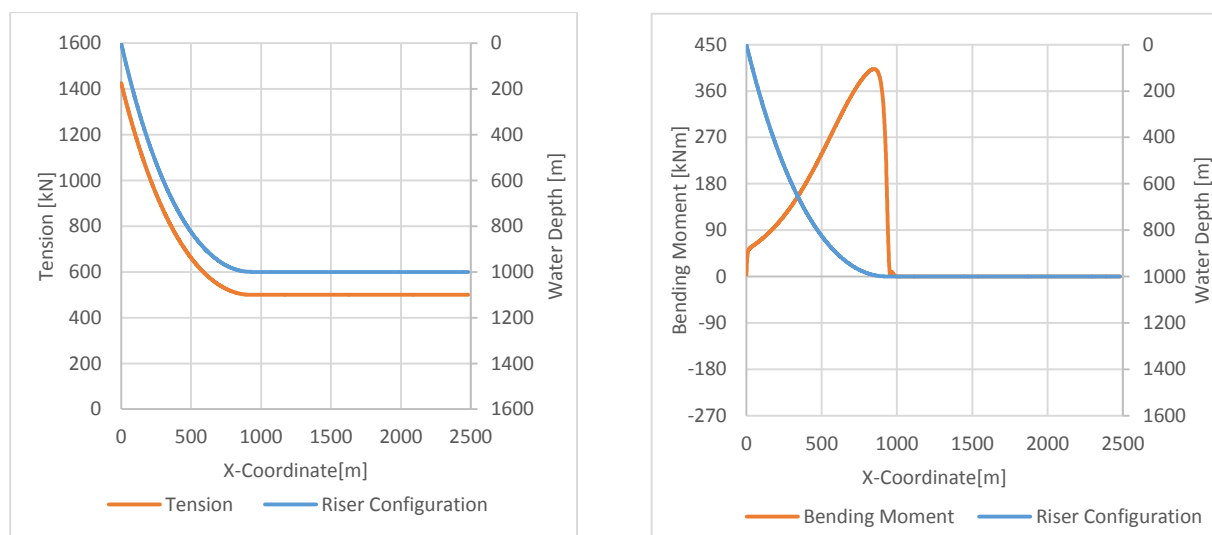


Fig. 6-20. Effective tension and bending moment along the riser length in the static configuration.

Fig. 6-21 shows the soil penetration and the respective soil force along the riser length in the TDP region. The initial penetration due to self-weight in the static condition is 5.53 mm and is characterized by the flat-line behind the TDP. Shortly behind the TDP, penetration increases gradually to a maximum of 19.9 mm before decreasing again. The maximum penetration is located approximately 10 m from the TDP. The maximum soil resistance is 1.36 kN/m and is located at the maximum penetration point.

The soil force shown in Fig. 6-21 is due to virgin penetration of the pipe into the soil. The results can be validated by manual calculation using Eq. [4-41].

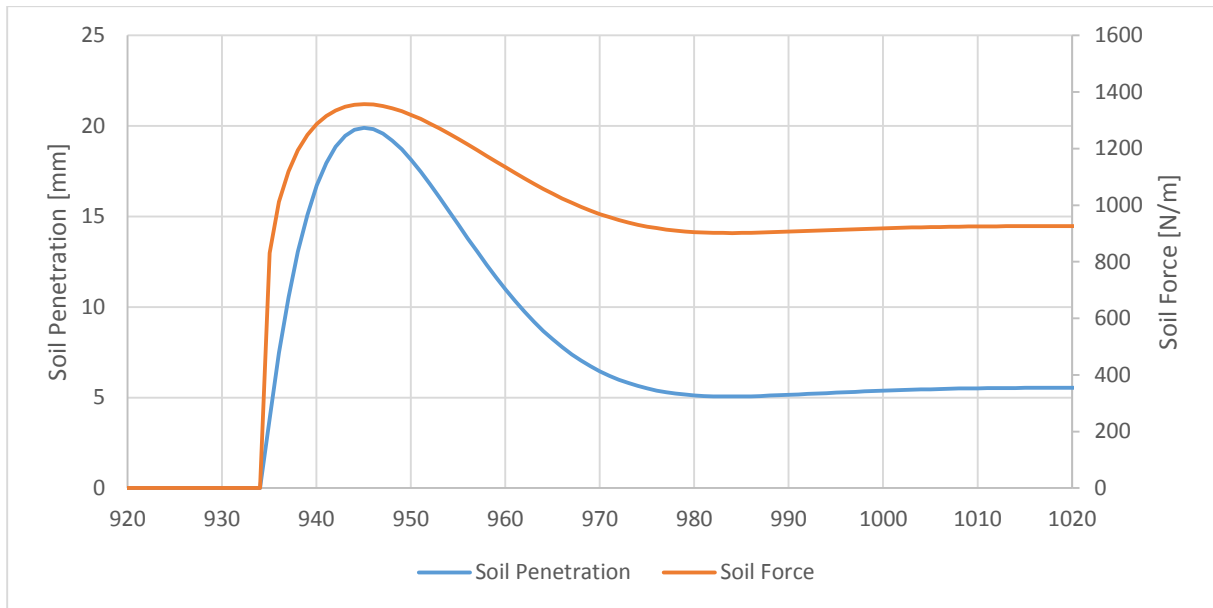


Fig. 6-21. Soil force and penetration along the riser length.

### 6.6.3 Dynamic Analysis

Fig. 6-22 demonstrates how the penetration develops with every cycle. It can be seen that with each cycle the penetration at TDP deepens, and TDP moves toward the hang-off point. The maximum penetration at the first cycle is  $0.051D$ , and it increases by 66% to  $0.084D$  at the end of the tenth cycle. The TDP moves from 934 m to 928 m. It can also be observed from Table 6-5 that the coordinate of the bottom point is not fixed and can change. It is also worth mentioning that with each cycle, the increment of penetration is decreasing (see Table 6-5).

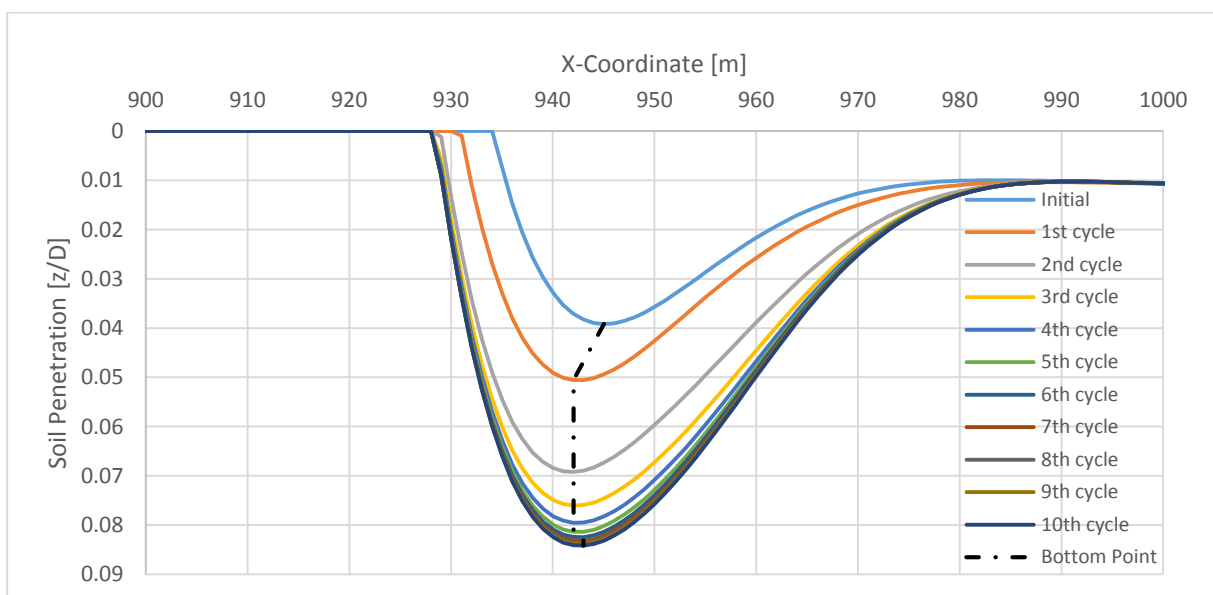


Fig. 6-22. Penetration development around the TDP region.

Table 6-5 Bottom Point Locations and Penetration Depths

Cycle	1	2	3	4	5	6	7	8	9	10
X-Cor	942.04	942.04	942.04	942.04	942.04	943.04	943.04	943.04	943.04	943.04
z/D	0.051	0.069	0.076	0.080	0.081	0.082	0.083	0.084	0.084	0.084

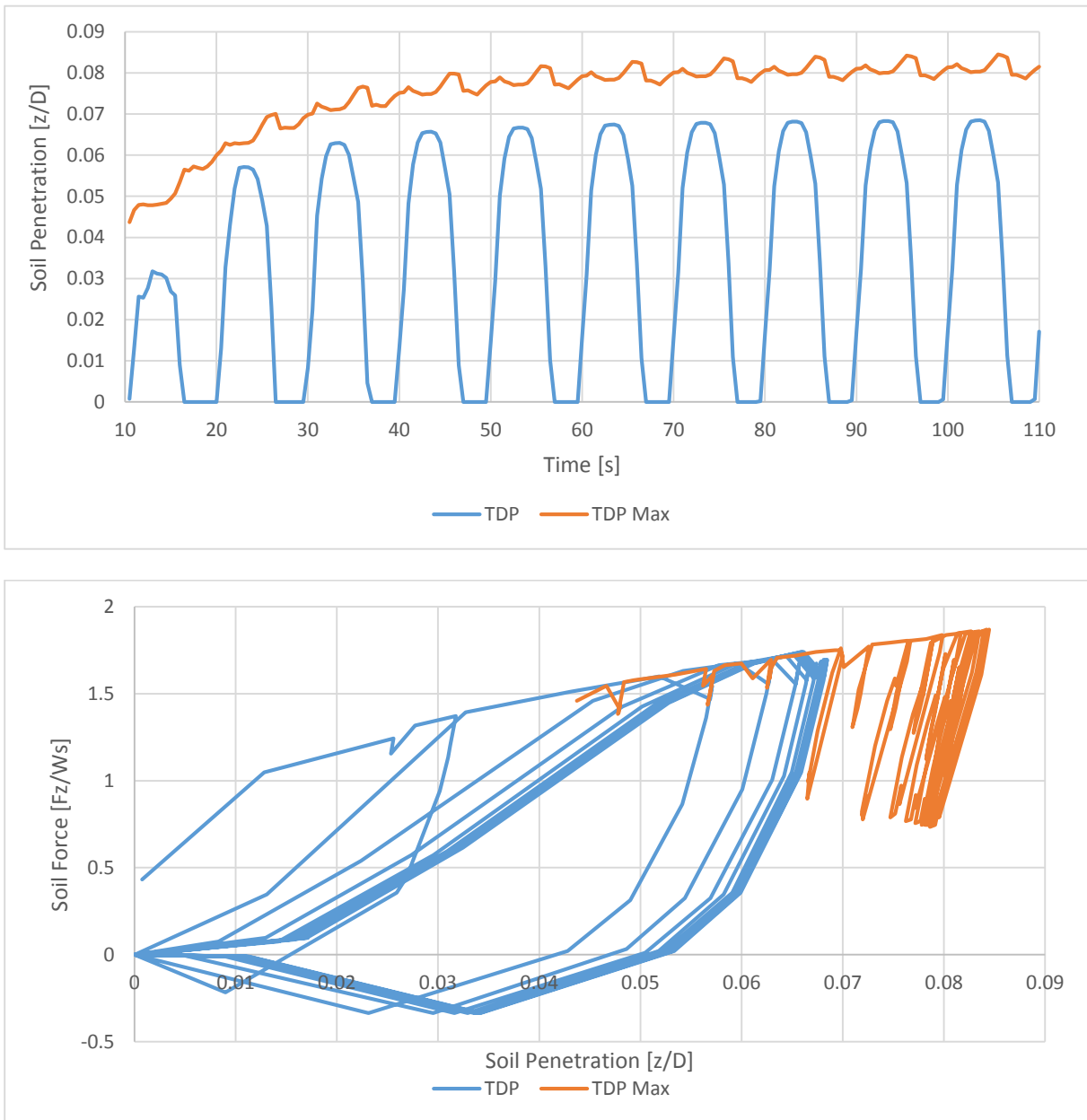


Fig. 6-23. Soil penetration and force at maximum penetration point (TDP Max) and TDP.

The force-displacement curve at the TDP and the maximum penetration point (TDP Max) reveals different pipe-soil behaviours, as shown in Fig. 6-23. At the TDP region, it is characterized by large displacement cycles and large suction forces, which reduce the vertical movement. At the maximum penetration point (TDP Max), the pipe-soil behaviour is characterized by small displacement cycles and is never separated from the seabed; therefore, no suction force is encountered.

The bending moment along the riser length at the minimum of heave motion is presented in Fig. 6-24. The figure shows that the location of the peak bending moment moves toward the hang-off point at the end of the tenth cycle. This is in-line with the movement of TDP shown in Fig. 6-22 and demonstrates the effect of penetration development (trenching) with each cycle.

Table 6-6 Bending Moment Ranges at TDP

Cycle	1	2	3	4	5	6	7	8	9	10
TDP [kN.m]	118.01	159.64	166.41	169.01	168.28	168.44	168.25	168.33	168.34	168.38
TDP Max[kN.m]	77.97	97.88	97.37	97.10	95.20	94.11	93.79	93.74	93.16	93.09

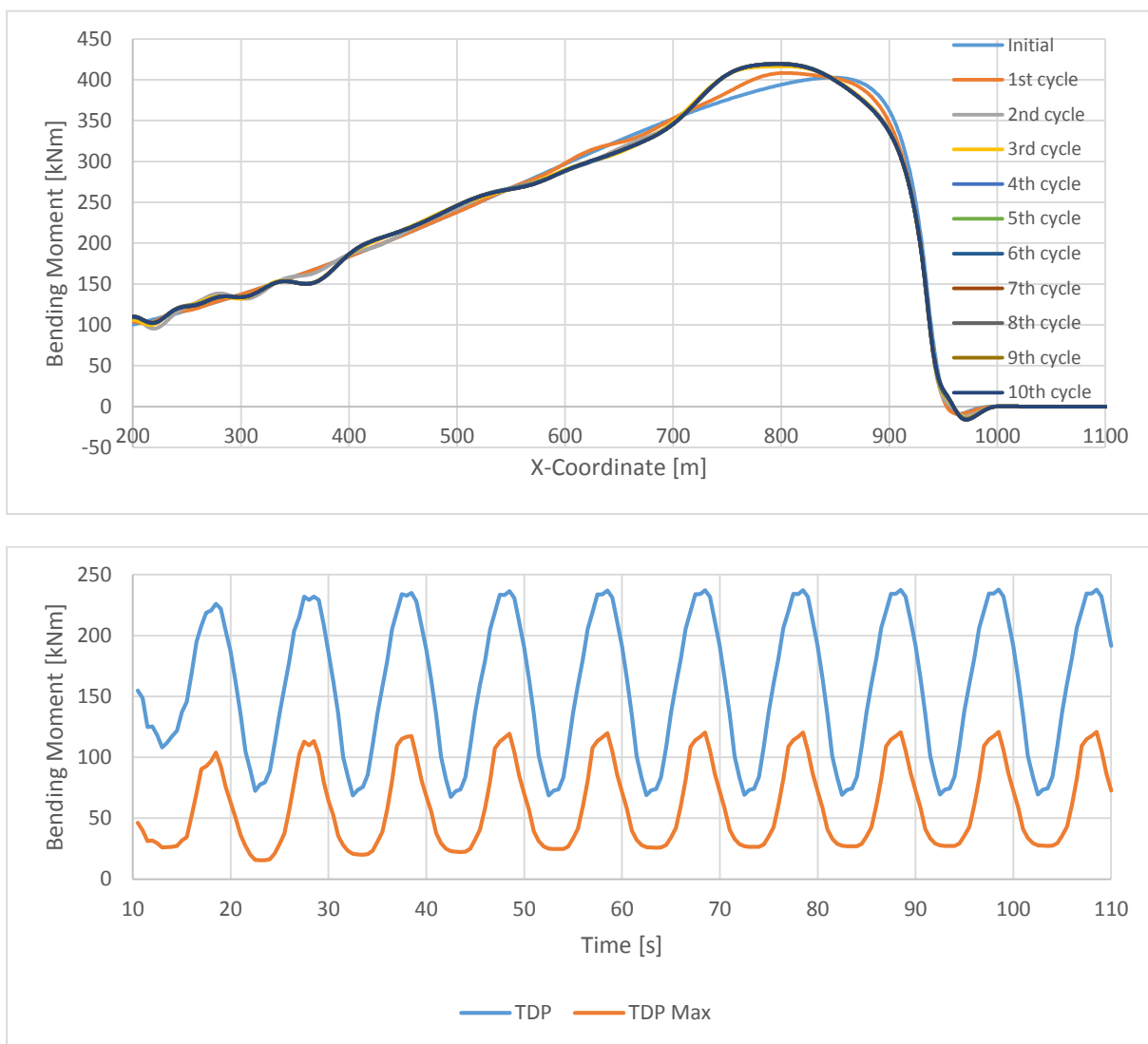


Fig. 6-24. Bending moment range (top) and history (bottom) for non-linear soil model analysis.

Looking at the moment history reveals higher bending moments at TDP compared to TDP Max. The maximum bending moment at TDP is 232 kNm. With respect to fatigue, that moment range is higher at TDP than at TDP Max. The moment variation increases slightly as the penetration

develops, as shown in Table 6-6. Fig. 6-25 shows the moment envelope at the tenth cycle. It can be seen that the TDP region has the highest moment variation at the end of simulations. From the results, it can be concluded that the TDP region is the most crucial area for fatigue analysis.

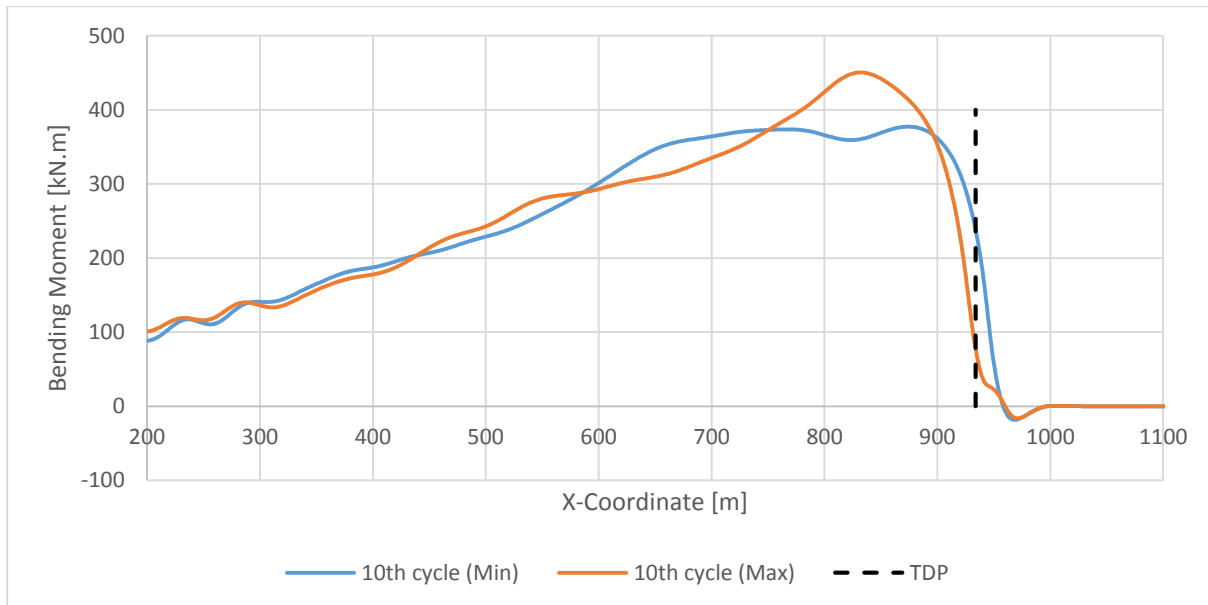


Fig. 6-25. Maximum and minimum bending moment at the tenth cycle.

#### 6.6.4 Soil Strength Sensitivity

The sensitivity of the pipe-soil interaction due to soil strength is the focus of this section. Three seabed strengths (soft clay) have been chosen as the case study, as can be seen in Table 6-7. In addition, seabed with a linear material model is used as a comparison. The soil stiffness used for the linear model is 0.167 MN/m<sup>2</sup>.

Table 6-7 Case List for Vertical Soil Strength Sensitivity Study

Case Name	Soil Strength ( $s_u$ )	Soil Strength Gradient ( $s_g$ )	Equivalent Soil Stiffness
Linear	-	-	0.167 MN/m <sup>2</sup>
Low	1 kPa	0.8 kPa/m	0.167 MN/m <sup>2</sup>
Medium	1.5 kPa	1.2 kPa/m	0.67 MN/m <sup>2</sup>
High	2 kPa	1.5 kPa/m	1.8 MN/m <sup>2</sup>

Dynamic responses are presented for the soil penetration development (trenching), bending moment, and effective tension at TDP in each soil model.

Fig. 6-26 shows the penetration at the minimum of the tenth heave cycle. The figures demonstrate that with higher strength, the soil is harder to penetrate, which causes difference in penetration development. Compared with the linear model, it can be seen that results from the non-linear model show a deeper trench and smoother curvature. It therefore can be concluded that the non-linear model can simulate correct behaviour of the pipe.

Table 6-8 shows how the maximum penetration in each soil model develops. It can be seen that the trench develops faster in very soft clay compared to harder soil. In harder clay, the increment is quite low and reaches maximum penetration earlier. In the linear model, no trench development is observed.

Table 6-8 Maximum Normalized Penetration (z/D) for Various Soil Models

Cycle	1	2	3	4	5	6	7	8	9	10
Low	0.051	0.069	0.076	0.080	0.081	0.082	0.083	0.084	0.084	0.084
Medium	0.024	0.032	0.035	0.037	0.037	0.038	0.038	0.038	0.038	0.038
High	0.014	0.018	0.019	0.020	0.020	0.020	0.020	0.020	0.020	0.020
Linear	0.021	0.021	0.021	0.021	0.021	0.021	0.021	0.021	0.021	0.021

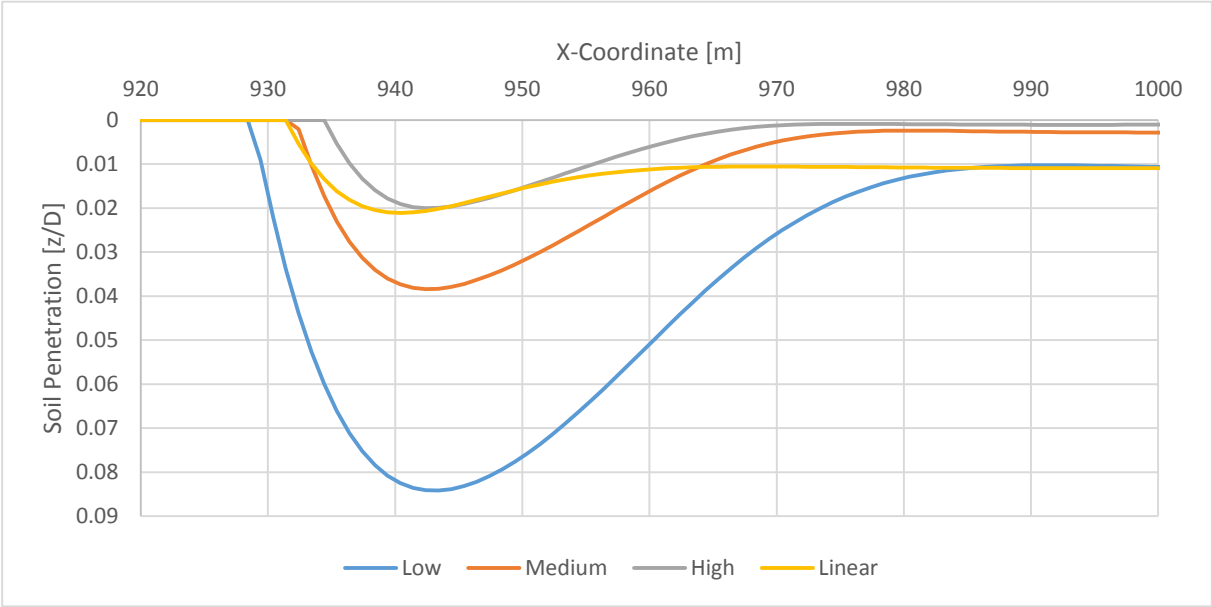


Fig. 6-26. Soil penetration at the tenth cycle for various seabeds, verticals strength.



From the penetration at the TDP, it can be seen that in high seabed stiffness, the curvature is smoother for the high soil strength model. Therefore, it also affects the bending moment at the TDP region considerably. Fig. 6-27 shows the bending moment history in the TDP region for all tested seabed models. The figure shows that the non-linear model gives significantly lower moment variation compared to the linear model.

It can be seen that in heave minimum, the difference between non-linear soil models is small due to the trench reducing the curvature. The high soil model gives a higher moment range compared to the low or medium soil model due to lower trench depth.

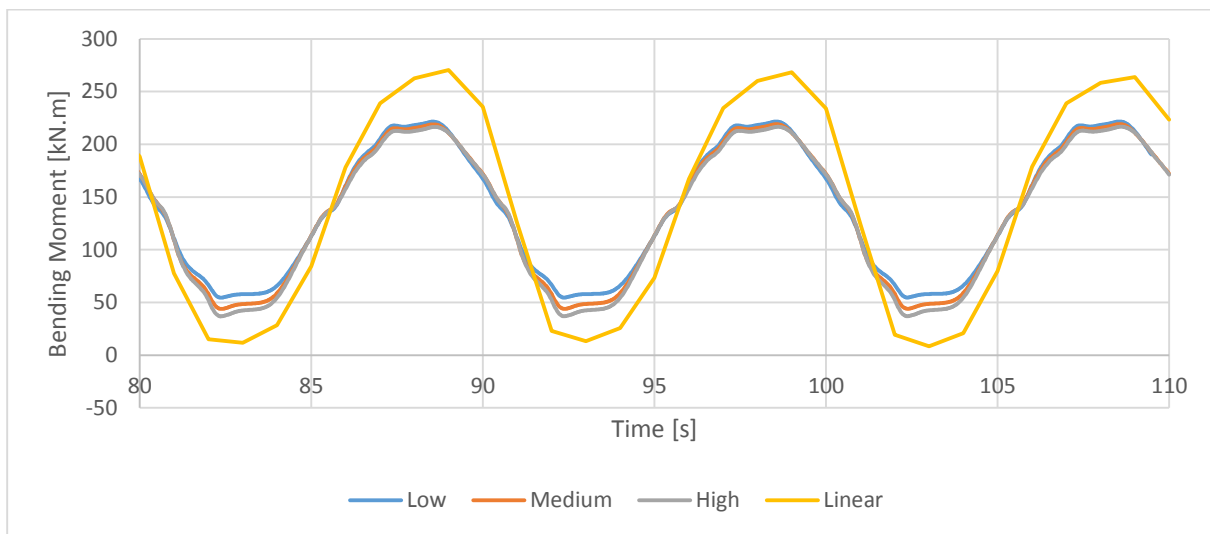


Fig. 6-27. Bending moment history for various seabeds, vertical strength at TDP.

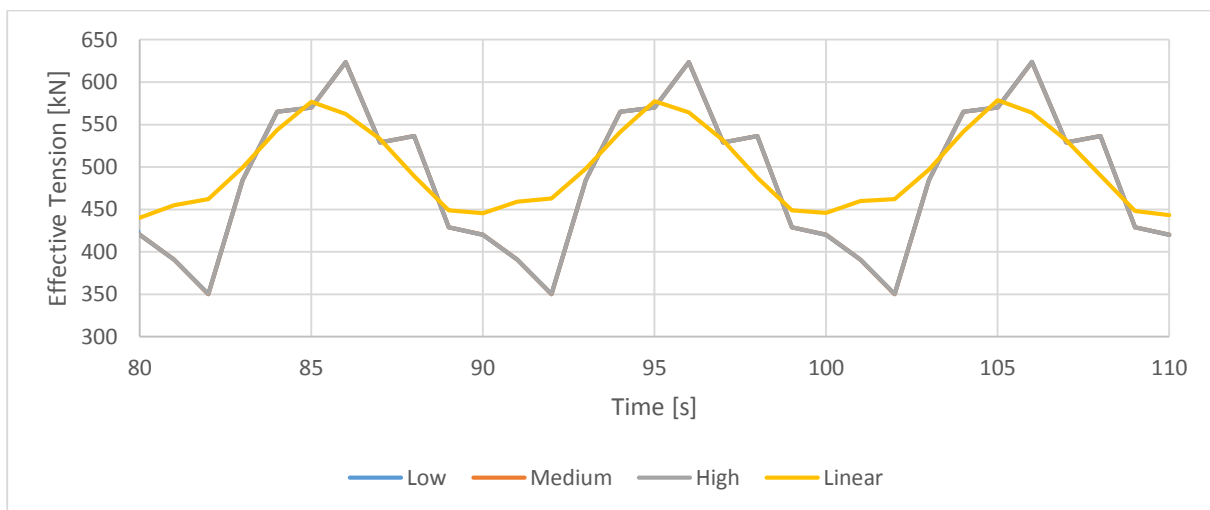


Fig. 6-28. Effective tension history at TDP for various soil models.

Fig. 6-28 shows the effective tension history at TDP. The figure demonstrates another difference between the linear and non-linear models. For the non-linear model, the tension variation is higher due to the inclusion of hysteresis damping in the analysis.

With respect to fatigue, the stresses are mainly dominated by bending moment; therefore, using the non-linear model will improve the fatigue life of SCR at TDP. One also can conclude that the softer soil will give a lower moment range, and therefore a higher fatigue life.

Table 6-9 Results Summary for Soil Strength Sensitivity Analysis

Soil Model	Max Penetration	Max Bending Moment [kN·m]	Max. Effective Tension [kN]
Low	0.084D	229.891	630.224
Medium	0.038D	224.001	630.128
High	0.020D	221.327	630.098
Linear	0.021D	270.417	598.881

### 6.6.5 Suction Force Sensitivity

Soil suction force that is experienced by the riser during uplifting is a crucial aspect in riser-soil interaction. It is therefore important to study the effect of different suction force magnitudes to the development of bending moment at the TDP region.

The suction force of the non-linear soil model is governed by following equations:

$$F_{z2} = -f_{suc}F_{z1} \quad [6-2]$$

$$z_2 = z_1 - \frac{(1 + \omega)F_{z1}}{k_o} \frac{1 + f_{suc}}{\omega - f_{suc}} \quad [6-3]$$

In this section, four suction factors,  $f_{suc}$  which is 0.2, 0.4, 0.6, and 0.8 are investigated. To ensure correct behaviours of the soil, the  $\omega$  parameter is also increased to 0.4, 0.6, 0.8, and 1.0. The soil penetration at the TDP is shown in Fig. 6-29. The effect of suction force is very obvious, with a higher suction factor resulting in lower uplift displacement. Lower uplift displacement means that the trench will be deeper with high suction factor, as demonstrated in the figure.

Fig. 6-30 shows the bending moment history at TDP. The effect is quite apparent, where a higher moment range is observed for high suction factor. Higher suction force results in smoother curvature during uplift, which lower the bending moment. The effect on effective tension is negligible according to the results shown in Fig. 6-31. The results are summarized in Table 6-10.

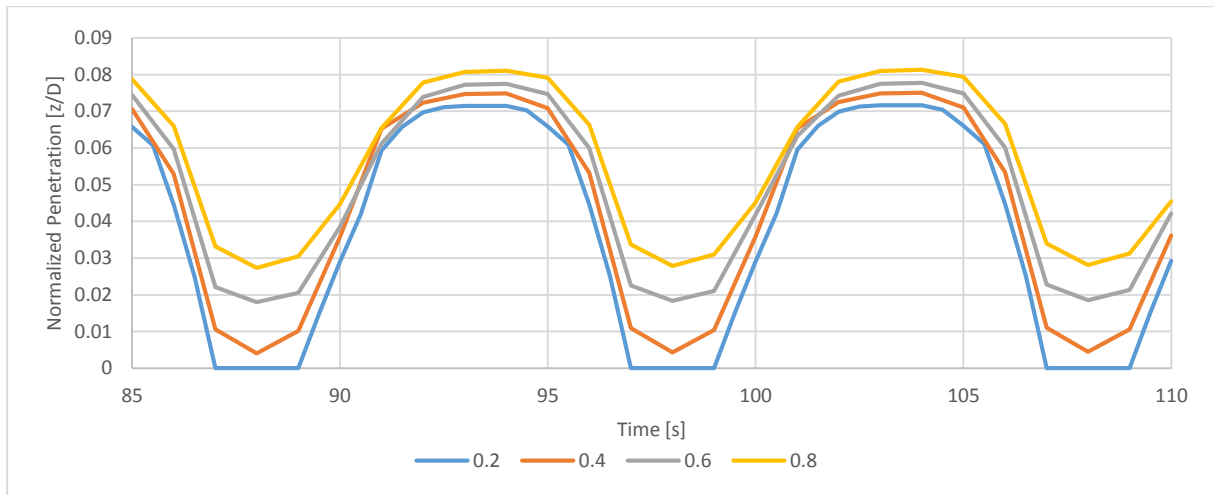


Fig. 6-29. Soil penetration in TDP for various suction factors.

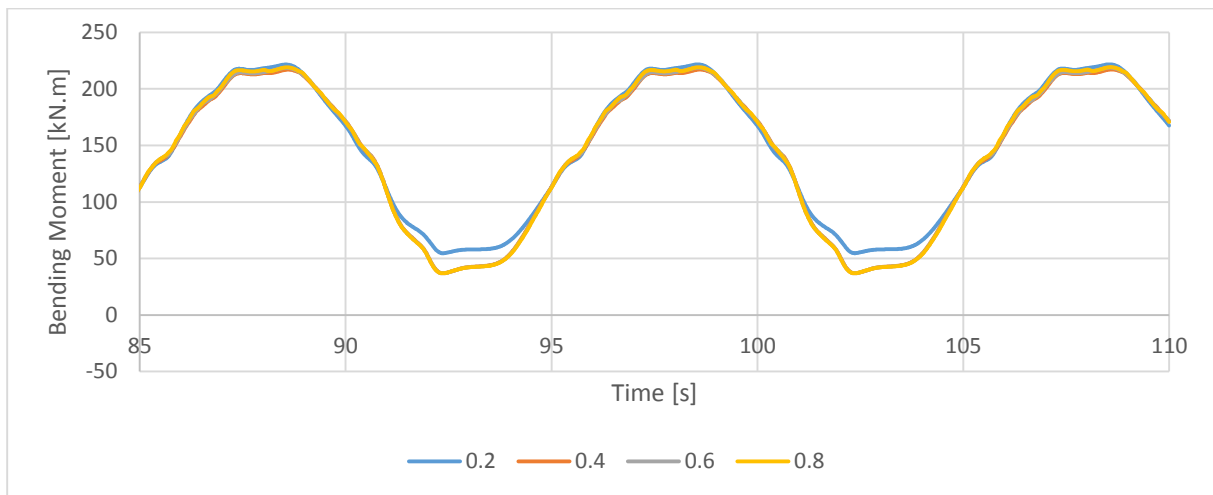


Fig. 6-30. Bending moment history at TDP for various suction factors.

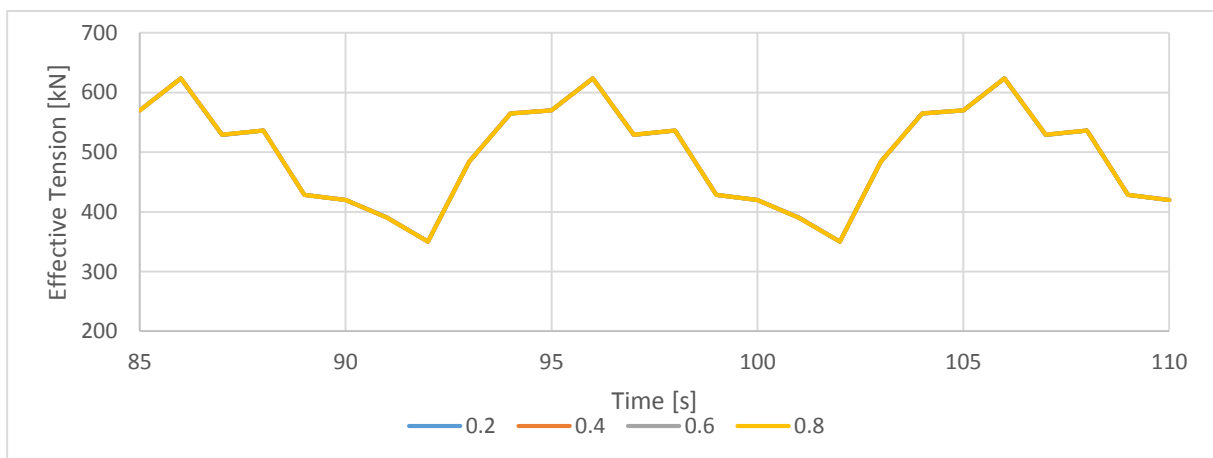


Fig. 6-31. Effective tension history at TDP for various suction factors.

Table 6-10 Results Summary for Suction Factor Sensitivity Analysis

Suction factor	Max Penetration at TDP	Max Bending Moment [kN·m]	Maximum Tension [kN]
0.2	0.072D	229.891	630.224
0.4	0.075D	232.759	623.862
0.6	0.077D	238.067	623.915
0.8	0.081D	270.417	623.948

6.6.6 Heave Amplitude Sensitivity

Heave amplitude is an important parameter in design of SCR because it will affect the moment and tension distribution. This section will study the sensitivity of SCR response to changes in heave amplitude. The amplitudes used in the analysis are 0.5 m, 1 m, 2 m, and 3 m. The soil penetration along the x-coordinate at the end of simulation (110 s) can be seen in Fig. 6-32. The soil gradually increases with every cycle, and the case with the highest heave amplitude gives the deepest trench. The figure also shows that the TDP region becomes wider with higher heave amplitude.

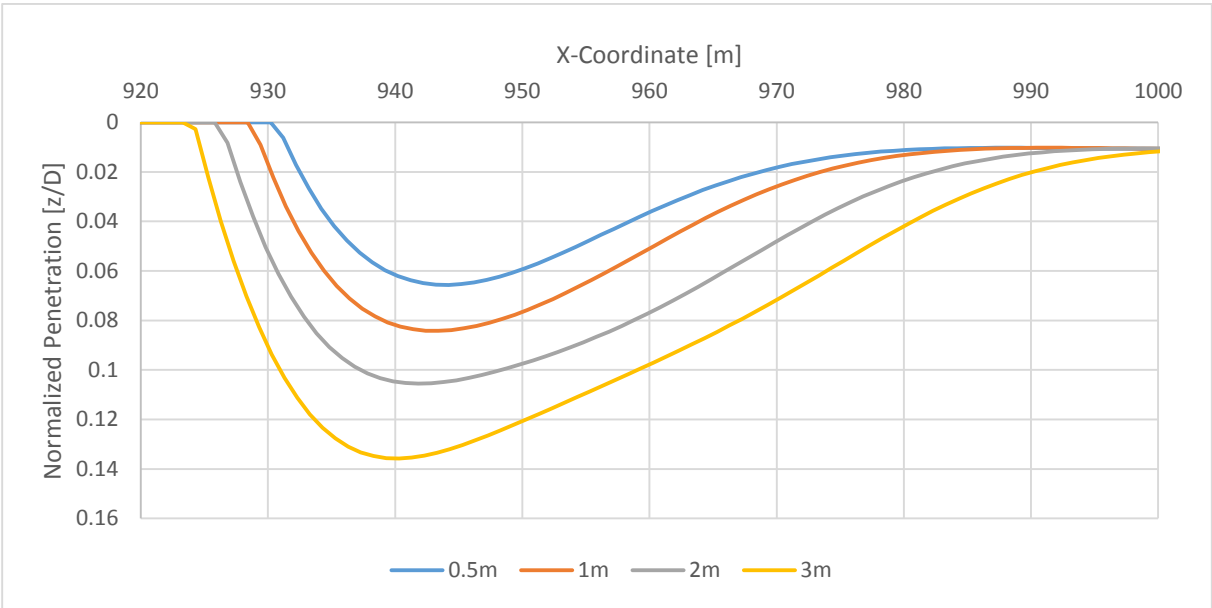


Fig. 6-32. Soil penetration (normalized) for various heave amplitudes.

The trench developed in each cycle makes the curvature smoother in the TDP region and results in a lower maximum bending moment. Fig. 6-33 shows the bending moment at TDP for different heave amplitudes. It is obvious that heave amplitude has a significant effect on moment variations. The heave motion is also observed to have a significant impact on effective tension, as shown in Fig. 6-34. Therefore, it can be concluded that higher heave motion will result in higher moment range and accumulates more fatigue damage.

Table 6-11 Result Summary for Heave Amplitude Sensitivity Analysis

Heave Amplitude	Maximum Penetration	Maximum Bending Moment [kN·m]	Maximum eff. tension [kN]
0.5 m	0.06D	194.886	602.333
1 m	0.08D	229.891	630.224
2 m	0.11D	269.453	848.189
3 m	0.13D	306.482	784.434

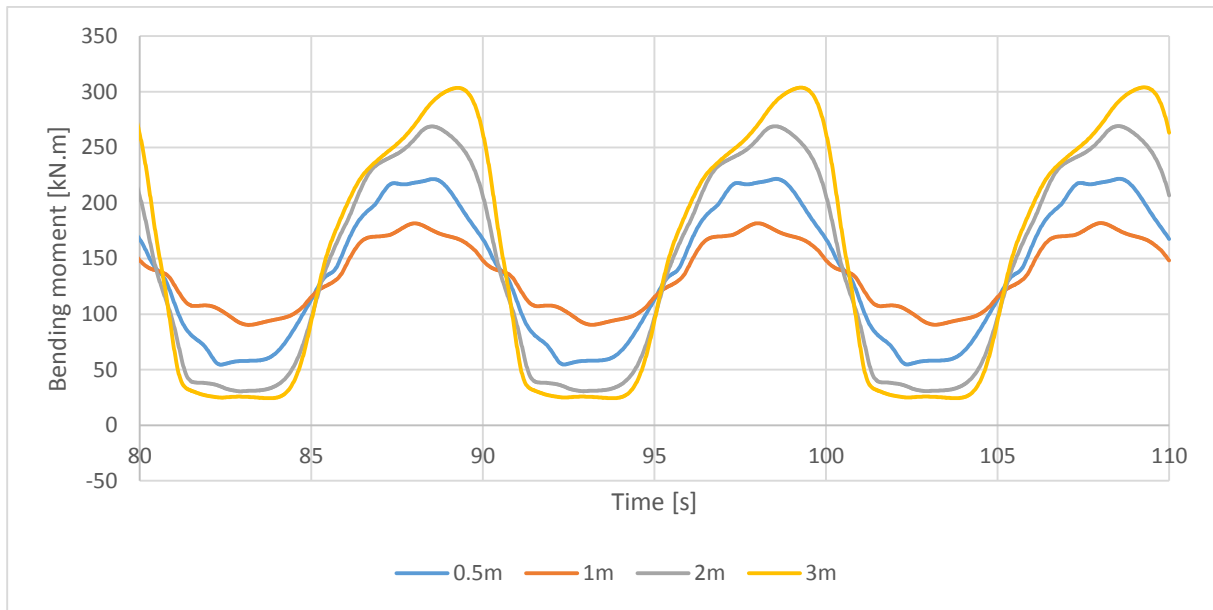


Fig. 6-33. Bending moment history at TDP for various heave amplitudes.

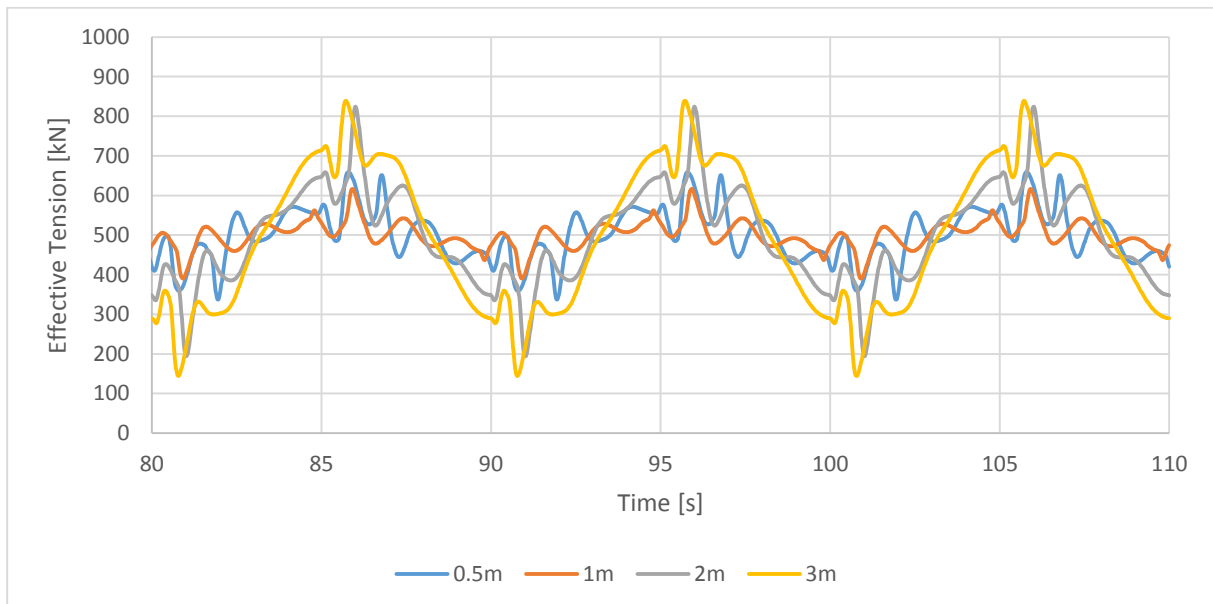


Fig. 6-34. Effective tension history at TDP for various heave amplitudes.

## CHAPTER 7 CONCLUSION

The main objective of the thesis is to develop a working non-linear soil model for use in pipelines and risers designed for soft clay. In deepwater, soft clay is frequently encountered, and its interaction with risers and pipelines highly influences the design. The typical use of said models is to describe the pipe-soil interaction in a simplified and easy-to-implement way. The development focuses on the interaction between risers (SCR) and soil at TDP in the vertical direction, and lateral buckle of pipelines in the lateral direction.

Mathematical models of soil in the vertical and lateral directions that are already widely used in industry are presented in this thesis. The description of pipe-soil interaction in the models is typically in the form of a force-displacement relationship. The relationship is often derived from dimensional analysis and fitting the curve using a high number of test data.

In vertical pipe-soil interaction, the proposed model can simulate non-linear soil behaviours. It is shown that the interaction is a very path-dependent process and generally consists of four main paths. The first path is the backbone curve which models the pipe initial penetration into the soil. The second path is the elastic rebound which occurs during load reversal. In this path, suction force is mobilized by the soil. The third path, called partial pipe-soil separation, describes the soil resistance after maximum suction force is exerted by the soil until full separation. The fourth path describes the re-contact process between the pipe and the soil. If all main paths are passed during one cycle, the resulting force-displacement curve is called the main 'bounding' loop. If reversal occurs before all main paths are passed, the force-displacement curve will enter an 'arbitrary' loop until the pipe moves further. To correctly simulate the behaviours in the time-domain, 16 'memory' parameters are identified.

In lateral non-linear pipe-soil interaction, two main components of soil resistance are encountered. The first component, friction force, is also known as the Coulomb model. The second component is called soil passive/remaining resistance. The soil passive resistance is shown to be time-dependent and a function of soil penetration and vertical force. The proposed soil model of soil passive resistance generally can be divided into three main paths. In the first path, known as the elastic regime, the soil force can be found from the soil elastic stiffness. In the second path, which is the plastic regime, the pipe started to dig into the soil and build up high soil resistance. In the third path, called the residual force path, the pipe breaks out of the soil trench and begins to drag soil along the way. The dragged soil provides resistance on top of the friction force, and if lateral displacement is quite large, it will build up the soil berm,

which gives a very high lateral resistance. Three non-linear models are presented in this thesis: DNV, PONDUS and SAFEBUCK Berm model. Each model has its own characteristics, which are explained in detail. Thirty six memory parameters have been identified for use in calculating the lateral soil force in the time-domain.

Using the mathematical models presented in this thesis, two soil subroutines have been developed. The first subroutine, called DNVMODEL-Y, contains the non-linear soil models from three different sources (DNV, PONDUS, and SAFEBUCK). The second subroutine is called AUBENY-Z and contains a non-linear non-degradation vertical soil model developed by Aubeny et al. The formulation of the subroutines is performed using FORTRAN programming language and is implemented in conjunction with SIMLA for complete pipe-soil interaction analysis. The formulation methods of the subroutines are discussed in detail in the thesis.

The validation of the soil subroutines is accomplished with two methods. The first method is by comparing the results with comparable works/software. The second method is by ascertaining the results with some forced displacement loads. Both results from stand-alone subroutines and the SIMLA model have been validated.

Some applications of soil subroutines are discussed in detail in the thesis. Regarding lateral pipe-soil interaction, it is found that soil stiffness can affect the buckling shape of the pipelines. Two buckling shapes are identified. The first one is a long arch shape, and the second one is a 'snaking' shape. The thesis also includes several analysis cases regarding application of the non-linear soil model in HP/HT pipelines during cyclic thermal loading. It is shown that the non-linear model can limit the walk/cycle compared to the Coulomb model. Comparison with the Coulomb model using various friction coefficients also is presented and discussed in detail.

Regarding vertical pipe-soil interaction, some example applications using a specified deepwater SCR is presented. The results show that the implemented non-linear model can simulate the interaction accurately. Effects of trenching of the SCR in the TDP region are thoroughly investigated. Several sensitivity analyses concerning the soil parameters are also conducted to study the effect on penetration/trench development and bending moment.

## CHAPTER 8 FURTHER WORKS

Due to time constraints, a few aspects of the non-linear pipe-soil interaction are not included in the current version of soil subroutines. The lateral soil model, DNVMODEL-Y, has a fairly well-established small displacement force-displacement model based on the DNV and PONDUS models. However, for large displacement, the current Berm model may be too simplified and does not correctly represent the soil berm resistance. Part of the reason is due to lack of references regarding the force-displacement curve for large displacement. Most of the research projects proposed the berm resistance in terms of the friction model, which cannot fit with the model derived from DNV and PONDUS. If, in the future, a force-displacement curve for the Berm model is invented, it can be included inside the subroutine to increase its versatility.

Regarding the vertical soil model, the current version of AUBENY-Z only includes the non-linear non-degradation soil model. It is recognized that soil degradation can contribute to fatigue life of SCR. Again, due to time constraints, the vertical soil model with degradation effect is not included. The soil model for that exists and is in a similar format to the non-degradation soil model. Therefore, upgrading the vertical soil model is a real possibility in the near future.

Another development also can be pursued to find a method to combine lateral and vertical pipe-soil interaction. Both vertical and lateral soil models are developed by different research projects and tailored for different purposes. It could, however, be interesting to see if both models could be combined to make a complete description of the soil model in the Y-Z plane.

The current subroutines do not include any soil model in the axial direction. In the analysis presented in this thesis, axial direction pipe-soil interaction is modelled using Coulomb friction. The applicability of this method and the interaction between the axial and lateral soil models can be the focus of further study.

Last, further study of applications of non-linear soil models in practical pipelines and risers are proposed. Examples include the use of realistic thermal data to investigate the pipeline walking phenomenon or calculation of buckling loads in design of pipelines. In the vertical direction, the application of realistic vessel motion with six degrees of freedom is recommended. However, the user should be well aware of the limitations and applicability of the programs before progressing to such analyses.



## CHAPTER 9 REFERENCES

- [1] C. P. Aubeny, G. Biscontin and J. Zhang, "Seafloor Interaction with Steel Catenary Riser," Texas A&M University, Austin, Texas, 2006.
- [2] D. Bruton, D. White, M. Carr and C. Cheuk, "Pipe-soil interaction during lateral buckling and pipeline walking—The SAFEBUCK JIP," in *Offshore Technology Conference*, Houston, 2008.
- [3] W. Dunlap, R. Bhonala and D. Morris, "Burial of Vertically Loaded Offshore Pipelines," in *22nd Annual Offshore Technology Conference, number OTC 6375*, Houston, Texas, 1990.
- [4] E. Giertsen, R. Verley and K. Schrøder, "CARISIMA: A CATENARY RISER/SOIL INTERACTION MODEL FOR GLOBAL RISER ANALYSIS," in *OMAE*, Vancouver, 2004.
- [5] C. P. Aubeny, H. Shi and J. Murff, "Collapse Load for cylinder embedded in trench in cohesive soil," in *International Journal of Geomechanics*, 2005.
- [6] V. Richard and K. M. Lund, "A Soil Resistance Model for Pipelines Placed on Clay Soils," in *OMAE*, 1995.
- [7] T. Sotberg and R. L. Verley, "A Soil Resistance Model For Pipelines on Sandy Soils," *OMAE*, Vols. V-A, Pipeline Technology, pp. 123-131, 1992.
- [8] D. Bruton, D. White, C. Cheuk, M. Bolton and M. Carr, "Pipe/Soil Interaction Behaviour During Lateral Buckling," *SPE Journal of Projects, Facilities and Construction*, vol. 1(3), pp. 1-9, 2006.
- [9] H. Brennodden, D. Sveggen and J. Murf, "Full-scale pipe-soil interaction tests," in *Offshore Technology Conference*, Houston, Texas, 1986.
- [10] H. Brennodden, J. Lieng and R. Verley, "An energy-based pipe-soil interaction model," in *Offshore Technology Conference*, Houston, Texas, 1989.
- [11] DNV, "DNV-RP-F109 "On-Bottom Stability Design of Submarine Pipelines"," DNV, Hovik, 2011.
- [12] T. Sotberg, T. Holthe, K. M. Lund and R. T. Igland, "PONDUS Technical Manual," SINTEF, Trondheim, 1994.
- [13] Q. Bai and Y. Bai, "6 - Soil and Pipe Interaction," in *Subsea Pipeline Design, Analysis, and Installation*, Boston, Gulf Professional Publishing, 2014, pp. 121-151.
- [14] C. Cardoso and R. M. S. Silveira, "Pipe Soil Interaction Behaviour for Pipelines Under Large Displacement on Clay Soils - A Model for Lateral Residual Friction Factor," in *Offshore Technology Conference*, Houston, 2010.
- [15] MARINTEK, "MARINTEK," 1 May 2011. [Online]. Available: <https://www.sintef.no/globalassets/upload/marintek/pdf-filer/software/simla.pdf>. [Accessed 09 May 2015].
- [16] S. Sævik, O. D. Økland, G. S. Baarholm and J. K. Gjølsteen, SIMLA Version 3.16.0 User Manual, Trondheim: MARINTEK, 2015.

- [17] M. Carr, F. Sinclair and D. Bruton, "Pipeline Walking—Understanding the Field Layout Challenges, and Analytical Solutions Developed for the SAFEBUCK JIP," in *Offshore Technology Conference (OTC)*, Houston, 2006.

**APPENDIX A      INPUT FILES****PONDUS Input File (Validation Case 1)**

```

50PONDUS (5 lines with descriptive text to follow)
PONDUS   LONG PIPE WITH REGULAR SINE WAVE, Nov. 2004
         INPUT FILE:   example1.ipon
         OUTPUT FILE:  example1.opon
         Ragnar T Igland   2004-11-10

FILES
' IDENT  FILENAME
  PON    ex1_plot.dat
  INO    node11_1.dat
  OCT    timeseriesresults1.ts
EXECUTION
' IRUN   ICOD      TSTART   IOPFAC  FACH   FACL   ICOMP  IREL   STRTUP
  1      0         0
UNIT
' SCALE
  METERS
MATERIAL
' EMOD   RNYC      THERM    RHOS    RHOC    RHOI    YIELD  RHOW
  2.1E11 0.3       1.2E-7  7.86E3  3.05E3  100.    4.15E8 1025.
PIPEDATA
' PLEN   NEL       DEPTH    XSTART  INODF   FSH
  125.   10        60.
' I      L        HDIA     SDIA     STHICK  RMASS   WSUB
  0      0        0.2032  0.2032  0.01
BOUNDARY
' BCOTL  BCORL     BCOTR    BCORR   IOPAX   SKAL    SKAR    RMYL    RMYR
  -1     -1       0        -1      1
SOIL
' I      L        ISOIL    SKA     RMY
' 0      0        1        50.E3  0.4
  0      0        2        800.   65.E3  0
HYDRO
' I      L        CM      CD      CL      CMR
  0      0        3.0    1.5    0.0
REGWAV
' H      T        FI      VC
  12.    10.     90.    0.0
TEPRTE
' IOPF
  2
' PRES   FTOT
  0.     0.
SOLVE
' DT     NTIMX    IOPDIS
  0.01  35000     1
' EPS    MAXIT    IOPINT   ALPHA1  ALPHA2  ALPHA3  EPSNM
  0.00001 10     1       0.     0.0    0.0
PRINT
' IPRINT
  1
' NNP    NEP      ITPR     INODT   ITPRT
  11     10      5        11     5
' INP1   INP2     . . . . . INPNNP
  1      2      3 4 5 6 7 8 9 10 11
' IEP1   IEP2     . . . . . IEPNEP
  1      2      3 4 5 6 7 8 9 10

```

```
PLOT
' ISTEP   ISTET   ISTE0
  1000     5       5
' NTN
  10
' INOD     IDA     IOCT
  11       1       1
  11       2       1
  11       3       1
  11       4       1
  11       5       1
  11       6       1
  11       7       1
  11       8       0
  11      -2       0
  11     -11       0
' NTE
  2
' IEL      IDB     IOCT
  1         1       1
  1         3       1
END
```

PONDUS Input File (Validation Case 2)

```

50PONDUS (5 lines with descriptive text to follow)
PONDUS LONG PIPE WITH REGULAR SINE WAVE, Nov. 2004
INPUT FILE: example1.ipon
OUTPUT FILE: example1.opon
Ragnar T Igland 2004-11-10

FILES
' IDENT FILENAME
  PON ex2_plot.dat
  INO nodell.dat
  OCT timeseriesresults2.ts
EXECUTION
' IRUN ICOD TSTART IOPFAC FACH FACL ICOMP IREL STRTUP
  1 0 0
UNIT
' SCALE
  METERS
MATERIAL
' EMOD RNYC THERM RHOS RHOC RHOI YIELD RHOW
  2.1E11 0.3 1.2E-7 7.86E3 3.05E3 100. 4.15E8 1025.
PIPEDATA
' PLEN NEL DEPTH XSTART INODF FSH
  125. 10 60.
' I L HDIA SDIA STHICK RMASS WSUB
  0 0 0.2032 0.2032 0.01
BOUNDARY
' BCOTL BCORL BCOTR BCORR IOPAX SKAL SKAR RMYL RMYR
  -1 -1 0 -1 1
SOIL
' I L ISOIL SKA RMY
' 0 0 1 50.E3 0.4
  0 0 2 800. 65.E3 0
HYDRO
' I L CM CD CL CMR
  0 0 3.0 1.5 0.0
REGWAV
' H T FI VC
  25. 10. 90. 0.0
TEPRTE
' IOPF
  2
' PRES FTOT
  0. 0.
SOLVE
' DT NTIMX IOPDIS
  0.01 9900 1
' EPS MAXIT IOPINT ALPHA1 ALPHA2 ALPHA3 EPSNM
  0.00001 10 1 0. 0.0 0.0
PRINT
' IPRINT
  1
' NNP NEP ITPR INODT ITPRT
  11 10 1 11 1
' INP1 INP2 . . . . . INPNNP
  1 2 3 4 5 6 7 8 9 10 11
' IEP1 IEP2 . . . . . IEPNEP
  1 2 3 4 5 6 7 8 9 10
PLOT
' ISTEP ISTET ISTE0
  1000 1 1
' NTN

```

```
10
' INOD      IDA      IOCT
11          1         1
11          2         1
11          3         1
11          4         1
11          5         1
11          6         1
11          7         1
11          8         0
11         -2         0
11        -11         0
' NTE
2
' IEL      IDB      IOCT
1          1         1
1          3         1
END
```

## APPENDIX B SOURCE CODES

### DNVMODEL-Y SOURCE CODE

```

=====
!Lateral Riser-Soil Motion Model[CLAY]
!DEVELOPED BY : ARIFIAN AGUSTA IRMAN
!MASTER STUDENT, NTNU
=====
subroutine ma dnvlateral(x input,IOP,lsnum,input_array,work_array,opt,res)
implicit none

!Input definiton
double precision,intent(in)::x input
integer,intent(in)::IOP,lsnum
double precision,dimension(*)::input_array
integer,intent(in),dimension(*)::opt

!Internal variable definiton
double precision::x1,D,zi,gs,kc,x2,x3,f,ws_prev,deltaf,slq,x0,x3berm
double precision::xd,x1n,x2n,x3n,x_rev,ke,fe,zfr1,k_clay,x12,x12n
double precision::fl,fr1,ws,gc,su,fr2,s,fr3,f_rev,fr,ds,ve
double precision::E,z2m,z3,z2,ad,zpm,z_prev,fx_prev
double precision::zinit
double precision,dimension(3)::x
double precision::EFAC1,ENER1,ENER0,EFAC0,DELEN,D2,D1,XEL,XCROSS
integer::i,path,opt1,opt2,opt3
integer::lstart,vsign

!Internal variable definition for berm model
double precision::pos_rev,xpos_rev,xberm,fberms,xneg_rev,neg_rev
double precision::fberm_max,berm_pcmt,berm_cycles
double precision::fberms_neg,xberm_neg

!Output defintion
double precision::z,fx,a,kx
double precision,intent(out),dimension(4)::res
double precision,dimension(*)::work_array
!integer,allocatable,dimension(:)::pathrec

!Unpacking option array
opt1=opt(1)
opt2=opt(2)
opt3=opt(3)

!Unpacking input array
D=input_array(1) !Pipe diameter[m]
ws=input_array(2) !Submerged weight [N/m]
gs=input_array(3) !Soil submerged weight
su=input_array(4) !Seabed undrained shear strength
fl=input_array(5) !Lift Force
ke=input_array(6) !Soil Elastic stiffness for linear case (IOP=1)
x(1)=x input

!Defining maximum berm cycles
if(OPT2>0)then
berm_cycles=OPT2
end if

!Unpacking work array
=====
!!
i=int(work_array(1)) !Load step number(internal)
x(2)=work_array(2) !X at i-1
x(3)=work_array(3) !X at i-2
path=int(work_array(4)) !Path identifier from previous iteration
fx_prev=work_array(5) !Fx from previous iteration
z_prev=work_array(6) !Soil penetration from previous iteration
f_rev=work_array(7) !Last known reversal point (force)
x_rev=work_array(8) !Last known reversal point (displacement)
xd=work_array(9) !Energy from previous iteration
XCROSS=work_array(10) !Highest known amplitude
ws_prev=work_array(11) !Last known amplitude
!Characteristic properties from previous iteration
x1=work_array(12)
x2=work_array(13)

```

```

x3=work_array(14)
x1n=work_array(15)
x2n=work_array(16)
x3n=work_array(17)
zi=work_array(18)
fr1=work_array(19)
fr2=work_array(20)
fr3=work_array(21)
z2=work_array(22)
z3=work_array(23)
E=work_array(24)
x12=work_array(25)
x12n=work_array(26)
pos rev=work_array(27)
neg rev=work_array(28)
xpos_rev=work_array(29)
xneg_rev=work_array(30)
fberms=work_array(31)
xberm=work_array(32)
fberms neg=work_array(33)
xberm neg=work_array(34)
lstart=int(work_array(35))
x3berm=work_array(36)
!Load step counting number
!=====
==!!

!CASE SELECTOR
SELECT CASE (IOP)
!=====
==!!
!CASE 1 - LINEAR SPRING
CASE(1)
z=zi
to initial embedment
a=0.050d0*x(1)
fx=ke*x(1)
force in linear case
kx=ke
stiffness
path=100
work_array(1:36)=0.0d0
work_array(4)=real(path)
goto 999
!CASE 2 - Contact Lost (Lifted out of seabed)
!=====
==!!
CASE(2)
work_array(1:36)=0.0d0
z=0
a=0
fx=0
condition
kx=0
path=200
work_array(4)=real(path)
i=0
goto 999
!CASE 3 - NON-LINEAR MODEL/PLASTIC DEFORMATION
!=====
==!!
CASE(3)
!Skipping the initial calculation
if(i>0)then
goto 100
end if

!Innate Properties calculation(Initial Only)
gc=su/(D*gs)
kc=(su*D)/(ws-fl)
IN EVERY ITERATION
zi=zinit(D,su,ws,gs,fl)
fr1=fr(su,d,gs,zi,ws,fl)
path=0
lstart=lsnum
step number
fe=0.2*(ws-fl)+fr1
soil model
!FL NEED TO BE UPDATED
!Initial penetration
!Elastic limit-FR1
!Starting path number
!Record starting load
!Elastic limit of the

```



```

xel=fe/ke                                     !Elastic limit of the
displacement                                  !The first crossing
xcross=0
for plastic displacement

!DNV Characteristic Limit
x1=xel                                         !Limit of elastic
range
x2=0.50d0*D                                  !Breakout-limit
x3=D                                           !DNV RULE(0.5 for DNV,
0.75 for PONDUS)
x1n=-x1                                       !Negative range limit
x2n=-x2
x3n=-x3

!Modifying the characteristic limit according to PONDUS MANUAL
if (OPT3==2) then
  x12=xel
  x12n=-xel
  x2=0.75d0*D
  x2n=-x2
  k_clay=gs*D**2/ws
  x3=(0.6*(5.5/k_clay+1)+x2/D)*D
  x3n=-x3
end if

if (zi>0.5*D) then
  zi=0.5d0*D
end if

!Transition from Linear to Non-Linear
100 if (i==0) then
  if (x(1)>xel) then
    write(*,*) "The Linear Model displacement exceed the elastic limit of Non-Linear Model"
    stop
  end if
end if

!Internal load step counting
i=lsnum-(lstart-1)

!Amplitude of plastic deformation
a=abs(x(1)-xcross)
if (a/D<0.05) then
  aD=0.05
elseif (a/D>=0.05) then
  aD=a/D
end if

!PATH 01 - ELASTIC RANGE
01 if (path==0.or.path==15) then

  !Path Branching
  if (x(1)>x1.and.x(1)>x(2)) then
    path=12
    if (OPT3==2) then
      path=20
      goto 20
    end if
    goto 12
  elseif (x(1)<x1n.and.x(1)<x(2)) then
    path=121
    if (OPT3==2) then
      path=21
      goto 20
    end if
    goto 12
  end if

  fx=f_rev+ke*(x(1)-x_rev)
  z=zi

  if (x(1)<x(2)) then
    path=15
  elseif (x(1)>x(2)) then
    path=0
  end if
end if

```

```

      kx=ke
    end if

!PATH 20 - EXTENDED ELASTIC RESISTANCE (ONLY FOR OPT3=2!)
20  if(path==20.or.path==21)then
    !PATH BRANCHING Requirement
    if(x(1)<x12n.and.path==21)then
      path=121
      goto 12
    elseif(x(1)>x12.and.path==20)then
      path=12
      goto 12
    end if

    if(x(1)<x(2).and.path==20)then
      path=14
      goto 14
    elseif(x(1)>x(2).and.path==21)then
      path=14
      goto 14
    end if

    ZPM=0

    if(E>0)then

      S=(ws-f1)/(d*su)
      D1=f1
      DELEN=abs(D1*(x(1)-x(2)))           !Incremental
energy  EFAC0=(0.12*(S**0.637)*(aD)**(-0.25))**(1/0.32)
      ENER0=su*(D**2)*(z_prev/D)**(1/0.32)/EFAC0           !Energy from
previous iteration
      ENER1=ENER0+DELEN
      EFAC1=0.12*(S**0.637)*(aD)**(-0.25)
      ZPM=EFAC1*(ENER1/(su*D**2))**0.32-EFAC1*(ENER0/(su*D**2))**0.32           !Incremental
penetration
      E=ENER1
      DELEN=0

    end if

    if(path==21)then
      z=z_prev+(ZPM*D)
      fx=-(0.2*(ws-f1)+f1)
      kx=0
    elseif(path==20)then
      z=z_prev+(ZPM*D)
      fx=(0.2*(ws-f1)+f1)
      kx=0
    end if
  end if

!PATH 12 - BREAKOUT BUILD-UP
12  if(path==12.or.path==121)then
    !Reloading before breakout
    if(x(1)<x(2).and.path==12)then
      path=14
      goto 14
    elseif(x(1)>x(2).and.path==121)then
      path=14
      goto 14
    end if

    S=(ws-f1)/(d*su)

    !Direction identifier
    if(path==12)then
      vsign=1
    else
      vsign=-1
    end if

    !PENETRATION FOR ELASTIC LIMIT
    gc=su/(D*gs)

```

```

      kc=(su*D)/(ws-f1)                                !FL NEED TO
BE UPDATED IN EVERY ITERATION
      zfr1=(0.0071d0*(gc**0.3d0/kc)**3.2d0+0.062d0*(gc**0.3d0/kc)**0.7d0)*D  !INITIAL
PENETRATION [m] - PONDUS
      fr1=fr(su,d,gs,zfr1,ws,f1)

      IF(OPT3==1)then
        FR1=fr(su,d,gs,zi,ws,f1)
      END IF

      if (fx_prev<(0.2*(ws-f1)+fr1).and.path==12)then
        fx_prev=(0.2*(ws-f1)+fr1)
      elseif (fx_prev>-(0.2*(ws-f1)+fr1).and.path==121)then
        fx_prev=(0.2*(ws-f1)+fr1)*vsign
      end if

      FR2=fr(su,d,gs,z_prev,ws,f1)
      ve=(0.2*ws)/ke
      D1=fx_prev-0.2*(ws-f1)
!Passive resistance from previous iteration
      D2=(fr2-fr1)/(x2-x12)*(x(1)-ve)-x12)+fr1
!Passive resistance for t2 from previous curve
      if(path==121)then
        D1=abs(fx_prev+0.2*ws)
!Passive resistance from previous iteration
        D2=(fr2-fr1)/(x2n-x12n)*(x(1)-ve)-x12n)+fr1
!Passive resistance for t2 from previous curve
      end if
      DELEN=0.5*(D1+D2)*(x(1)-x(2))*vsign
!Incremental energy
      EFAC0=(0.12*(S**0.637)*(aD)**(-0.25))**(1/0.32)
      ENER0=su*(D**2)*(z_prev/D)**(1/0.32)/EFAC0
!Energy from previous iteration
      ENER1=ENER0+DELEN
      EFAC1=0.12*(S**0.637)*(aD)**(-0.25)
      ZPM=EFAC1*(ENER1/(su*D**2))**0.32-EFAC1*(ENER0/(su*D**2))**0.32
!Incremental penetration
      E=ENER1
      DELEN=0
      Z=Z_PREV+(ZPM*D)

      !Calculate new FR2 (Breakout-Resistance)
80      FR2=fr(su,d,gs,z,ws,f1)
      D2=(fr2-fr1)/(x2-x12)*(x(1)-x12)+fr1
!Passive resistance for t2 from previous curve
      if(path==121)then
        D2=(FR2-FR1)/(x2n-x12n)*(x(1)-x12n)+fr1
      endif

      IF(X(2)==X(1))THEN
        SLQ=0
      ELSE
        SLQ=(D2-D1)/(X(1)-X(2))
      ENDIF

      f=SLQ*(1/ke)*vsign
      deltaf=f/(1+f)*ke*(x(1)-x(2))-1/(1+f)*0.2*(ws-ws_prev)
      fx=fx_prev+deltaf

      !SOIL STIFFNESS
      KX=(FR2-FR1)/(X2-X12)

      !Maximum penetration (Z2-max)
      if(((z/D)<=0.5).and.((aD)>=0.05))then
        s=ws/(D*s_u)
        gc=su/(D*gs)
        z2m=(1.1*s*gc**0.54)*(aD)**(0.17))*D
      elseif((z/D)>0.5)then
        z2m=0.5*D
      end if

      !Maximum penetration reached path
      if(z>z2m)then
        z=z2m
        goto 80
      end if

```

```

!Path Branching Requirement-Breakout
if(x(1)>x2.or.x(1)<x2n)then
  z2=z_prev

  if(opt1==2)then
    z3=zinit(D,su,ws,gs,fl)          !PONDUS MANUAL
  elseif(opt1==1)then
    z3=0.5*z2                        !DNV RULE
  end if

  if(x(1)<x2n.and.path==121)then
    path=131
    goto 131
  elseif (x(1)>x2)then
    path=13
    goto 13
  end if
end if
end if

!After breakout-Positive Loading
13 if(path==13)then
  !Path branching requirement
  if(x(1)<x(2))then
    path=14
    !Logical if current reversal is less than previous known reversal, reset the cycle
    counting to zero
    if(x(2)<(xpos_rev-0.1*D))then
      pos_rev=1
    else
      pos_rev=pos_rev+1
    end if
    xpos_rev=x(2)
    goto 14
  end if
  FR3=fr(su,d,gs,z3,ws,fl)

  !LINEAR INTERPOLATION OF Z (BASED ON DNV MODEL)
  IF(OPT3==1)then
    z=z2+(z3-z2)/(x3-x2)*(x(1)-x2)

  ELSEIF(OPT3==2)then
    FR2=fr(su,d,gs,z_prev,ws,fl)
    SLQ=(FR3-FR2)/(x3-x2)
    F=SLQ*(1/ke)
    X0=X(2)-X2
    DS=FR2+SLQ*(x(1)-(x2+x0))/(1+F)
    gc=su/(D*gs)
    Z=(abs(DS)/(4.13*D*su*gc**(-0.392)))**(1/1.31)
    Z=Z*D
    END IF

    if(z<z3)then
      if(z_prev>z3)then
        x3berm=x(1)
      endif
      fx=(fr3+0.2*(ws-fl))
      z=z3
      kx=0
      IF(OPT2>0)then
        !Activating the berm resistance model
        if(pos_rev>0)then
          if(x(1)<xpos_rev.and.x(1)>((xpos_rev+x3berm)*0.5))then
            path=99
            xberm=(xpos_rev+x3berm)*0.5
            fberms=fx_prev
            goto 99
          end if
        end if
      end if
    else
      FR2=fr(su,d,gs,z,ws,fl)
      D1=fx_prev-0.2*(ws_prev)
      D2=FR2
      IF(X(2)==X(1))then
        SLQ=0

```

```

ELSE
SLQ=(D2-D1)/(x(1)-x(2))
END IF

F=SLQ*(1/ke)
deltaf=F/(1+F)*KE*(x(1)-x(2))-1/(1+f)*0.2*(ws-ws_prev)
fx=fx_prev+deltaf
kx=(FR3-FR2)/(X3-X2)
end if
end if

!After Breakout, Negative Loading
131 if(path==131)then
!Path branching requirement
if(x(1)>x(2))then
path=14
!Logical if current reversal is less than previous known reversal, reset the cycle
counting to zero
if(x(2)>(xneg_rev+0.1*D))then
neg_rev=1
else
neg_rev=neg_rev+1
end if
xneg_rev=x(2)
goto 14
end if
FR3=fr(su,d,gs,z3,ws,f1)
IF(OPT3==1)THEN
!LINEAR INTERPOLATION OF Z FOR DNV MODEL
z=z2+(z3-z2)/(x3n-x2n)*(x(1)-x2n)

ELSEIF(OPT3==2)then
!PONDUS MODEL
FR2=fr(su,d,gs,z_prev,ws,f1)
SLQ=-(FR3-FR2)/(x3n-x2n)
F=SLQ*(1/ke)
X0=X(2)-X2N !Origin's translated distance
DS=FR2-SLQ*(x(1)-(x2n+x0))/(1+F)
gc=su/(D*gs)
Z=(abs(DS)/(4.13*D*su*gc**(-0.392)))**(1/1.31)
Z=Z*D

END IF
if(z<z3)then
if(z_prev>z3)then
x3berm=x(1)
endif
fx=-(fr3+0.2*(ws-f1))
z=z3
kx=0
IF(OPT2>0)then
!Activating the berm resistance model
if(neg_rev>0)then
if(x(1)>xneg_rev.and.x(1)<((xneg_rev+x3berm)*0.5))then
path=98
xberm_neg=(xneg_rev+x3berm)*0.5
fberms_neg=fx_prev
goto 98
end if
end if
end if
else
FR2=fr(su,d,gs,z,ws,f1)
D1=abs(fx_prev)-0.2*(ws_prev)
D2=FR2
if(X(2)==X(1))then
SLQ=0
else
SLQ=-(D2-D1)/(x(1)-x(2))
endif
F=SLQ*(1/ke)
deltaf=F/(1+F)*KE*(x(1)-x(2))-1/(1+f)*0.2*(ws-ws_prev)
fx=fx_prev+deltaf
kx=(FR3-FR2)/(X3-X2)
end if
end if
end if

```

```

!Reversal Path-New Curve Definition
14 if(path==14)then

    !REVERSAL POINT
    f_rev=fx_prev
    x_rev=x(2)
    xcross=x(2)

=====
    !PONDUS MODEL REVERSAL
=====
    if(OPT3==2)then
        gc=su/(D*gs)
        kc=(su*D)/(ws-fl)                                !FL NEED TO
BE UPDATED IN EVERY ITERATION
        zfr1=(0.0071d0*(gc**0.3d0/kc)**3.2d0+0.062d0*(gc**0.3d0/kc)**0.7d0)*D !INITIAL
PENETRATION [m] - PONDUS
        fr1=fr(su,d,gs,zfr1,ws,fl)
        zi=z_prev

!Modifying the characteristic limit according to PONDUS MANUAL
fe=fr1+(0.2*(ws-fl))                                !Elastic limit
xel=fe/ke                                            !Elastic limit for displacement
x1=xel+(x_rev-f_rev/ke)
x1n=-xel+(x_rev-f_rev/ke)

if(x_rev>x2.or.x_rev<x2n)then
    xd=x_rev-x2
    if(x_rev<x2n)then
        xd=x_rev-x2n
    end if
    x12=x12+xd
    x12n=x12n+xd
    x2=x2+xd
    x2n=x2n+xd
    x3=x3+xd
    x3n=x3n+xd
end if

=====
    !DNV MODEL REVERSAL
=====
    elseif(OPT3<2)then
        zi=z_prev                                !DNV require previous penetration as initial
penetration for new curve
        fr1=fr(su,d,gs,zi,ws,fl)                !DNV MODEL
        fe=fr1+(0.2*(ws-fl))                    !Elastic limit
        xel=fe/ke                                !Elastic limit for displacement
        xd=x_rev-f_rev/ke

!Shifting the characteristic limit
x1=xel+xd
x2=0.50*D+xd
x3=D+xd
x1n=-xel+xd
x2n=-0.50*D+xd
x3n=-D+xd
x12=x1
x12n=x1n

    end if

=====
=====

!Renaming the path based on loading direction
if (x(1)<x(2))then
    path=15
elseif(x(1)>x(2))then
    path=0
endif

```

```

        goto 01
    end if

    !BERM RESISTANCE MODEL
99  if (path==99) then
        if (pos_rev >= berm_cycles) then
            pos_rev = berm_cycles
        end if

        if (x(1) < x(2)) then
            path = 13
            goto 13
        end if
        z = z3
        Fberm_max = 1.5 * (ws - fl) + fberms
        SAFEBUCK JIP RESEARCH
        Berm_pcnt = (1 / berm_cycles) * pos_rev
        berm_resistance_in_the_current_cycles
        fx = fberms + ((Fberm_max - fberms) * berm_pcnt) / (xpos_rev - xberm) * (x(1) - xberm)
        kx = berm_pcnt * (Fberm_max - fberms) / (xpos_rev - xberm)

    END IF

98  if (path==98) then
        if (neg_rev >= berm_cycles) then
            neg_rev = berm_cycles
        end if

        if (x(1) > x(2)) then
            path = 131
            goto 131
        end if
        Fberm_max = 1.5 * (ws - fl) + abs(fberms_neg)
        !BASED ON SAFEBUCK JIP RESEARCH
        Berm_pcnt = (1 / berm_cycles) * (neg_rev)
        !Maximum berm resistance in the current cycles
        fx = fberms_neg + ((-Fberm_max - fberms_neg) * berm_pcnt) / (xneg_rev - xberm_neg) * (x(1) - xberm_neg)
        kx = berm_pcnt * (-Fberm_max - fberms_neg) / (xneg_rev - xberm_neg)
        z = z3
    END IF

END SELECT

!UPDATING WORK ARRAY
!=====
=====
work_array(1) = real(i)
work_array(2) = x_input
if (i > 2) then
work_array(3) = x(2)
end if
work_array(4) = real(path)
work_array(5) = fx
work_array(6) = z
work_array(7) = f_rev
work_array(8) = x_rev
work_array(9) = xd
work_array(10) = xcross
work_array(11) = ws
work_array(12) = x1
work_array(13) = x2
work_array(14) = x3
work_array(15) = x1n
work_array(16) = x2n
work_array(17) = x3n
work_array(18) = zi
work_array(19) = fr1
work_array(20) = fr2
work_array(21) = fr3
work_array(22) = z2
work_array(23) = z3
work_array(24) = E
work_array(25) = x12
work_array(26) = x12n
work_array(27) = pos_rev
work_array(28) = neg_rev
work_array(29) = xpos_rev
!Iteration number
!X at i-1
!X at i-2
!Path identifier from previous iteration
!Fx from previous iteration
!Soil penetration from previous iteration
!Last known reversal point (force)
!Last known reversal point (displacement)

```

```

work_array(30)=xneg_rev
work_array(31)=fberms
work_array(32)=xberm
work_array(33)=fberms_neg
work_array(34)=xberm_neg
work_array(35)=real(lstart)
work_array(36)=x3berm
!=====
=====
!Updating Result Array
999 res(1:4)=(/z,fx,a,kx/)

end subroutine ma dnvlateral

!!=====SUB-
ROUTINES=====!!
function fr(su,d,gs,z,ws,fl)
implicit none
double precision::gc,kc
double precision::su,D,gs,z,ws,fl
double precision::fr
gc=su/(D*gs)
kc=(su*D)/(ws-fl)
fr=(4.13*kc/(gc**0.392)*(z/d)**1.31)*(ws-fl)
end function fr

function zinit(D,su,ws,gs,fl)
implicit none
double precision::gc,kc,D,su,gs,ws,fl
double precision::zinit
gc=su/(D*gs)
kc=(su*D)/(ws-fl)
!INITIAL PENETRATION [m] - PONDUS
zinit=(0.0071d0*(gc**0.3d0/kc)**3.2d0+0.062d0*(gc**0.3d0/kc)**0.7d0)*D
end function zinit

```

## VERTICAL SOIL MODEL SOURCE CODES (AUBENY-Z)

```

!=====
!           VERTICAL RISER-SOIL MODEL [CLAY]           !
!=====
subroutine vsm(z input,IOP,lsnum,input array,work array,opt,res real,res int)
implicit none

!INPUT DEFINITION
double precision,intent(in)::z input
double precision,dimension(*)::input array
integer,dimension(*)::opt

!Internal Variable definition
double precision,dimension(3)::z
integer::i,path,IOP,lsnum,lstart
double precision::D,s0,fsuc,w,phi,sg,k0,a,b,ks
double precision::p_prev,P1,P2,Y1,Y2,Y3,zr,zrb,pr,prb,pref,pref2
double precision::P01,P12,P23,P31,P31r
double precision::K01,K12,K23,K31,K31r,z_d,p_dum,PE,ERR, P_d

```



```

double precision::z_dum1, z_dum2

!OPTION DEFINITION (PENDING)

!OUTPUT DEFINITION
double precision::p,kz
double precision,dimension(*)::work array
double precision,dimension(*),intent(out)::res real
integer,dimension(*),intent(out)::res int

!Unpacking input array
z(1)=z input
D=input array(1)
s0=input array(2)
fsuc=input array(3)
w=input_array(4)
phi=input_array(5)
sg=input array(6)
ks=input array(7)
a=input array(8)
b=input array(9)

!=====
!Unpacking work array
i=work array(1)           !Load step number
z(2)=work array(2)       !Z from i-1
z(3)=work_array(3)       !Z from i-2
p_prev=work_array(4)     !P from previous iteration
path=work_array(5)       !Path identifier
k0=work array(6)         !Soil stiffness(vertical)
P1=work array(7)
P2=work array(8)
Y1=work_array(9)
Y2=work_array(10)
Y3=work array(11)
zrb=work array(12)
zr=work array(13)
prb=work_array(14)
pr=work_array(15)
lstart=work_array(16)
z d=work array(17)

!=====

!CASE SELECTOR
SELECT CASE (IOP)
!=====
!CASE 1 - INITIAL LINEAR SPRING
CASE(1)
p=ks*z(1)
kz=ks
path=100
!In case of contact lost in linear spring, no suction is considered
if(z(1)<0)then
  path=101
end if

!=====
!CASE 3 - NON - LINEAR MODEL
CASE(3)

if(i>0)then
  goto 100
end if

!Calculating the equivalent backbone curve
z_dum1=z(2)
z_dum2=10*z(2)
Pe=ks*z(2)
P d=P01(z dum2,D,s0,sg,a,b)
err=100
if(path==100)then
do while(P_d<Pe)
  P_d=P01(z_dum2,D,s0,sg,a,b)
  z_dum2=2*z dum2
end do

do while(err>1e-5)

```

```

z_d=0.5*(z_dum1+z_dum2)
Pe=ks*z(2)
P dum=P01(z d,D,s0,sg,a,b)
if(P dum<Pe)then
  z_dum1=z_d
elseif(P_dum>Pe)then
  z dum2=z d
endif
err=abs(P dum-Pe)
end do
end if
!Initial calculation
p_prev=P01(z(2),D,s0,sg,a,b)
k0=660.0*s0
lstart=lsnum
path=0

!Transition from Linear to Non Linear, check
100 if(i==0)then
  if(z(1)<0)then
    write(*,*)"The penetration is negative, try reducing the starting time"
    stop
  end if
end if

!Internal load step counting
i=lsnum-(lstart-1)

!Initial penetration
01 if (path==0) then
  p=P01(z(1),D,s0,sg,a,b)
  kz=K01(z(1),D,s0,sg,a,b)
  if(z(1)<z_d)then
    p=P01(z d,D,s0,sg,a,b)
    kz=0
  end if
end if

!The definition of first reversal point and cycles important resistance reversal points
if (i>2) then
  if (z(1)<z(2).and.z(2)>z(3).and.path==0)then
    Y1=z(2)
    P1=p_prev
    Y2=Y1-(((1+w)*P1/k0)*((1+fsuc)/(w-fsuc)))
    Y3=Y2-phi*(Y1-Y2)
    P2=-fsuc*P1
    if (z(1)<Y2.and.z(1)>Y3)then
      path=23
      goto 23
    elseif (z(1)<Y3)then
      path=30
      goto 30
    else
      path=12
      goto 12
    end if
  end if
end if

!Point 1 to Point 2
12 if (path==12)then
  p=P12(z(1),Y1,P1,P1,k0,w,-1)
  kz=K12(z(1),Y1,P1,k0,w,-1)
  if (z(1)<=Y2)then
    path=23
    goto 23
  else if (z(1)>z(2))then
    path=121
    zrb=z(2)
    prb=p_prev
    goto 121
  end if
end if

!Reloading between Point 1 and Point 2
121 if (path==121)then

```

```

    pref=P31(z(1),Y1,Y3,P1)
    p=P12(z(1),zrb,prb,P1,k0,w,1)
    kz=K12(z(1),zrb,p1,k0,w,1)
    !Ensuring the reversal within the bounding loop
    if (p>pref) then
        !print *, "Hit upper bound, iteration no:",i
        !print *, "Original value:",p,"Reference Value (P31):",pref
        p=pref
        path=31
        goto 31
    end if
    !Unloading in Path 1-2-1
    if (z(1)<z(2))then
        path=122
        zr=z(2)
        pr=p_prev
        goto 122
    end if
    if (z(1)>=Y1)then
        path=0
        goto 01
    end if
end if

!Unloading in Path 1-2-1
122 if (path==122)then
    pref=P12(z(1),Y1,P1,P1,k0,w,-1)
    pref2=P23(z(1),Y2,Y3,P2)
    p=P12(z(1),zr,pr,P1,k0,w,-1)
    kz=K12(z(1),zr,p1,k0,w,-1)
    if (p<pref .and. z(1)>Y2) then
        !print *, "Hit lower bound 1, iteration no:",i
        !print *, "Original value:",p,"Reference Value (P12):",pref
        p=pref
        path=12
        goto 12
    elseif (p<pref2 .and. z(1)<Y2)then
        !print *, "Hit lower bound 2, iteration no:",i
        !print *, "Original value:",p,"Reference Value (P23):",pref
        p=pref2
        path=23
        goto 23
    end if
    !Reloading in Path 1-2-1
    if (z(1)>z(2))then
        path=121
        zrb=z(2)
        prb=p_prev
        goto 121
    end if
end if

!Point 2 to Point 3
23 if (path==23)then
    p=P23(z(1),Y2,Y3,P2)
    kz=K23(z(1),Y2,Y3,P2)
    !Reloading
    if (z(1)>z(2))then
        path=231
        zrb=z(2)
        prb=p_prev
        goto 231
    end if
    if (z(1)<=Y3)then
        path=30
    end if
end if

!Reloading between Point 2 and Point 3
231 if (path==231)then
    p=P31r(z(1),Y1,zrb,P1,Prb)
    kz=K31r(z(1),Y1,zrb,P1,Prb)
    if (z(1)<z(2))then
        path=122
        zr=z(2)
        pr=p_prev
        goto 121
    end if
end if

```

```

        end if
        if(z(1)>=Y1)then
            path=0
            goto 01
        end if
    end if

!Full Separation
30 if (path==30)then
    p=0
    kz=0
    if (z(1)>z(2) .and. z(1)>=Y3) then
        path=31
        goto 31
    end if
end if

!Recontact
31 if (path==31)then
    p=P31(z(1),Y1,Y3,P1)
    kz=K31(z(1),Y1,Y3,P1)
    if(z(1)<z(2))then
        path=122
        zr=z(2)
        pr=p prev
        goto 122
    end if
    if (z(1)>=Y1)then
        path=0
        goto 01
    end if
end if

END SELECT

!Updating iteration number

!=====
!Updating work array
work_array(1)=i                !Load step number
work_array(2)=z(1)            !Z from i-1
if(i>2)then
work_array(3)=z(2)            !Z from i-2
end if
work_array(4)=p                !P from previous iteration
work_array(5)=path            !Path identifier
work_array(6)=k0              !Soil stiffness(vertical)
work_array(7)=P1
work_array(8)=P2
work_array(9)=Y1
work_array(10)=Y2
work_array(11)=Y3
work_array(12)=zrb
work_array(13)=zr
work_array(14)=prb
work_array(15)=pr
work_array(16)=lstart
work_array(17)=z d
!=====

!Updating result array
res_real(1:2)=(/p,kz/)

!Updating contact status array (1-contact, 0-contact lost)
if(path==30.or.path==101)then
    res_int(1)=0
else
    res_int(1)=1
end if

end subroutine vsm

!=====FUNCTION PAGE=====
function P01(y,D,s0,sg,a,b)

```

```

implicit none
double precision::P01,y,D,s0,sg,a,b
P01=(a*(y/D)**b)*(S0+Sg*y)*D;
end function P01

function K01(z,D,s0,sg,a,b)
implicit none
double precision::z,D,s0,sg,K01
double precision::a,b
if(z<=0)then
  K01=0
else
  K01=(a*b*(S0+Sg*z)*(z/D)**(b-1)+D*a*sg*(z/D)**b)
end if
end function K01

function P12(y,Y1,Prb,P1,k0,w,x)
implicit none
double precision :: P12,y,y1,prb,p1,k0,w
integer::x
P12=Prb+(y-Y1)/(1/k0+x*(y-Y1)/((1+w)*P1));
end function P12

function K12(z,z1,p1,k0,w,x)
implicit none
double precision::z,z1,p1,k0,w,K12,A
integer::x
A=1/k0+x*(z-z1)/((1+w)*P1)
K12=1/A+x*(z1-z)/(((1+w)*P1)*A**2)
end function K12

function P23(y,Y2,Y3,P2)
implicit none
double precision::y,Y2,Y3,P2
double precision::Y0,Ym,P23
Y0=(Y2+Y3)/2;
Ym=(Y2-Y3)/2;
P23=P2/2+P2/4*(3*(y-Y0)/Ym-((y-Y0)/Ym)**3);
end function P23

function K23(z,Y2,Y3,P2)
implicit none
double precision::z,Y2,Y3,P2
double precision::Y0,Ym,K23
Y0=(Y2+Y3)/2;
Ym=(Y2-Y3)/2;
K23=P2/4*(3/Ym-3*(z-Y0)**2/(Ym**3));
end function K23

function P31(y,Y1,Y3,P1)
implicit none
double precision::y,Y1,Y3,P1
double precision::P31,Y0,Ym
Y0=(Y1+Y3)/2;
Ym=(Y1-Y3)/2;
P31=P1/2+P1/4*(3*(y-Y0)/Ym-((y-Y0)/Ym)**3);
end function P31

function K31(z,Y1,Y3,P1)
implicit none
double precision::z,Y1,Y3,P1
double precision::K31,Y0,Ym
Y0=(Y1+Y3)/2;
Ym=(Y1-Y3)/2;
K31=P1/4*(3/Ym-3*(z-Y0)**2/(Ym**3));
end function K31

function P31r(y,Y1,Yrb,P1,Prb)
implicit none
double precision::y,Y1,Yrb,P1,Prb
double precision::y0,ym,P31r
Y0=(Y1+Yrb)/2;
Ym=(Y1-Yrb)/2;
P31r=(P1+Prb)/2+(P1-Prb)/4*(3*(y-Y0)/Ym-((y-Y0)/Ym)**3);
end function P31r

function K31r(z,Y1,Yrb,P1,Prb)

```

```
implicit none
double precision::Y1, Yrb, P1, Prb
double precision::y0, ym, K31r, z
Y0=(Y1+Yrb)/2;
Ym=(Y1-Yrb)/2;
K31r=(P1-Prb)/4*(3/Ym-3*(z-Y0)**2/(Ym**3));
end function K31r
```

**APPENDIX C Excerpt of SIMLA User Manual****3.32.13 DNVMODEL-Y (CONT126)**

**MATERIAL MNAME DNVMODEL-Y ISOIL SKA GAMS TPOND [SU SG IMODEL  
IBERM IPONDUS]**

**ISOIL:** Soil type (unit: -)

**1 :** Clay - only clay allowed in this version

**2 :** Sand

**SKA:** Elastic soil stiffness (unit : FL<sup>-2</sup>)

**GAMS:** Soil submerged weight (unit : FL<sup>-3</sup>)

**TPOND:** Time at which the DNVMODEL-Y model is to be activated

**SU:** Undrained shear strength (unit: FL<sup>-3</sup>). Optional parameter for **ISOIL=1** (clay) only.

**SG:** Soil strength gradient (unit: FL<sup>-3</sup>). Optional parameter for **ISOIL=1** (clay) only.

**IMODEL:** Definition of penetration breakthrough, 1= dnvmodel, 2= pondus model. Optional parameter for **ISOIL=1** (clay) only.

**IBERM:** Berm resistance parameter expressing how many diameters of movement needed to activate full berm resistance, if zero then berm resistance is not activated. Optional parameter for **ISOIL=1** (clay) only.

**IPONDUS:** 1-DnV soil modelling, 2=Pondus soil modelling. Optional parameter for **ISOIL=1** (clay) only.

**3.32.14 AUBENY-Z (CONT126)**

**MATERIAL MNAME AUBENY-Z ISOIL SKA GAMS TPOND [SU SG FSUC W PHI BACKBC1 BACKBC2 ]**

**ISOIL:** Soil type (unit: -)

**1 :** Clay - only clay allowed in this version

**2 :** Sand

**SKA:** Elastic soil stiffness (unit : FL<sup>-2</sup>)

**GAMS:** Soil submerged weight (unit : FL<sup>-3</sup>)

**TPOND:** Time at which the AUBENY-Z model is to be activated

**SU:** Undrained shear strength (unit: FL<sup>-3</sup>). Optional parameter for **ISOIL=1** (clay) only.

**SG:** Soil strength gradient (unit: FL<sup>-3</sup>). Optional parameter for **ISOIL=1** (clay) only.

**FSUC:** Suction factor (unit: -). Optional parameter for **ISOIL=1** (clay) only.

**W:** Asymptota (unit: -). Optional parameter for **ISOIL=1** (clay) only.

**PHI:** Separation point ratio (unit: -). Optional parameter for **ISOIL=1** (clay) only.

**BACKB1:** Backbone curve parameter 1 (unit: -). Optional parameter for **ISOIL=1** (clay) only.

**BACKB2:** Backbone curve parameter 2 (unit: -). Optional parameter for **ISOIL=1** (clay) only.